. SCUOLA INTERNAZIONALE SUPERIORE DI STUDI AVANZATI

SISSA Digital Library

Foxg1 bimodally tunes L1-mRNA and -DNA dynamics in the developing murine neocortex

Original
Foxg1 bimodally tunes L1-mRNA and -DNA dynamics in the developing murine neocortex / Liuzzi, G.; Artimagnella, O.; Frisari, S.; Mallamaci, A.. - In: DEVELOPMENT. - ISSN 0950-1991. - 151:10(2024), pp. 1-85. [10.1242/dev.202292]

Availability:
This version is available at: 20.500.11767/139330 since: 2024-06-03T15:17:20Z

Publisher:

Published
DOI:10.1242/dev.202292

Terms of use:

Testo definito dall'ateneo relativo alle clausole di concessione d'uso

Publisher copyright

note finali coverpage

(Article begins on next page)

17 July 2024

Foxg1 bimodally tunes *L1*-mRNA and -DNA dynamics in the developing murine neocortex

Gabriele Liuzzi[*], Osvaldo Artimagnella[‡], Simone Frisari[§] and Antonello Mallamaci[*]

Laboratory of Cerebral Cortex Development, SISSA, Trieste, Italy

[*]Corresponding authors
e-mail: amallama@sissa.it; gliuzzi@sissa.it
[‡]Present address: IRCCS Centro Neurolesi "Bonino-Pulejo", Messina, Italy.
[§]Present address: Department of Medicine, Surgery and Health Sciences, University of Trieste, Trieste, Italy

Keywords: Foxg1, L1 retrotransposon, transcription, retro-transcription, cerebral cortex

SUMMARY STATEMENT

This study reports the bimodal tuning of *L1* retrotransposon transcription and retrotranscription exerted by *Foxg1* brain patterning gene in the developing rodent neocortex.

ABSTRACT

Foxg1 masters telencephalic development via a pleiotropic control over its progression. Expressed within the central nervous system (CNS), *L1* retrotransposons are implicated in progression of its histogenesis and tuning of its genomic plasticity. Foxg1 represses gene transcription, and *L1* elements share putative Foxg1 binding motifs, suggesting the former might limit telencephalic expression (and activity) of the latter. We tested such prediction, in vivo as well as in engineered primary neural cultures, by loss- and gain-of-function approaches. We showed that *Foxg1*-dependent, transcriptional *L1* repression specifically occurs in neopallial neuronogenic progenitors and post-mitotic neurons, where it is supported by specific changes in the *L1* epigenetic landscape. Unexpectedly, we discovered that Foxg1 physically interacts with *L1*-mRNA and positively regulates neonatal neopallium *L1*-DNA content, antagonizing the retrotranscription-suppressing activity exerted by Mov10 and Ddx39a helicases. To the best of our knowledge, *Foxg1* represents the first CNS patterning gene acting as a bimodal retrotransposon modulator, limiting transcription of *L1* elements and promoting their amplification, within a specific domain of the developing mouse brain.

© 2024. Published by The Company of Biologists Ltd.
This is an Open Access article distributed under the terms of the Creative Commons Attribution License (http://creativecommons.org/licenses/by/4.0), which permits unrestricted use, distribution and reproduction in any medium provided that the original work is properly attributed

Development • Accepted manuscript

INTRODUCTION

Foxg1 encodes for an evolutionarily ancient transcription factor that drives the development of the anterior brain (Hanashima et al., 2004). It promotes the activation of subpallial (Martynoga et al., 2005) and neo-paleo-pallial (Muzio and Mallamaci, 2005) morphogenetic programs, regulates pallial stem cells fate choice, promoting neuronogenesis at expenses of gliogenesis (Brancaccio et al., 2010; Falcone et al., 2019; Frisari et al., 2022), and commits neocortical neurons to distinct layer identities (Hanashima et al., 2004; Hou et al., 2019; Miyoshi and Fishell, 2012; Toma et al., 2014). Subsequently, Foxg1 stimulates neuronal morphological maturation (Brancaccio et al., 2010; Chiola et al., 2019; Yu et al., 2019; Zhu et al., 2019), and enhances electrical activity (Tigani et al., 2020; Zhu et al., 2019), being in turn transiently upregulated by the latter (Fimiani et al., 2016; Tigani et al., 2020). Experimental *Foxg1* knock-down in vivo reduces social interaction and results in selective impairment of specific learning and memory abilities (Miyoshi et al., 2021; Shen et al., 2006; Yu et al., 2019). In humans, several *FOXG1* copy number variations (CNVs) and structural mutations have been described. They lead to severe neuropathological scenarios, collectively referred to as FOXG1 syndrome, for which no cure is so far available (Brimble et al., 2023; ClinVar db_Foxg1; Florian et al., 2011; Mitter et al., 2018; Papandreou et al., 2016; SFARI db_Foxg1; Vegas et al., 2018). Traditionally recognized as a transcriptional transrepressor (Seoane et al., 2004), Foxg1 has more recently been implicated in straight control of extra-transcriptional functions, such as post-transcriptional ncRNA processing (Weise et al., 2019), translation (Artimagnella et al., 2022) and mitochondrial biology (Pancrazi et al., 2015).

Albeit tightly controlled (Faulkner and Billon, 2018; Goodier, 2016), transposable elements including *L1s* are actively transcribed. Specific ensembles of such elements are activated concomitantly with distinct, early histogenetic routines (He et al., 2021), and, in some cases, their transcription is required for the progression of these routines (Jachowicz et al., 2017; Macfarlan et al., 2012; Percharde et al., 2018). Moreover, a subset of full-length *L1s* is able to undergo somatic retrotransposition. As little as about 145 in humans, such retrotransposition-competent *L1s* are approximately 3000 in mice, including 900, 400 and 1800 ones belonging to A, Gf and Tf families, respectively (An, 2012; Floreani et al., 2022). Products of their somatic retro-transposition generally lack family-specific 5'UTRs (Singer et al., 2010), while retaining shared orf2 and 3'UTR regions. Clonal analysis robustly demonstrated that somatic retrotransposition takes place within the developing embryo at

Development • Accepted manuscript

different times and in variety of cell types, with special emphasis on the developing CNS (Bodea et al., 2018; Evrony et al., 2015; He et al., 2021; Richardson et al., 2014; Zhu et al., 2021). The magnitude of L1 neo-retrotransposition in the human CNS has been hotly debated, and human neocortical/ hippocampal neurons have been reported to harbor somatic L1 insertions at a frequencies between 0.2 and 80 events per neural cell (Baillie et al., 2011; Coufal et al., 2009; Evrony et al., 2012; Evrony et al., 2016; Upton et al., 2015). An increase in *L1*-DNA content (close to +30%) has been reported in mice as well, in both neocortical and hippocampal neurons, between embryonic day 15.5 (E15.5) and postnatal day 14 (P14) (Fontana et al., 2021).

A substantial fraction of Foxg1 protein is stably bound to chromatin (De Filippis et al., 2012), suggesting it might be implicated in long term gene repression. Next, motif enrichment analysis (MEA) of *L1* consensus sequence by Jaspar software (Mathelier et al., 2016) revealed a high score, putative FOXG1 binding site (RTAAACAW) within *L1-orf2* coding sequence (our unpublished data). Based on this information, we hypothesized that Foxg1 may be implicated in regulation of *L1* transcription. We tested this hypothesis within the murine embryonic neocortex. We showed that Foxg1-dependent *L1* repression mainly occurs in neuronogenic progenitors and post-mitotic neurons, accompanied by specific changes in the epigenetic landscape. Unexpectedly, we also found that Foxg1 positively influences neopallial *L1*-DNA content, counteracting the retrotranscription-suppressing activity exerted by Mov10 and Ddx39a helicases.

RESULTS

In vivo *Foxg1* down-regulation of *L1*-mRNA.

To investigate Foxg1 involvement in regulation of *L1* trascription, we compared *L1*-mRNA levels in the neocortex of P0 *Foxg1*$^{-/+}$ mice (Hébert and McConnell, 2000) (**Fig. S2A**) and wild type controls. As expected, we observed a substantial upregulation of *L1* expression in these mutants. It was detected by the diagnostic "*L1*.orf2" amplicon, common to all *L1* families, as well by the "*L1*.5'UTR.A, .Gf, and .Tf" amplicons (hereafter referred to also as *L1.A*, *L1.Gf* and *L1.Tf*), specific to their respective transposition-competent families (**S1**; **Table S1,** (Sookdeo et al., 2013; Storer et al., 2021). Its amplitude equalled +19.7±1.6% (p<0.014, n=7,7),

Development • Accepted manuscript

+17.2±0.3% (p<0.008, n=7,7), +33.0±0.1% (p<10^{-4}, n=7,7), and +15.8±0.5% (p<0.006, n=7,7), as for *L1.orf2, L1.A*, *L1.Gf* and *L1.Tf*, respectively (**Fig. 1).**

In vitro modeling of *L1-mRNA* progression in murine developing neocortex.

To ease the dissection of Foxg1 control over *L1* expression, we established three protocols, termed "type-I", "-II" and "-III", for the generation of primary neural cultures representing early, mid and late phases of pallial neuronogenesis, respectively (**Fig. 2A**). Characterized by progressively longer durations, such protocols differed for terminal exposure of neural cells to "pure pro-proliferative", "mixed pro-proliferative/pro-differentiative", and "pure pro-differentiative" media, respectively. Neural cells generated by these protocols were classified based on their Sox2/Tubb3 expression profiles (Hutton and Pevny, 2011; Menezes and Luskin, 1994). Type I cultures predominantly comprised $Sox2^{+}Tubb3^{-}$ presumptive neural stem cells (NSCs; 39.3±0.9%; n=3) and $Sox2^{-}Tubb3^{-}$ neuronogenic progenitors (NPs; 30.1±0.7%; n=3), with a limited $Tubb3^{+}$ neuronal output (30.6±1.2%; n=3). The prevalence of these two precursors decreased (to 22.2±1.4% and 16.6±1.1%, respectively; n=3) in Type II cultures, which were characterized by more frequent neurons (Ns; 61.2±2.0%; n=3). As expected, neuronal prevalence further increased in Type III cultures (71.7±1.0%; n=3).

Subsequently, we profiled these cultures for *L1*-mRNA expression levels, by qRT-PCR (**Fig. 2B**). A progressive increase in the expression of the pan-*L1* diagnostic amplicon "*L1.orf2*", was observed moving from "type I" to "type II" and "type III" cultures ("type I" culture-normalized values were: 1.00±0.11, 19.85±2.59, and 21.65±3.27, respectively, with $p_{(\text{type I - vs - type II})}$<$10^{-5}$, $p_{(\text{type II -vs - type III})}$<0.34, n=6,6,6). Similar progressions were also observed in cases of family-specific amplicons, namely *L1.5'UTR.A* ("type I" culture-normalized values: 1.00±0.39, 13.01±1.49, and 49.87±8.57, respectively, with $p_{(\text{type I - vs - type II})}$<$10^{-5}$, $p_{(\text{type II - vs - type III})}$< 10^{-3}, n=6,6,6), *L1.5'UTR.Gf* ("type I" culture-normalized values: 1.00±0.10, 11.16±3.10, and 33.31±7.14, respectively, with $p_{(\text{type I - vs - type II})}$<$10^{-2}$, $p_{(\text{type II - vs - type III})}$< 10^{-2}, n=5,6,6), and *L1.5'UTR.Tf* ("type I" culture-normalized values: 1.00±0.05, 23.41±7.26, and 72.48±11.49, respectively, with $p_{(\text{type I - vs - type II})}$<$10^{-2}$, $p_{(\text{type II - vs - type III})}$< 10^{-2}, n=5,6,5). This scenario points to a generalized upregulation of *L1* expression, associated with neocortical neuronogenesis progression.

To validate the biological plausibility of these results, we repeated this analysis *in vivo*, by comparing *L1* expression in neocortical tissue taken from E14.5 (mid-neuronogenic) and P0

Development • Accepted manuscript

(post-neuronogenic) mice (**Fig. 2C**). [Here, to enhance the robustness of the results, we normalized *L1* qRT-PCR values against a specific "gene quadruplet". This included three RNA-pol II-transcribed genes (*Gapdh*, *Rpl10a* and *Cltc*), characterized by comparable expression profiles in apical precursors (APs), basal progenitors (BPs), early neurons (eNS) and late neurons (lNs) (Telley et al., 2016) (**Table S3A**), as well as by poor sensitivity to *Foxg1* manipulation (Artimagnella and Mallamaci, 2020) (**Table S3B**). Additionally, the quadruplet also included RNA-pol I-transcribed *rDNA-45S*, from which the large majority of cell RNA complement is generated]. As expected, we observed a robust upregulation of *L1*-mRNAs in P0 compared to E14.5 neocortices, as evidenced by the amplicons "*L1.orf2*" (+122.3±47.7%, p<0.004, n=10,7), "*L1.5'UTR.A*" (+140.6±44.0%, p<0.001, n=10,7), "*L1.5'UTR.Gf*" (+149.6±51.4%, p<0.003, n=9,7), and "*L1.5'UTR.Tf*" (+91.0±28.1%, p<0.001, n=10,7). As a specificity control, a similar analysis was performed on the mesencephalic tectum (a CNS district not expressing *Foxg1*), harvested from the same animals. Intriguingly, this revealed an opposite E14.5 →P0 dynamics in *L1*-mRNA levels ("*L1.5'UTR.A*": -20.9±5.1%, p<0.045, n=9,8; "*L1.5'UTR.Gf*": -36.5±4.7%, p<0.013, n=10,8; and "*L1.5'UTR.Tf*" -24.3±5.3%, p<0.051, n=10,8).

Modeling *Foxg1* regulation of *L1*-mRNA.

To dissect Foxg1 control over *L1* transcription, we firstly evaluated *L1*-mRNA levels in "type II", mid-neuronogenic cultures, where *Foxg1* had been constitutively knocked down (**Table S2** and **Fig. S2B**) by CRISPR-Cas9 technology and lentiviral transgenesis (**Fig. 3A**). Consistently with findings in P0 *Foxg1*$^{-/+}$ pups (**Fig. 1**) and upon normalization against the "*Gapdh*, *Rpl10a*, *Cltc* and *rDNA18S* quadruplet", neocortical *Foxg1*-LOF cultures exhibited an increasing trend in *L1*-mRNAs from all three families, which - however - was not statistically significant (**Fig. 3A** and **S4A**).

Next, we examined *L1*-mRNA response to Foxg1 upregulation. To get insights into temporal and intra-neuronogenic lineage progression of Foxg1 modulation of *L1* expression, we run multiple *Foxg1*-OE assays, employing different, early-, mid- and late-neuronogenic, cultures, and driving the *Foxg1* transgene by means of the ubiquitous pPgk1 promoter and the cell-type specific, pNes, pTa1 and pSyn promoters, active in NSCs, NPs/Ns, and Ns, respectively (Brancaccio et al., 2010; Tigani et al., 2020). As a control, we used the *ALPP* gene, encoding

Development • Accepted manuscript

for human Placental alkaline phosphatase, hereafter referred to as *Plap* (Falcone et al., 2016).

Foxg1 overexpression in early-neuronogenic ("type I") cultures, driven by either pNes or pPgk1, resulted in a similar and generalized down-regulation of *L1*-mRNAs. Specifically, in case of pNes-manipulated cultures, L1.orf2, .A, .Gf, and .Tf signals were decreased by 29.1±4.1% ($p<10^{-4}$, n=9,9), 27.3±3.8% ($p<10^{-3}$, n=9,9), 23.2±5.0% (p<0.006, n=9,9), and 22.3±5.5% (p<0.008, n=9,9), respectively (**Fig. 3B**). Similarly, in pPgk1-manipulated cultures, these signals were reduced by 26.8±4.5% (p<0.006, n=6,6), 31.0±6.7% (p<0.004, n=6,6), 38.5±6.3% (p<0.003, n=6,6), and 32.2±5.0% (p<0.002, n=6,6), respectively (**Fig. 3C**).

Conversely, mid-neuronogenic ("type II") *Foxg1*-OE cultures showed different results depending on the promoter driving the *Foxg1* transgene. The most pronounceed *L1* downregulation was observed in *Foxg1*-OE^{pPgk1} cultures, with *L1*.orf2, .A, .Gf, and .Tf signals decreased by 42.9±6.1% (p<0.046, n=6,6), 61.4±4.4% (p<0.001, n=6,6), 68.1±2.9% (p<0.001, n=6,6), and 60.2±5.4% (p<0.003, n=6,6), respectively (**Fig. 3D**). A milder decline in *L1*-mRNA was observed in *Foxg1*-OE^{pTa1} cultures, where L1.A, .Gf, and .Tf signals decreased by 18.1±4.6% (p<0.025, n=7,5), 23.4±3.5% (p<0.004, n=7,5), and 16.1±4.3% (p<0.034, n=7,5), respectively (**Fig. 3E**). *L1*-mRNA levels were mostly unaffected in *Foxg1*-OE^{pSyn} "type II" cultures, except for the *L1*.Gf signal, which was reduced by 10.7±0.8% (p<0.024, n=6,5) (**Fig. 3F**).

Lastly, late-neuronogenic cultures ("type III"), again over-expressing *Foxg1* under the control of the pSyn promoter however over a longer duration, displayed a generalized *L1*-mRNA down-regulation, with L1.orf2, .A, .Gf, and .Tf signals decreased by 19.2±3.8% (p<0.004, n=7,8), 14.3±6.7% (p<0.007, n=7,8), 15.6±7.2% (p<0.003, n=7,8), and 21.3±4.0% (p<0.003, n=7,7), respectively (**Fig. 3G**).

While pointing to a general trend of *Foxg1*-dependent *L1* down-regulation, these results offer valuable insights into temporal and cell-type specific unfolding of this process. In this respect, it is important to distinguish between *late* neuronogenic cultures manipulated by a *pSyn-driven Foxg1* transgene (**Fig. 3G**) and *other cultures* (**Fig. 3B-F**).

In the former case the promoter was active in cells occupying a terminal position along the neuronogenic sequence and the culture was allowed to age sufficiently for robust Foxg1 protein accumulation within the same cell type where the promoter is active. In the light of these considerations, the interpretation of data obtained in *Foxg1*-OE^{pSyn}, "type III" cultures

Development • Accepted manuscript

(**Fig. 3G**) is straightforward, pointing to a consistent *neuronal* inhibition of *L1* elements belonging to all families by Foxg1. Remarkably, this inference was corroborated by the results of supplemental *Foxg1* manipulations, both OE and LOF, performed in pure neuronal cultures fully depleted of glial cells by araC supplementation (**Fig. 4**). In such neocortical neurons, constitutive *Foxg1* overexpression reduced the *L1*.orf2 qRT-PCR signal, by 25.2±8.7% (p<0.046, n=4,4) upon *Gapdh*-normalization (**Fig. 4**, graph (1)), by 33.5±8.7% (p<0.025, n=4,4) upon *Rpl10a*-normalization (**Fig. 4**, graph (2)), whereas constitutive *Foxg1*-knockdown (**Fig. S2C**) increased such signal, by 66.4±21.9% (p<0.016, n=4,4) upon *Rpl10a*-normalization (**Fig. 4**, graph (3).

Conversely, in case of "type I" and "type II" cultures, the promoters driving the *Foxg1* transgene were active in transient precursor types, within relatively short-lived preparations. Consequently, in such cases, Foxg1 protein accumulation could have taken place in a cell type where the promoter is no longer active, or the available time might have been not sufficient to get an appreciable protein upregulation at all. Because of that, *L1*-mRNA dynamics displayed by *Foxg1*-OE, "type I" and "type II" cultures required further clarification. In this respect, to get insights into the actual cell types where Foxg1 upregulation elicited an *L1*-mRNA decline, we (1) quantified the sizes of NSCs, NPs and Ns compartments of differently engineered cultures, (2) profiled each compartment for the distribution of Foxg1 protein cell content, and (3) finally looked for correlative evidences between results of (1,2) analyses and cumulative *L1*-mRNA dynamics specific to the corresponding cultures.

We found that, within early-neuronogenic, "type I", preparations, pNes-driven *Foxg1* elicited a prominent increase of NPs at the expense of NSCs, while keeping Ns to a minimum. Specifically, being f_X the prevalence of X-type cells within the entire cell population, values were: f_{NP}(*Foxg1*-GOF)=39.16±1.14% vs f_{NP}(ctrl)=11.93±2.58% ($p<1.03*10^{-5}$, n=6,5), and f_{NSC}(*Foxg1*-GOF)=57.81±1.53% vs f_{NSC}(ctrl)=84.58±2.81% ($p<2.83*10^{-6}$, n=6,5) (**Fig. 5A** (1)).

Moreover, we found that, within the same preparations, pNes-driven *Foxg1* specifically increased the frequency of both NSCs and NPs expressing Foxg1 at the highest levels (i.e. falling within the first decile), however such effect was far more prominent in case of NPs than in NSCs. Specifically, being ${}^{X}f_{dec1}$ the fraction of X-type cells falling in decile 1, values were: ${}^{NSC}f_{dec1}$(ctrl)=3.4% vs ${}^{NSC}f_{dec1}$(*Foxg1*-GOF)=15.4%, and ${}^{NP}f_{dec1}$(ctrl)=48.5% vs

Development • Accepted manuscript

$^{NP}f_{dec1}$(*Foxg1*-GOF)= 83.3% (**Fig. 5A** (2)). In this way, among cells moving to the first-decile upon *Foxg1* overexpression, (a) >4/5 belonged to the NP compartment and (b) less than 1/5 to the NSC one. [In fact, (a) $\Delta f_{NP*dec1}$ = f_{NP}(*Foxg1*-GOF) * $^{NP}f_{dec1}$(*Foxg1*-GOF) - f_{NP}(ctrl) * $^{NP}f_{dec1}$(ctrl) = 0.392 * 0.832 - 0.119 * 0.485 = 0.268), and (b) $\Delta f_{NSC*dec1}$ = f_{NSC}(*Foxg1*-GOF) * $^{NSC}f_{dec1}$(*Foxg1*-GOF) - f_{NSC}(ctrl) * $^{NSC}f_{dec1}$(ctrl) = 0.578 *0.154 - 0.846 * 0.034 = 0.060].

All that suggests that, within early-neuronogenic, "type I", cultures, the robust *L1*-mRNA downregulation evoked by ^{pNes}*Foxg1*-OE (**Fig. 3B**) mostly occurred in NPs, and NSCs contribution to this phenomenon was marginal, if any (**Fig. 7** (1)).

Next, we performed a similar analysis of mid-neuronogenic, "type II", preparations harboring the pTα1- and pPgk1-driven *Foxg1* transgenes, which exhibited the strongest impact on *L1*-mRNA dynamics (**Fig. 3D-F**). These transgenes altered only marginally culture compartments sizes, both eliciting a moderate shrinkage of the neuronal one (from 66.1±1.9% to 60.0±1.8%, with p<0.03 and n=5,6, as well as 62.0±0.9% to 53.6±1.6%, with p<0.01 and n=3,6, respectively) (**Fig. 5B** (1) and **5C** (1)). Intriguingly, while similarly perturbing neuronal Foxg1 expression levels, they distorted Foxg1 protein distribution in NPs according to different patterns. Specifically, the NP fraction "moving" to the first expression decile upon *Foxg1*-OE increased much more in ^{pPgk1}*Foxg1*-OE cultures (0.244 - 0.080 = 0.164) than in ^{pTα1}*Foxg1*-OE ones (0.122 - 0.058 = 0.064) (**Fig. 5B** (2) and **5C** (2)). Taking into account the stronger *L1* inhibition occurring in ^{pPgk1}*Foxg1*-OE compared to ^{pTα1}*Foxg1*-OE cultures (**Fig. 3DE**), this scenario suggests that down-regulation of *L1*-mRNA detected in *Foxg1*-OE mid-neuronogenic cultures may have primarily occurred in NPs (**Fig. 7** (2)).

In conclusion, results of our *Foxg1*-OE assays point to a negative impact of Foxg1 on *L1*-mRNA expression, both in NPs and Ns (**Fig. 7**), and mirror phenotypes displayed by *Foxg1*-LOF and -OE cultures further suggest that Foxg1 *physiologically tunes* these levels.

Mechanisms underlying Foxg1 control of *L1* transcription.

Foxg1 is mostly recognized to act as a transcriptional repressor (Falcone et al., 2019; Seoane et al., 2004). We wondered whether this also specifically applies to *L1*s. To address this question, we established early ("prot I"-type) neuronogenic cultures, both wild type (*Plap*-OE) and overexpressing Foxg1 (*Foxg1*-OE), and compared Foxg1-enrichment at their *L1* loci against IgG controls, by chromatin immuno-precipitation/quantitative polymerase chain

Development • Accepted manuscript

reaction (ChIP)-qPCR. We found that this enrichment was barely detectable in *Plap*-OE cultures and, conversely, statistically significant at all diagnostic amplicons in *Foxg1*-OE preparations ($p_{5'UTR.A}$<0.014, $p_{5'UTR.Gf}$<0.01, $p_{5'UTR.Tf}$<0.002, p_{orf2}<0.02, $p_{3'UTR}$<0.01, with n=4,4) (**Fig. 6A**). Considering the predominance of NSCs in early ("prot I"-type) *Plap*-OE cultures and their substantial conversion into NPs induced by *Foxg1*-OE (as depicted in **Fig. 5A** (1)), ChIP results shown in **Fig. 6A** may reflect selective Foxg1 recruitment at *L1* loci in NPs, but not in NSCs (**Fig. 7** (1)).

Subsequently, we run similar assays on chromatin prepared from mid-neuronogenic ("prot II"-type) cultures. In this instance, a clear Foxg1-enrichment was detectable at almost all diagnostic amplicons in *Plap*-OE controls ($p_{5'UTR.A}$<0.02, $p_{5'UTR.Gf}$<0.09, $p_{5'UTR.Tf}$<0.04, p_{orf2}<0.02, $p_{3'UTR}$<0.02, with n=5,5 or - case Gf - n=5,4) (**Fig. 6B**). Coupled with the high prevalence of NPs and Ns in all "prot II"-type cultures (as illustrated in **Fig. 5C** (1)), this observation points to Foxg1 binding to *L1* loci in NPs and/or Ns (**Fig. 7**).

In conclusion, both quantification of *L1*-mRNA levels and measure of Foxg1 protein recruitment to *L1* loci, in control and *Foxg1*-OE cultures, suggested us that Foxg1 control over L1 transcription should specifically occur in NPs and Ns. To confirm this inference, we transduced E11.5 neopallial precursors - either made loss-of-function for *Foxg1* or left inaltered - by a pTa1-mCherry transgene, driving selective mCherry expression in committed neuronogenic progenitors and their post-mitotic progenies (Brancaccio et al., 2010). Four days later, we dissociated the resulting neurospheres, sorted single cells based on red fluorescence intensity, and quantified *L1* transcripts in mCherry$^+$ and mCherry$^-$ fractions. It turned out that CRISPR/Cas9-mediated *Foxg1* knock-down did not affect *L1*-mRNA levels in mCherry$^-$ NSCs, while inducing a significant upregulation trend of them in mCherry$^+$ NPs and Ns [+64.29±24.89% (p<0.06), +81.31±26.20% (p<0.02), and +64.99±22.54% (p<0.03), with n=4,4, as for "*L1.5'UTR.A*", "*L1.5'UTR.Gf*", and "*L1.5'UTR.Tf*" amplicons, respectively] (**Fig. 8**). In essence, while significant in NPs and Ns, physiological Foxg1 contribution to *L1* repression is negligible in NSCs, as expected.

Several studies have underscored the significance of various epigenetic marks in tightly regulating L1 transcription (Bulut-Karslioglu et al., 2014; Day et al., 2010; Guler et al., 2017; He et al., 2019; Kim et al., 2014; Muotri et al., 2010; Protasova et al., 2021; Rangasamy, 2013). Additionally, inspection of the public Biogrid database (BioGRID db_FOXG1) revealed that Foxg1 physically interacts with key effectors modulating the epigenetic chromatin

Development • Accepted manuscript

landscape, including Histone deacetylase 2 (HDAC2), Lysine-specific demethylase 5B (KDM5B), Lysine-specific demethylase 1A (KDM1A). Thus, Foxg1 might influence *L1*-mRNA levels by modulating the epigenetic state of *L1* chromatin.

To explore this, we evaluated chromatin extracted from mid-neuronogenic cultures, *wild type* and *Foxg1*-OE, for its enrichment at *L1* loci for a number of key epigenetic markers: H3K4me3, H3K9me3, H3K27ac, and MeCP2 (**Fig. 8A,B**). We observed a remarkable enrichment for H3K4me3, H3K9me3, H3K27ac at all diagnostic amplicons analyzed, *L1*.5'UTR.A, .Gf, .Tf, .orf2 and.3'UTR, irrespective of culture genotype (about 60-1200-folds over IgG controls). Conversely, enrichment for MeCP2 over these controls was barely appreciable (<2-folds). Furthermore, enrichment for H3K4me3 showed a decreasing trend in *Foxg1*-OE compared to *Plap*-OE cultures ($p_{5'UTR.A}$<0.021, $p_{5'UTR.Gf}$<0.106, $p_{5'UTR.Tf}$<0.141, p_{orf2}<0.069, $p_{3'UTR}$<0.045, with *n*=4,3 and - in case of orf2 - n=3,3). Conversely, an opposite trend was evident for H3K9me3 ($p_{5'UTR.A}$<0.072, $p_{5'UTR.Gf}$<0.006, $p_{5'UTR.Tf}$<0.062, p_{orf2}<0.021, $p_{3'UTR}$<0.028, with *n*=5,5 and - in case of Tf - n=4,4)(**Fig. 8C**).

Overall, these results support the hypothesis that Foxg1-mediated modulation of *L1* transcription involves pervasive changes in the epigenetic state of these elements, namely a decrease in transcription-promoting H3K4me3 marks and an increase in heterochomatic H3K9me3 marks. Additionally, the high levels of H3K27ac observed in both controls and *Foxg1*-OE samples suggest a transient bivalent state of chromatin, capable of both silencing and transcription (He et al., 2019), while the low MeCP2 enrichment at mid-neuronogenic stages likely reflects relatively low expression of this protein (Diez-Roux et al., 2011).

Lastly, to further elucidate the mechanisms mediating Foxg1 impact on *L1* transcription, we took advantage of the neuropathogenic $FOXG1^{W308X}$ allele (Frisari et al., 2022), encoding for a prematurely truncated protein, lacking the binding domains for the Groucho/Tle co-repressor and the *KDM5B*-encoded JARID1B H3K4me2/3-demethylase (**Fig. 10**). Delivered to neuron-enriched cultures as a Tet^{ON}-driven transgene, $FOXG1^{W308X}$ led to a reduction of *L1*-mRNA levels, less pronounced compared to $FOXG1^{WT}$, -19.93±9.85% vs -43.94±10.39% (*n*=4,4), -18.47±5.27% vs -45.01±8.83% (*p*<0.021; *n*=4,4), -21.11±4.72 % vs -40.03±6.37% (*p*<0.038; *n*=4,4), and -31.94±6.24% vs -47.37±9.15% (*n*=4,4), as evaluated at diagnostic amplicons "orf2", "5'UTR.A" ", "5'UTR.Gf", and "5'UTR.Tf", respectively (**Fig. 10**). A consistent pattern emerged from comparisons of earlier, "mid-neuronogenic" cultures,

Development • Accepted manuscript

alternatively overexpressing the two FOXG1 alleles (**Fig. S3 and 3D**), suggesting that JARID1B and/or Groucho/Tle contribute to *Foxg1*-dependent *L1* repression.

Temporal progression of pallial *L1* DNA copy-number.

We wondered if, in addition to inhibiting *L1* transcription of *L1* elements, Foxg1 might further impact their DNA copy number. To get preliminary information about natural dynamics of *L1* DNA within the developing embryonic pallium, we scored early-, mid- and late-neuronogenic cultures for their cumulative *L1* copy number (**Fig. 11A**). For this purpose, we relied on the diagnostic 3'UTR amplicon (**Fig. S1**, **Table S1**), present in all *L1* repeats, including the prevailingly 5' truncated elements originating from somatic retrotransposition (Babushok et al., 2006). We found *L1* copy number did not change across early- and mid-neuronogenic cultures, whereas it was increased by 35.08±3.65% (p<0.001, n=5.7) in late-neuronogenic ones (**Fig. 11B**, (1)).

Actually, these results were obtained on DNA prepared by a dedicated, sample digestion procedure ("high PK"), aimed at extracting DNA with comparable efficacy regardless of the compaction state of chromatin. [Fulfillment of this requirement had been previously tested, by quantifying an X-chromosomal (*lyonizable*) *Mecp2* amplicon in DNA extracted from female and male tissues, and normalizing it against an autosomal amplicon (*Gfap)*. This gave a normalized, female-to-male *Mecp2* signal ratio, equalling 1.54±0.18, with $p_{♂-♀}$<0.053, n=3,2 (**Fig. S5**(1))]. To strenghten **Fig. 11B**, (1) results, we repeated the quantification of pallial *L1* content upon replacing the "high PK" protocol with a further improved version of it ("very high PK"). [With this latter protocol the female-to-male *Mecp2* signal ratio arose to 2.25±0.45 ($p_{♂-♀}$<0.016, n=3,2) and a similar 2.22±0.10 ratio was also obtained for an alternative X-chromosomal gene, *Cdkl5* ($p_{♂-♀}$<0.001, n=3,3) (**Fig. S5**(2,3)]. Moreover, as a control, we included in this last assay late-neuronogenic cultures pre-treated by chronic lamivudine, an established inhibitor of retro-transcription. "Very high PK" samples substantially replicated the outcome of "high PK" ones, with *L1* copy number increased in late-neuronogenic cultures by 1.31±0.16-folds compared to their mid-neuronogenic counterparts (p<0.04, n=8,8). Remarkably, this increase was fully suppressed by lamivudine (**Fig. 11B** (2)).

Development • Accepted manuscript

As mentioned above, assays referred to in **Fig. 11B** (1,2) were based on the "3'UTR" diagnostic amplicon. As a further control, we also quantified *L1*-DNA in mid- and late neuronogenic cultures by means of family-specific 5'UTR amplicons (**Fig. S1**, **Table S1**). As expected, no relevant changes were found (**Fig. 11B** (3,4,5), except an increasing trend in "5'UTR.A" **(Fig. 11B**(3)), possibly reflecting differential somatic RT failure in distinct *L1* families.

Finally, to validate the dynamics of *L1*-DNA observed in mid- vs late-neuronogenic cultures, we compared *L1*-DNA content in neocortices dissected from E14.5 vs P0 wild-type mice. As expected, the latter exceeded the former, by 23.8±4.7% ($p<0.0060$; n=8,7) (**Fig. 12**), corroborating our previous findings. Intriguingly, an increase of *L1*-DNA content over the same time interval was also detectable in the mesencephalic tectum, where its amplitude was even larger (+54.0±8.1%, with $p<0.0004$ and n=6,9) (**Fig. 12**).

Foxg1 impact on *L1*.DNA copy numbers

We have shown that *L1* copy number increases during neocortical neuronogenesis progression. To further investigate the role (if any) of *Foxg1* in this process, we compared *L1* DNA content in neocortices of *Foxg1*$^{-/+}$ neonates and their littermate wild type controls. When normalized against *Gfap* and *Nfia,* such content turned out to be decreased in *Foxg1*-LOF samples by 7.50±0.85% ($p<10^{-3}$, n=6,8), compared to controls (**Fig. 13**). To note, this variation accounts for approximately one third of the increment in neocortical *L1* copies detectable over the same time interval in wild type mice (**Fig. 12**). Moreover, this decrease occurred in mutants characterized by *Foxg1*-mRNA levels reduced by only 33.59±6.17% ($p<0.02$, n=8,7) compared to wild-type controls (**Table S2**).

To corroborate these findings, we repeated the evaluation of *L1* copy number in primary, late-neuronogenic cultures manipulated by CRISPR-Cas9 technology, which allowed us to achieve a more pronounced *Foxg1* down-regulation, by 65.37±2.68% ($p<10^{-7}$, n=8,8), (**Table S2**). Remarkably, in this case, *L1* copy number was reduced by 15.23±2.19% (upon normalization against *Gfap* and *Nfia*, with $p<10^{-3}$, n=8,8) (**Fig. 14B**(1)), corresponding to about two thirds of the "physiological" increment mentioned above (**Fig. 12**).

To achieve a more comprehensive understanding of Foxg1 role in tuning *L1* copy number, we overexpressed it in late-neuronogenic cultures, under the control of pTa1 and pPgk1 promoters, and evaluated the impact of these manipulations on *L1* DNA content. As

Development • Accepted manuscript

expected, we found that *L1*-DNA content was increased by "pTa1-driven *Foxg1",* by 37.11±16.35%, with $p<0.03$, and $n=9,9$ (**Fig. 14B**(4)). Conversely, no *L1*-DNA increase was elicited by "pPgk1-driven *Foxg1"* (**Fig. 14B**(3)), possibly due to the stronger *L1*-mRNA downregulation triggered by such transgene compared to its pTa1 counterpart (**Fig. 3D,E**). These results collectively indicate that Foxg1 plays a crucial role in *L1*-DNA amplification and its *fine physiological tuning*. To note, such amplification-promoting activity must be particularly robust, as it emerged despite the concurrent, *Foxg1*-induced down-regulation of *L1*-mRNA, namely the *template* from which new *L1* DNA is generated.

Mechanisms underlying Foxg1 impact on *L1* copy number

We wondered: how does Foxg1 impact *L1* DNA content? We considered two possible scenarios: (1) it acts indirectly, as a "professional transcription factor" modulating the transcription of genes encoding for key effectors involved in synthesis and/or degradation of new somatic *L1* copies; (2) it straightly regulates these processes, through physical interaction with factors implicated in them and/or with *L1*-mRNA.

As for (1), we inspected a database of genes mis-regulated upon Foxg1 overepression in neocortical neuronal cultures (Artimagnella and Mallamaci, 2020). We found that mRNA encoding for Apobec1, an inhibitor of *L1* retro-transposition (Ikeda et al., 2011), is halved in *Foxg1*-OE samples (**Table S4A**), which suggests Foxg1 might promote retro-transposition, by mitigating such inhibition.

As for (2), we interrogated the public Biogrid database for Foxg1 interactors implicated in retro-transposition control and found two well known antagonizers of *L1* retro-transposition, Mov10 and Ddx39a (Goodier et al., 2012)(**Table S4B**). We co-manipulated expression levels of each of them alongside *Foxg1* in late-neuronogenic cell preparations, and evaluated the impact of such manipulations on *L1*-DNA content (**Fig. 15A**). Intriguingy, in a sensitized *Foxg1*-lof environment, "wild-type" levels of both *Mov10* and *Ddx39a* led to statistically significant decreases in *L1*-DNA copy number compared to their knock-down counterparts [-16±3% with $p<0.035$ $n=7$, as well as -18±3% with $p<0.018$, and $n=6$, respectively]. Conversely, in a *Foxg1*-wt environment, a decrease was only detectable in *Ddx39a* "wild type" compared to *Ddx39a* knock-down samples [-15±3%, with $p<0.015$, and n=10]. Notably, two-ways ANOVA analysis of results indicated *statistical* interaction among

Development • Accepted manuscript

Foxg1 and both *Mov10* (p<0.026) and *Ddx39a* (p<0.058) variables (**Fig. 15B**), pointing to a likely *functional* interaction among Foxg1 and the helicases encoded by these two genes. Furthermore, we reasoned that Foxg1 could counteract Mov10 and Ddx39a, by preventing them from interacting with *L1*-mRNA. This might be achieved by chelating the helicase in order and/or shielding its *L1*-RNA interactor. While the former phenomenon has been previously documented (Li et al., 2015), to assess the latter, we run a set of RNA-immunoprecipitation (RIP) assays, by which we quantified "5'UTR", "orf2" and "3'UTR" *L1* diagnostic amplicons in anti-Foxg1-immunoprecipitated RNA (**Fig. 16**). Consistent with our prediction, we found a robust enrichment of Foxg1 at both 5' and 3' ends of L1-mRNA. Normalized agaist IgG controls, this enrichment was 3.11±0.20 folds at "L1.5'UTR.A" (p<10^{-4}, n=5,3), 1.85±0.28 folds at "L1.5'UTR.Gf" (p<0.043, n=5,3), 4.13±0.51 folds at "L1.5'UTR.Tf" (p<0.003, n=5,3), and 3.89±0.55 folds at "L1.3'UTR" (p<0.004, n=5,3) (**Fig. 16** (1,2,3,5)). Foxg1 enrichment was lower at "L1.orf2", where statistical significance was not reached (**Fig. 16** (4)).

DISCUSSION

Foxg1 plays a central role in telencephalic development, exerting a highly pleiotropic control over it. *L1* is a prominent retrotransposon family modulating progression of neocortical histogenesis and contributing to plasticity of neuronal genomic DNA. In this study, we systematically investigated the impact of the former on the biology of the latter within the developing murine neocortex. Main results were as follows.

As suspected, we found that *L1*-mRNA encoded by all three retro-transposition-competent families (A, Gf and Tf) was increased in *Foxg1*-LOF mouse neonates compared to wild type controls (**Fig. 1**). To model *Foxg1*-dependent *L1* regulation across neuronogenic progression, firstly, we developed an integrated culture-set, representing early-, mid- and late-phases of neuronogenesis in vitro. This set exhibited a progressive increase in *L1*-mRNA expression, paralleling in vivo *L1*-mRNA dynamics (**Fig. 2**). Then, we manipulated Foxg1 levels at different stages of the neuronogenic progression, both up and down, via multiple approaches, taking advantage of distinctive neural cell type-specific promoters (**Fig. 3,4**). We evaluated the impact of these manipulations on the sizes of NSCs, NPs and Ns compartments, and we mapped changes of Foxg1 protein levels to these compartments

Development • Accepted manuscript

(**Fig. 5**). Additionally, we profiled Foxg1 binding to *L1* chromatine at different steps of neuronogenic progression (**Fig. 6**). Integrated analysis of these results provided us robust evidence that Foxg1 represses *L1* expression selectively in NPs and Ns (**Fig. 7**). This repression was confirmed by quantifying *L1*-mRNA in NSCs and NPs+Ns fractions, FACsorted from *Foxg1*-LOF preparations (**Fig. 8**). As expected, we found that such repression was associated with reduced H3K4me3 and increased H3K9me3 marks along the entire retrotransposon (**Fig. 9**). Furthermore, a prematurely truncated, human neuropathogenic, loss-of-function variant of FOXG1 downregulated *L1*-mRNA too, although to a lesser extent than its "healthy" counterpart (**Fig. 10 and S3**).

Before investigating the potential impact of *Foxg1* on *L1*-DNA copy number, we profiled the progression of this number in early-, mid- and late-neuronogenic cultures, and we found that it increased by approximately 35% in late ones, in a retro-transcription-dependent way (**Fig. 11**). A similar increase was observed in vivo as well, in neonatal compared to mid-neuronogenic embryonic neocortex, suggesting the former phenomenon to be genuine (**Fig. 12**). Then, unexpectedly, we discovered that Foxg1 down-regulation, both in vivo and in vitro, resulted in a remarkable, Foxg1-dose-dependent reduction in *L1*-DNA content, up to two thirds of the natural increase observed in vivo. Consistently, mild Foxg1 overexpression in mid-neuronogenic cultures increased *L1*-DNA, further suggesting that Foxg1 *tunes* physiological amplification of this DNA (**Fig. 13,14**). We hypothesized that Foxg1 intervention in *L1* retrotranscription might involve two helicases, Mov10 and Ddx39a, known to antagonize retrotransposition and physically interact with Foxg1 protein. Interestingly, Foxg1 desensitized neocortical neurons to the activity of these helicases, resulting in increased *L1*-DNA copy number (**Fig. 15**). Finally, we found that Foxg1 binds to *L1*-mRNA, particularly at its 5' and 3' ends (**Fig. 16**).

As a general methodological note, the interpretation of results originating from gene overexpression-assays requires a special caution, because of paradoxical dominant-negative effects, potentially evoked by gene product over-abundance. In this respect, it is worthy mentioning that in our OE assays *Foxg1* expression gains usually fell below 5x, at both mRNA and protein levels (**Table S2, and Fig. S2**). More importantly, phenotypes evoked by Foxg1 overexpression generally mirrored those elicited by gene knock-down (see, for example, **Fig. 3A** vs **Fig. 3B-G**, or **Fig. 4(2)** vs **Fig. 4(3)**), suggesting that they provide a qualitatively genuine representation of the physiological functions played by Foxg1 in natural contexts.

Development • Accepted manuscript

Concerning the scientific outcome of our study, two main messages emerged from it: (1) we demonstrated that *L1*-mRNA levels progressively increase as neopallial neurono-genesis goes on, and Foxg1 limits this increase (**Fig. 3,4**). Noticeably, Foxg1 control of *L1*-mRNA applies to all three retrotransposition-competent L1 families (**Fig. 1,3**) and it is achieved by direct Foxg1 binding to *L1* chromatin (**Fig. 6**), triggering a prominent change in its epigenetic state (**Fig. 9**).

(2) we documented a natural upregulation of pallial *L1*-DNA content occurring during late-intrauterine development, and discovered that, albeit associated to an opposite *L1*-mRNA dynamics (**Fig. 3**), moderate fluctuations of Foxg1 levels around the baseline generally result in colinear variations in such *L1*-DNA content (**Fig. 13,14** (1,2,4)).

Actually, the increasing progression of *L1*-mRNA levels we documented in the murine neopallial neuronogenic lineage is not novel. Indeed, it recalls similar phenomena previously reported to take place in human embryonic neocortex (Garza et al., 2023) and adult hippocampus (Muotri et al., 2010). Conversely, novel is the impact exerted by Foxg1 on *L1*-mRNA expression. Thus, Foxg1 adds to the small transcription factor set known to control *L1* transcription in the CNS (Blaudin De Thé et al., 2018; Kuwabara et al., 2009; Liu et al., 2019; Muotri et al., 2005; Nandi et al., 2016; Sanchez-Luque et al., 2019). In this context, it recalls Sox2. However, Sox2 was documented to repress *L1* transcription in adult NSCs (Kuwabara et al., 2009), while Foxg1 has been shown to act in embryonic neuronal progenitors and neurons (**Fig. 7 and 8**). Moreover, Sox2 is expressed in the apical compartment of the entire neuraxis (Pevny and Lovell-Badge, 1997), Foxg1 is mainly confined to the telencephalon (Tao and Lai, 1992). Notably, to our knowledge, Foxg1 is the first patterning gene proven to limit *L1* expression within a specific domain of the developing mouse brain (Blaudin De Thé et al., 2018; Kuwabara et al., 2009).

Moreover, even the increase of *L1*-DNA content we documented in the developing mouse neocortex is not novel. Indeed, it is qualitatively and metrically consistent with results of a previous study, run in the perinatal rodent brain (Fontana et al., 2021). Conversely, novel is the impact exerted by Foxg1 on *L1*-DNA copy number. In this respect, we hypothesized that *Foxg1* control of *L1*-DNA content could take place via two helicases, Mov10 and Ddx39a, reported to antagonize *L1* retro-transcription (Goodier et al., 2012) and physically interact with Foxg1 protein (Li et al., 2015). We ruled out transcription as a mediator of this mechanism. In fact, while resulting in *Mov10*- and *Ddx39a*-mRNA

Development • Accepted manuscript

downregulation, by -45.3% and -17.6%, respectively, with padj<0.05 (Artimagnella and Mallamaci, unpublished data), *Foxg1* knock-down did not increase *L1*-DNA content, but rather *reduced* it. Conversely, we noticed that *Foxg1* knock-down made the decline of *L1*-DNA evoked by higher levels of *Mov10* and *Ddx39a* more pronounced (**Fig. 15**). In addition, we showed that Foxg1 protein normally binds to *L1*-mRNA (**Fig. 16**). Hence, we propose that Foxg1 may ease *L1*-mRNA retro-transcription largely by preventing the interaction among the two helicases and such mRNA (Goodier et al., 2012), competitively or due to steric hindrance. Such involvement in retrotranscription control adds to Foxg1 implication in other non-transcriptional metabolic routines, such as post-transcriptional ncRNA processing (Weise et al., 2019), translation (Artimagnella et al., 2022) and mitochondrial biology (Pancrazi et al., 2015).

Such bimodal Foxg1 impact on *L1* biology is remarkable. Mechanistically, it is tempting to speculate the the transient down-regulation *Foxg1* physiologically undergoes in newborn pyramids (Miyoshi and Fishell, 2012) may be instrumental in allowing sufficient accumulation of *L1*-mRNA needed for subsequent robust retro-transcription. From a broader perspective, it has been shown/suggested that different products of L1 activity (RNA, orf1/2 proteins, DNA) have been evolutionarily highjacked for distinctive aspects of cell physiology and metabolism (Blaudin De Thé et al., 2018; Chow et al., 2010; Madabhushi et al., 2015; Mangoni et al., 2023; Muotri and Gage, 2006), so likely requiring differential tuning of their dosages. Thanks to its bimodal impact on L1 transcription and retrotranscription, Foxg1 might contribute to such complex regulation. To note, the relationship between *L1*-mRNA and and *L1*-DNA levels apparently depends on the CNS structure in order. Differently from neocortex, a huge amplification of *L1*-DNA content is achieved within the late-gestational tectum, despite the concomitant down-regulation of the "underlying" *L1*-mRNA level (**Fig. 2,12**). This might reflect an intrinsically different regulation of L1 biology in telencephalon vs mesencephalon and/or a developmental heterochrony between these two structures.

Actually, at the moment, we ignore the functional meaning of *Foxg1* control over *L1* biology. Concerning Foxg1-dependent modulation of *L1*-mRNA levels, two considerations may help addressing this issue. On one side, *Foxg1* exerts a multifaceted impact on neocortical histogenesis, (1) stimulating the NSC-to-NP transition ((Falcone et al., 2019) **Fig. 5A**(1)), (2) inhibiting NPs exit from cell cycle (Brancaccio et al., 2010), (3) promoting

Development • Accepted manuscript

postmitotic neuronal differentiation (Chiola et al., 2019; Frisari et al., 2022; Tigani et al., 2020; Yu et al., 2019; Zhu et al., 2019) and migration (Miyoshi and Fishell, 2012), and (4) antagonizing gliogenesis (Brancaccio et al., 2010; Falcone et al., 2019; Frisari et al., 2022). On the other side, it has been shown that specific ensembles of transposable elements are transcribed concomitantly with the progression of certain early histogenetic routines (He et al., 2021). In some cases, such transcription has been proven to be necessary for the advancement of these routines (Jachowicz et al., 2017; Macfarlan et al., 2012; Percharde et al., 2018). It is tempting to speculate this might apply to cortical histogenesis as well. In this respect, shortly after the submission of this manuscript, Mangoni et al reported an in depth dissection of the complex phenotype originating by *L1*-mRNA knock-down in the developing neocortex (Mangoni et al., 2023). In this study, *L1*-mRNA was dampened via RNAi, by an order of magnitude comparable with that we elicited via *Foxg1*-OE (**Fig. 3D**). Intriguingly, this resulted in a variety of histogenetic anomalies, some of which (such as increased NSC progression to neuronogenesis, impaired neuronal radial migration, and decreased astrogenesis) were highly reminiscent of the developmental phenotype evoked by *Foxg1*-OE (**Fig. 5A** (1), (Falcone et al., 2019; Miyoshi and Fishell, 2012)). This suggests that *L1* response to *Foxg1* may contribute to *Foxg1* regulation of these processes.

Then, concerning Foxg1 impact on *L1*-DNA copy number, it has been proposed that somatic retrotransposition may help diversifying neuronal genome and, therefore, neuronal functional properties (Muotri and Gage, 2006; Singer et al., 2010). By upregulating *L1*-DNA copy number, Foxg1 might enhance this phenomenon.

Finally, beyond its physiological occurrence in the developing rodent embryo, the relationship between *FOXG1* and *L1* elements could be relevant to the etiopathogenesis of the human *FOXG1* syndrome. Deficient FOXG1 activity linked to *FOXG1* hemizygosity or heterozygosity for LOF-alleles might lead to *L1*-mRNA upregulation, while supernumerary or GOF *FOXG1* alleles might result in exaggerated *L1*-DNA neo-synthesis. Both scenarios are of potential neuropathogenic interest (Suarez et al., 2018), and an early patient treatment with FDA-approved inhibitors of retrotranscription (New drugs for HIV infection, 1996) might mitigate consequences of *FOXG1*-GOF mutations. However, major differences characterize cortical histogenesis and *L1* biology in humans and rodents (Pinson and Huttner, 2021; Rosser and An, 2012). For these reasons, these issues deserve further in depth investigations.

Development • Accepted manuscript

MATERIALS AND METHODS

Animal handling

Animal handling and subsequent procedures were in accordance with European and Italian laws [European Parliament and Council Directive of 22 September 2010 (2010/63/EU); Italian Government Decree of 4 March 2014, n° 26]. Experimental protocols were approved by SISSA OpBA (Institutional SISSA Committee for Animal Care).

Embryos and animals were generated at the SISSA mouse facility, as follows:

- wild-type ones were generated by breeding CD1 parents, purchased from Envigo Laboratories, Italy;
- *Foxg1*$^{+/-}$ ones (and their wild type controls) were generated by breeding CD1-backcrossed, *Foxg1*$^{+/-}$ males (Hébert and McConnell, 2000) to wild type CD1 females
- *Rosa26*$^{pCAG\text{-}Cas9\text{-}2P2\text{-}Egfp)/+}$ ones were generated by breeding *Rosa26*$^{pCAG\text{-}Cas9\text{-}2P2\text{-}Egfp)/+}$ males [originating from a line obtained by intercrossing a R*osa26*$^{(pCAG\text{-}flSTOP\text{-}Cas9\text{-}2P2\text{-}Egfp)/+}$ founder (Platt et al., 2014) to constitutive cre-expressors (Tang et al., 2002), and kept on a C57Bl/6 background] to wild type CD1 females.

Animals were staged by timed breeding and vaginal plug inspection. Where due, pregnant females were sacrificed by cervical dislocation.

As for genotyping:

- *Rosa26*$^{pCAG\text{-}Cas9\text{-}2P2\text{-}Egfp)/+}$ embryos were distinguished from their wild type littermates by inspection under fluorescence microscope
- *Foxg1*$^{+/-}$ embryos were distinguished from their wild type littermates by PCR genotyping, as previously described (Muzio and Mallamaci, 2005).

Molecular sexing was performed by a dedicated procedure, run in parallel with the microdissection of neural tissue of interest. For this purpose, a skin fragment from each embryo was collected and DNA extracted from it was used for fast, PCR-based genotyping. Males were distinguished by an oligo pair specifically amplifying the Y-chromosome-located *Uty* gene (see **Table 1**).

In general, extraction of genomic DNA employed for genotyping and preparation of the PCR reaction mix were performed by a KAPA HotStart Mouse Genotyping Kit Roche (KK7351), according to Manufacturer's instructions.

Development • Accepted manuscript

Primary neocortical cultures: early-, mid-, and late-neuronogenic ones

E11.5 - E12,5 mouse neocortical primordia were dissected and mechanically dissociated to single cells by gentle pipetting. Dissociated cells were quantified in a Burker chamber and then plated in 24-multiwell plates (Falcon) at 100 - 300 cells/uL, in pro-proliferative medium (1:1 DMEM-F12, 1X Glutamax (Gibco), 1X N2 supplement (Invitrogen), 1mg/ml BSA, 0.6% Glucose, 2 µg/ml mouse heparin (Stemcell technologies), 1X Pen/strept (Gibco), 10µg/ml Fungizone (Gibco), 20 ng/ml bFGF (invitrogen), 20 ng/mL EGF (Invitrogen). If required, neural cells were transduced with a LV mix, each LV at a multeplicity of infection (m.o.i.) ≥8, sufficient to infect almost the totality of neural cells in these conditions (Brancaccio et al., 2010). Neural cells were subsequently cultured according to three different schedules, aiming to model early, mid and late phases of neuronogenic progression:

(1) Protocol I (Prot-I), early-neurogenic cultures Already plated in pro-proliferative medium (see above) at 300 cells/µL, cells were kept in such medium up to day in vitro 1-3 (DIV1-DIV3), and then processed for analysis.

(2) Protocol II (Prot-II), mid-neuronogenic cultures 20 hours after plating cells in pro-proliferative medium (see above) at 300 cells/µL, their medium was further supplemented with 5% FBS. Cells were kept in the resulting medium up to DIV3, and then processed for analysis.

(3) Protocol III (Prot-III), late-neuronogenic cultures 20 hours after plating cells in pro-proliferative medium (see above) at a 100 cells/µL, their medium was further supplemented with 5% FBS, and - next - daily hemi-replaced by "1:1 DMEM-F12, 1X Glutamax (Gibco), 1X N2 supplement (Invitrogen), 1mg/ml BSA, 0.6% Glucose, 2 µg/ml mouse heparin (Stemcell technologies), 1X Pen/strept (Gibco), 10µg/ml Fungizone (Gibco), 5% FBS (Gibco)", up to DIV9, when cells were processed for analysis. When due, medium was further supplemented from DIV4 to DIV9 by 10 µM Lamivudine (L1295-10MG, Sigma Aldrich), assuming a conventional 3 days drug halflife.

In general, lentiviral transgenes were activated at day in vivo 0 (DIV0, i.e. the dissection day) by 2µg/mL doxycyclin (Sigma #D9891-10G) medium supplementation, and kept on by further doxycyclin supplementation, performed assuming a conventional 2 days drug halflife.

Development • Accepted manuscript

Primary neocortical cultures: neuron-enriched ones

Cortical tissue from E16.5 mice was chopped to small pieces for 5 min, in the smallest volume of ice-cold "1X PBS - 0,6% D-glucose - 5mg/ml DNaseI (Roche #10104159001)". After enzymatic digestion in "2.5X trypsin (Gibco #15400054) - 2mg/ml DNaseI" for 5 min, and its inhibition with "DMEM-glutaMAX (Gibco) – 10% FBS (Euroclone) - 1X Pen-Strep", cells were spun down and transferred to differentiative medium [Neurobasal-A, 1X Glutamax (Gibco), 1X B27 supplement (Invitrogen), 25µM L-glutamate (Sigma), 25µM β-Mercaptoethanol (Gibco), 2% FBS, 1X Pen/Strept (Gibco), 10µg/ml fungizone (Gibco)]. Cells were counted and plated onto 0.1mg/ml poly-L-Lysine (Sigma #P2636) pre-treated 12-multiwell plates (Falcon), $8x10^5$ cells per well in 0.6-0.8 ml differentiative medium. 10µM Cytosine β-D-arabinofuranoside (AraC; Sigma #C6645) was added to the medium at DIV1. Cells were kept in culture 8 days.

When required, lentiviral culture transduction was performed at DIV1, and TetON-regulated transgenes were activated, generally by 2µg/ml doxycyclin (Sigma #D9891-10G) medium supplementation at DIV4. Limited to **Fig. 10**, doxycyclin was employed at 200ng/ml, starting from DIV2.

Lentiviral vectors

Third generation self-inactivating (SIN) lentiviral vectors (LVs) were generated as previously described (Follenzi and Naldini, 2002) with minor modifications. Resuspended in "DMEM glutaMAX - 10x FBS - 1x Pen/Strep" HEK293T cells were plated on 10cmØ plates, $8*10^6$ cells/plate. Three days later, they were co-transfected with the transfer vector plasmid plus three auxiliary plasmids (pMD2-VSV.G; pMDLg/pRRE; pRSV-REV), in the presence of LipoD293™ (SigmaGen #SL100668). The conditioned medium was collected 24 and 48 hours after transfection, filtered and ultracentrifuged at 50.000 g on a fixed angle rotor (JA25.50 Beckmann Coulter) for 150 min at 4°C. Lentiviral pellets were then resuspended in (BSA-free) 1X PBS (Gibco). LVs were titrated by Real Time quantitative PCR after infection of HEK293T cells, as previously reported (Sastry et al., 2002). One end point fluorescence titrated LV was included in each PCR titration session and PCR-titers were adjusted to fluorescence-equivalent titers throughout the study.

The full list of LVs employed for this study is reported in **Table 2**. Performances of *Foxg1*-modulating LV transgenes were monitored by qRT-PCR. Results are summarized in **Table S2**.

Development • Accepted manuscript

Fluorescence activated cell sorting (FACS).

Acute preparations of early, proliferating neocortical precursors were transduced by lentiviral mixes including LV_pTα1-mCherry, expressing the corresponding red fluoroprotein in committed neuronogenic progenitors and their postmitotic progenies. Four days later, the resulting neurospheres were treated by 1x Trypsin at 37°C for 2 min, transferred to 10%FBS-containing medium for trypsin inactivation, and dissociated by gentle pipetting. Neural cells were pooled, spun at 200 g, and resuspended at $1*10^6$ cells/ml, in a dedicated flow cytometry buffer (a phenol red-free medium including 1X PBS, 25mM HEPES, and 2% FBS). Cell suspensions were filtered by a 70μm strainer (pluriSelect #43-10070-70), and transferred to flow cytometer tubes (pluriSelect #05-03040-01). Cells were profiled by a Biorad S3 Cell cytofluorimeter. First, forward scatter (FSC) and side scatter (SSC) parameters were used to exclude debris and cell aggregates. Next, analytical gates R3-R4, were set, for alternative $mCherry^{+/-}$ categorizations. $mCherry^-$ and $mCherry^+$ preparations (highly enriched in NSCs and "NPs + Ns", respectively) were collected and employed for subsequent RNA profiling.

Genomic DNA isolation and qPCR amplicon quantitation

DNA was isolated from neocortical tissue as well as from primary pallial cultures. Neocortices from E14.5 embryos and P0 pups were microdissected, cut into small pieces for <5 min in the smallest volume of ice-cold 1X PBS - 0.6% glucose, and kept on ice. Minced neural tissue was further dissociated to single cells by 2X trypsin at 37^OC for 5 min, followed by gentle pipetting and enzyme inactivation by FBS. On the other side, primary cell cultures were straightly treated by 0.3X trypsin at 37^OC for 5 min, again followed by gentle pipetting and enzyme inactivation by FBS. Next, in both cases, cells were counted in a Burker-chamber, split into aliquots of 10^6 cells each, pelletted for 5 min at 200g, and stored at -80°C for subsequent use.

Single cell aliquots were processed by the “FlexiGene DNA Kit; Qiagen”, according to Manufacturer's instructions, with the following modifications:

1) PK was employed at 0.6mg/mL (high PK) and 1.2 mg/mL (very high PK);

2) PK sample incubation was extended to 6 hrs;

3) following precipitation, the DNA pellet was washed three times by 70% ethanol.

Development • Accepted manuscript

Finally, DNA was resuspended in water and quantified by DS-11spectrophotometer (DeNovix).

Quantification of genomic amplicons (*L1* elements and X-chromosome genes) was performed starting from 10ng DNA per each reaction, by means of the SsoAdvanced SYBR Green SupermixT“platform (Biorad), according to Manufacturer's instructions. PCRs were run on a BioRad CFX96TM Thermal Cycler. Primer sequences and thermal reaction profiles are reported in **Table 1**. Each amplicon was qPCR-analyzed in technical triplicate, and results averaged. Averages were normalized against levels of selected autosomal amplicons, as reported in Figures (depending on cases, the level of a single reference gene or the geometrical average of >1 of them were employed). As specified in Legends to Figures, biological replicates were DNA preparations originating (1) from different embryo/neonate individuals or (2) individually transduced and cultured cell aliquots, taken from pooled neural cells preparations.

Validation of family-specific, diagnostic mL1 primers.

Genomic DNA extracted from P0 wild type neocortices was employed as substrate to obtain mL1 amplicons. PCRs were primed by family-specific oligonucleotide pairs [A5utr.t3L(oM)/F and A5utr.t3L(oM)/R; Gf5utr.t3L(oM)/F and Gf5utr.t3L(oM)/R; Tf5utr.t1L(M)/F and Tf5utr.t1L(M)/R] and a 3'UTR-specific pair [AM.mL1-pan3utr/F and AM.mL1-pan3utr/R]. They were catalyzed over 40 cycles by SsoAdvanced, as described in **Table 1**. Amplicons were cloned by a TOPO^{TM}-TA cloning kit (Invitrogen #K4575J10), according to Manufacturer's instructions. For each amplicon, at least six clones were double-strand sequenced via Sanger method, by a Commercial operator (Eurofins). Sequences were aligned by Clustal Omega and further processed to generate experimental, SEQ.A.x, SEQ.Gf.x, SEQ.Tf.x and SEQ.3'UTR consensuses. Similarly, harvested from the Dfam database (https://www.dfam.org) under accession numbers DF0001807, DF0001809, DF0001811, DF0001816, DF0001819, DF0001821, DF0001823, DF0001849, DF0001851, DF0001864, DF0001866, DF0001868, DF0001806, DF0001808, DF0001810, DF0001815, DF0001818, DF0001820, DF0001822, DF0001848, DF0001850, DF0001863, DF0001865 and DF0001867, family specific L1 5'UTR and 3'UTR sequences were aligned by Clustal Omega and further processed to generate family-specific DFAM.A, DFAM.Gf and DFAM.Tf, and "pan-L1"

Development • Accepted manuscript

DFAM.3'UTR consensuses. Finally, each SEQ consensus was aligned against the corresponding DFAM consensus.

Chromatin Immunoprecipitation (ChIP) assay

Chromatin Immunoprecipitation-quantitative Polymerase Chain Reaction assays (ChIP-qPCRs) were performed on chromatin aliquots prepared from $3.0*10^5$ cells (αFoxg1-ChIP) or $1.0*10^5$ cells (αH3K4me3-, αH3K9me3-, αH3K27ac-, and αMeCP2-ChIP).

ChIP analysis was performed by the MAGnify™ Chromatin Immunoprecipitation System kit (Invitrogen), according to Manufacturer's instructions, with minor modifications. Briefly, chromatin was fixed by 1% formaldehyde for 10 min at RT. After cell lysis, fixed chromatin was sonicated by a Soniprep 150 apparatus according to the following settings: (1) on ice; 5s ON, 55 s OFF; oscillation amplitude 5 µm; 4 cycles (αFoxg1-ChIP); (2) on ice; 5s ON, 55 s OFF; oscillation amplitude 5 µm; 5 cycles (αH3K4me3-, αH3K9me3-, αH3K27ac-, and αMeCP2-ChIP). Agarose gel electrophoresis was employed to estimate quality of sonicated chromatin.

Sonicated chromatin was immunoprecipitated for 2h at 4°C in a final volume of 100 µL, keeping the tubes in a rotating device, using the following, agarose bead-bound antibodies:

- αFoxg1 (rabbit polyclonal, Abcam #ab18259), 10 µg/reaction;
- αH3K4me3 (rabbit polyclonal, Abcam #ab8580), 3 µg/reaction;
- αH3K9me3 (rabbit polyclonal, Active Motif #39161), 3 µg/reaction;
- αH3K27ac (rabbit polyclonal, #ab177178), Abcam, 3 µg/reaction;
- αMecP2 (rat polyclonal IgG2a serotype, Active Motif #61291), 3 µg/reaction.

Next, immunoprecipitated DNA was purified according to Manufacturer's instructions. Last, 1/30 of each immunoprecipitated (IP) DNA sample was amplified by qPCR. For each sample, qPCRs were performed in technical triplicate. Averages were normalized against input chromatin and further normalized against controls. Experiments were performed at least in biological triplicate. Results were evaluated by Student's t-test, via Excel software.

Total RNA extraction

Total RNA was extracted from both primary neural cultures and acutely dissected neocortical samples using TRIzol Reagent (Thermofisher #15596026) according to the Manufacturer's instructions. RNA was precipitated using isopropanol and GlycoBlue

Development • Accepted manuscript

(Ambion) overnight at -80°C. After two washes with 75% ethanol, RNA was resuspended in 20µl sterile nuclease-free deionized water. Agarose gel electrophoresis and spectro-photometric measurements (DS-11, DeNovix) were employed to estimate its concentration, quality and purity.

RNA Immunoprecipitation (RIP)

RNA immunoprecipitation was performed starting from primary neural cultures.

Before starting cells processing, for each RIP reaction, 10µl of protein A/G Dynabeads (Thermofisher #492024) were coupled with 10µg of αFoxg1 (ChIP-grade, rabbit polyclonal, Abcam #ab18259), or 10µg of rabbit IgG (Millipore #12370) as control, according to Manufacturer's protocols. "Pre-clearing" control beads were prepared omitting antibody coupling.

Cells were washed once with ice-cold 1x PBS. 75µl ice-cold lysis buffer was added to each well (of 12-multiwell plate) and kept on ice for 10 min. Next, cells were scraped and lysed by vigorously pipetting up and down, paying attention not to make bubbles. Lysate collected from 10 wells (about $8x10^6$ cells; corresponding to a αFoxg1/IgG biological samples pair), was “pipetted up and down and kept 10 min on ice" twice, then it was centrifuged at 2000g for 10 min at 4°C, and then centrifuged at 16000g for 10 min at 4°C. The supernatant resulting from each sample was incubated with pre-clearing beads (pre-equilibrated in lysis buffer) for 30 min at 4°C on roller-shaker. Then, preclearing beads were separated with a magnet, and supernatant was incubated with antibody-coupled beads (pre-equilibrated in lysis buffer), overnight at 4°C on roller-shaker. 10% of supernatant (Input, IN-RIP) was stored on ice. The day after, beads were collected with a magnet and washed five times with 0.5ml ice-cold high-salt buffer. [Lysis buffer: 25mM TRIS-HC1, 150mM KCl (Ambion), 10mM $MgCl_2$ (Ambion), 1% (vol/vol) NP-40 (Thermo Fisher Scientific), 1X EDTA-free protease inhibitors (Roche), 0.5 mM DTT (Invitrogen), 10 µl/ml rRNasin (Promega), 10 µl/ml SuperaseIn (Applied Biosystems). High-salt buffer: 25mM TRIS-HCI, 350mM KCl (Ambion), 10mM $MgCl_2$ (Ambion), 1% (vol/vol) NP-40 (Thermo Fisher Scientific), 1X EDTA-free protease inhibitors (Roche), 0.5mM DTT (Invitrogen)]. For each sample, RNA immunoprecipitated (IP-RIP) and Input were extracted with Trizol™ LS reagent according to manufacturer's instructions. For each sample, a supplementary extraction was used to improve the total RNA yield. RNA was precipitated using isopropanol and GlycoBlue over-night at -80°C. After two washes with

Development • Accepted manuscript

75% ethanol, the RNA was resuspended in 10µl sterile nuclease-free deionized water. Agarose gel electrophoresis and spectrophotometric measurements (NanoDrop ND-1000) were employed to estimate quantity, quality and purity of the resulting RNA.

Total and immunoprecipitated RNA quantitation.

RNA preparations from total RNA samples, and RIP samples were treated by TURBO^{TM}DNase (2U/µl) (Thermofisher # AM2238) for 1h at 37°C, following Manufacturer's instructions. cDNA was produced by reverse transcription (RT) by Superscript III^{TM} (Thermofisher #18080093) according to Manufacturer's instructions, in the presence of random hexamers. Then, the RT reaction was diluted 1:5 (in case of both RIP and total RNA samples), and 1µl of the resulting cDNA was used as substrate of any subsequent quantitative PCR (qPCR) reaction. Limited to intron-less amplicons and for RIP-derived samples, negative control PCRs were run on RT(-) RNA preparations. qPCR reactions were performed by the SsoAdvanced SYBR Green Supermix^{TM} platform (Biorad #1725270), according to Manufacturer's instructions. For each transcript under examination and each sample, cDNA was qPCR-analyzed in technical triplicate, and results averaged. In case of total RNA, mRNA levels were normalized against the geometrical average of *Rpl10a*,*Gapdh*, *Cltc* and *Rn18S* levels (or a subset of them, see Legends to Figures). In case of RIP samples, IP samples were normalized against Inputs. Primer sequences reported in **Table 1**. Data analysis was performed using Microsoft Excel.

Immunofluorescence: sample preparation

Brains were dissected out from P0 mouse pups, fixed in 4% paraformaldehyde at 4°C overnight, transferred to 30% sucrose/1xPBS, kept at 4°C until equilibration, included in OCT (Bio-Optica) and sliced at 30µm. Slices were attached to Superfrost N^{+} glass slides (ThermoScientific), which were stored at -80°C. Before immunolabeling, slides were transferred to RT for 10' and washed in 1xPBS for 30' for OCT removal.

In case of primary neural cell preparations, cells were dissociated by 0.3X trypsin digestion for 4 minutes at RT, followed by gentle (10 times) pipetting and 1:1 v/v trypsin inactivation by FBS-containing medium. Cells were resuspended at 200 cells/µL and 1 mL of suspension was plated on a 12mmØ glass coverslip previously coated by 0.1mg/ml poly-L-Lysine. Cells

Development • Accepted manuscript

were kept in 5% CO2, at 37°C for 1 hour, fixed in 4% PFA at RT for 15 minutes, and finally washed 3 times in 1x PBS.

Fixed/washed cells/brain sections were treated with blocking mix (1X PBS - 10% FBS -1 mg/ml BSA - 0.1% Triton X-100) for at least 1 hour at room temperature (RT). Next, they were incubated with primary antibodies in blocking mix, overnight at 4°C. The day after, samples were washed 3 times in "1X PBS – 0.1% Triton X-100" (5 min each) and then incubated with secondary antibodies in blocking mix, for 2 hours at RT. Samples were finally washed 3 times in "1X PBS – 0.1% Triton X-100" (5 min each), subsequently counterstained with DAPI (4', 6'-diamidino-2- phenylindole), and mounted in Vectashield Mounting Medium (Vector). The following primary antibodies were used: αSox2, rabbit polyclonal, (clone 2Q178, Abcam #ab6142, 1:400); αTubb3, mouse monoclonal, (clone Tuj1, Covance #MMS-435P, 1:1000); αFoxg1 antibody (rabbit polyclonal, Abcam #ab18259, 1:500); αRFP (specifically recognizing mCherry), rat monoclonal (Antibodies online #ABIN334653, 1:500); αEGFP (Enhanced Green Fluorescent Protein), chicken polyclonal (GenTex #GTX13970, 1:1000). Secondary antibodies were conjugates with Alexa Fluor 488, Alexa Fluor 594 and Alexa Fluor 647 fluorophores (Invitrogen, 1:500).

Image acquisition and analysis

Immuno-stained cells/brain sections were photographed on a Nikon Eclipse TI microscope, equipped with a 20X objective, by a Hamamatsu 1394 ORCA-285 camera (**Fig. 2**), or a Nikon C1 confocal system (**Fig. 5, S2**). Hamamatsu photos were collected as 1344x1024 pixel files. Nikon C1 photos were collected as 3μm Z-stacks (0.3μm steps) of 1024x1024 pixel images. Images were analyzed by Adobe Photoshop CS6 (**Fig. 2**) and Volocity 5.5.1 (**Figure 5, S2**) softwares. Resulting numerical data were further processed by Microsoft Excel software.

Specifically in case of **Fig. 5** analysis, the following strategy was implemented. Acutely transduced by LV_pTα1-mCherry (firing in NPS and Ns) at moi=8, NSCs, NPs and Ns were recognized by their $mCherry^{-}Tubb3^{-}$, $mCherry^{+}Tubb3^{-}$ and $mCherry^{\pm}Tubb3^{+}$ profiles, respectively. Moreover, for each cell, nuclear Foxg1 protein content was quantified by Volocity 5.5.1 analysis of aFoxg1-IF signal. Data referring to an equal number of cells from 6 biological replicates of control samples were collected, cumulatively ranked and employed to establish boundaries between contiguous (aFoxg1-IF signal) deciles (here "biological replicates" are aliquots of neural cells originating from the same starting pool, each

Development • Accepted manuscript

independently transduced and cultured). Next, starting from 6 and 5 biological replicates of control and *Foxg1*-OE samples, respectively, distinctive cell types (NSCs, NP, and Ns) of different genotypes (control or mis-expressing Foxg1), falling within different decile bins were quantified, normalized against total cells of the same type and genotype, and finally plotted against decile number. Cumulatively, >17,000 neural cells were scored for this analysis.

As for **Fig. S2**, Foxg1 protein level were revealed by αFoxg1/αrabbit-Alexa488 immunofluorescence, and quantified by Volocity 5.5.1 analysis, run over the entire cell population. For each test, at least six biological replicates were employed. Here, "biological replicates" are columns of midparietal neocortex taken from different brains, each including at least 2,500 cells (**Fig. S2A**), or aliquots of neural cells originating from the same starting pool, each independently transduced and cultured (**Fig. S2B,C**).

Statistical analysis

When not otherwise stated, experiments were performed at least in biological triplicate. Statistical tests employed for result evaluation, *p* values, and definitions of *n* (number of biological replicates) are provided in each Figure. Full primary data referred to by all Figures are reported in **Table S5**.

AUTHORS' CONTRIBUTIONS

Contribution	*Contributor*
Conceptualization	GL, AM
Data Curation	GL, AM
Formal Analysis	GL, AM
Funding Acquisition	AM
Investigation	GL (performed all experiments), SF (provided materials for Fig. 10) OA (provided materials for Fig. 4 and 16)
Methodology	AM
Project Administration	AM
Software	GL, AM
Supervision	AM
Visualization	GL, AM
Writing – Original Draft Preparation	GL, AM
Writing – Review & Editing	AM

Development • Accepted manuscript

ACKNOWLEDGEMENTS

We thank Laura Rigoldi for embryo sexing.

COMPETING INTERESTS

The Authors declare no conflict of interests.

FUNDING

We thank:

(1) International FOXG1 Research Foundation (Grant to A.M.)

(2) SISSA (intramural funding to A.M.)

DATA AVAILABILITY

All relevant data can be found within the article and its supplementary information.

REFERENCES

An, W. (2012). L1 expression and regulation in humans and rodents. *Front. Biosci.* **E4**, 2203–2225.

Artimagnella, O. and Mallamaci, A. (2020). RNASeq profiling of Foxg1-GOF neocortical neurons.v2.

Artimagnella, O., Esposito, M., Sanges, R. and Mallamaci, A. (2022). Foxg1 regulates translation of neocortical neuronal genes, including the main NMDA receptor subunit gene, Grin1. 2022.10.05.510986.

Babushok, D. V., Ostertag, E. M., Courtney, C. E., Choi, J. M. and Kazazian, H. H. (2006). L1 integration in a transgenic mouse model. *Genome Res.* **16**, 240–250.

Baillie, J. K., Barnett, M. W., Upton, K. R., Gerhardt, D. J., Richmond, T. A., De Sapio, F., Brennan, P. M., Rizzu, P., Smith, S., Fell, M., et al. (2011). Somatic retrotransposition alters the genetic landscape of the human brain. *Nature* **479**, 534–537.

BioGRID db_FOXG1. https://thebiogrid.org/108580/summary/homo-sapiens/foxg1.html

Development • Accepted manuscript

Blaudin De Thé, F., Rekaik, H., Peze-Heidsieck, E., Massiani-Beaudoin, O., Joshi, R. L., Fuchs, J. and Prochiantz, A. (2018). Engrailed homeoprotein blocks degeneration in adult dopaminergic neurons through LINE-1 repression. *EMBO J.* **37**, e97374.

Bodea, G. O., McKelvey, E. G. Z. and Faulkner, G. J. (2018). Retrotransposon-induced mosaicism in the neural genome. *Open Biol.* **8**, 180074.

Brancaccio, M., Pivetta, C., Granzotto, M., Filippis, C. and Mallamaci, A. (2010). Emx2 and Foxg1 inhibit gliogenesis and promote neuronogenesis. *Stem Cells Dayt. Ohio* **28**, 1206–1218.

Brimble, E., Reyes, K. G., Kuhathaas, K., Devinsky, O., Ruzhnikov, M. R. Z., Ortiz-Gonzalez, X. R., Scheffer, I., Bahi-Buisson, N., Olson, H., and the FOXG1 Research Foundation (2023). Expanding genotype–phenotype correlations in FOXG1 syndrome: results from a patient registry. *Orphanet J. Rare Dis.* **18**, 149.

Bulut-Karslioglu, A., De La Rosa-Velázquez, I. A., Ramirez, F., Barenboim, M., Onishi-Seebacher, M., Arand, J., Galán, C., Winter, G. E., Engist, B., Gerle, B., et al. (2014). Suv39h-dependent H3K9me3 marks intact retrotransposons and silences LINE elements in mouse embryonic stem cells. *Mol. Cell* **55**, 277–290.

Chiola, S., Do, M. D., Centrone, L. and Mallamaci, A. (2019). *Foxg1* Overexpression in Neocortical Pyramids Stimulates Dendrite Elongation Via *Hes1* and pCreb1 Upregulation. *Cereb. Cortex* **29**, 1006–1019.

ClinVar db_Foxg1 https://www.ncbi.nlm.nih.gov/clinvar/?term=Foxg1[gene].

Coufal, N. G., Garcia-Perez, J. L., Peng, G. E., Yeo, G. W., Mu, Y., Lovci, M. T., Morell, M., O'Shea, K. S., Moran, J. V. and Gage, F. H. (2009). L1 retrotransposition in human neural progenitor cells. *Nature* **460**, 1127–1131.

Day, D. S., Luquette, L. J., Park, P. J. and Kharchenko, P. V. (2010). Estimating enrichment of repetitive elements from high-throughput sequence data. *Genome Biol.* **11**, R69.

Development • Accepted manuscript

De Filippis, R., Pancrazi, L., Bjørgo, K., Rosseto, A., Kleefstra, T., Grillo, E., Panighini, A., Cardarelli, F., Meloni, I., Ariani, F., et al. (2012). Expanding the phenotype associated with FOXG1 mutations and in vivo FoxG1 chromatin-binding dynamics. *Clin. Genet.* **82**, 395–403.

Diez-Roux, G., Banfi, S., Sultan, M., Geffers, L., Anand, S., Rozado, D., Magen, A., Canidio, E., Pagani, M., Peluso, I., et al. (2011). A high-resolution anatomical atlas of the transcriptome in the mouse embryo. *PLoS Biol.* **9**, e1000582.

Evrony, G. D., Cai, X., Lee, E., Hills, L. B., Elhosary, P. C., Lehmann, H. S., Parker, J. J., Atabay, K. D., Gilmore, E. C., Poduri, A., et al. (2012). Single-Neuron Sequencing Analysis of L1 Retrotransposition and Somatic Mutation in the Human Brain. *Cell* **151**, 483–496.

Evrony, G. D., Lee, E., Mehta, B. K., Benjamini, Y., Johnson, R. M., Cai, X., Yang, L., Haseley, P., Lehmann, H. S., Park, P. J., et al. (2015). Cell Lineage Analysis in Human Brain Using Endogenous Retroelements. *Neuron* **85**, 49–59.

Evrony, G. D., Lee, E., Park, P. J. and Walsh, C. A. (2016). Resolving rates of mutation in the brain using single-neuron genomics. *eLife* **5**, e12966.

Falcone, C., Filippis, C., Granzotto, M. and Mallamaci, A. (2015). Emx2 expression levels in NSCs modulate astrogenesis rates by regulating EgfR and Fgf9. *Glia* **63**, 412–422.

Falcone, C., Daga, A., Leanza, G. and Mallamaci, A. (2016). Emx2 as a novel tool to suppress glioblastoma. *Oncotarget* **7**, 41005–41016.

Falcone, C., Santo, M., Liuzzi, G., Cannizzaro, N., Grudina, C., Valencic, E., Peruzzotti-Jametti, L., Pluchino, S. and Mallamaci, A. (2019). Foxg1 Antagonizes Neocortical Stem Cell Progression to Astrogenesis. *Cereb. Cortex N. Y. N 1991* **29**, 4903–4918.

Faulkner, G. J. and Billon, V. (2018). L1 retrotransposition in the soma: a field jumping ahead. *Mob. DNA* **9**, 22.

Fimiani, C., Goina, E., Su, Q., Gao, G. and Mallamaci, A. (2016). RNA activation of haploinsufficient Foxg1 gene in murine neocortex. *Sci. Rep.* **6**, 39311.

Development • Accepted manuscript

Floreani, L., Ansaloni, F., Mangoni, D., Agostoni, E., Sanges, R., Persichetti, F. and Gustincich, S. (2022). Analysis of LINE1 Retrotransposons in Huntington's Disease. *Front. Cell. Neurosci.* **15**, 743797.

Florian, C., Bahi-Buisson, N. and Bienvenu, T. (2011). *FOXG1*-Related Disorders: From Clinical Description to Molecular Genetics. *Mol. Syndromol.* **2**, 153–163.

Follenzi, A. and Naldini, L. (2002). [26] Generation of HIV-1 derived lentiviral vectors. In *Methods in Enzymology*, pp. 454–465. Elsevier.

Fontana, C., Marasca, F., Provitera, L., Mancinelli, S., Pesenti, N., Sinha, S., Passera, S., Abrignani, S., Mosca, F., Lodato, S., et al. (2021). Early maternal care restores LINE-1 methylation and enhances neurodevelopment in preterm infants. *BMC Med.* **19**, 42.

Frisari, S., Santo, M., Hosseini, A., Manzati, M., Giugliano, M. and Mallamaci, A. (2022). Multidimensional Functional Profiling of Human Neuropathogenic FOXG1 Alleles in Primary Cultures of Murine Pallial Precursors. *Int. J. Mol. Sci.* **23**, 1343.

Garza, R., Atacho, D. A. M., Adami, A., Gerdes, P., Vinod, M., Hsieh, P., Karlsson, O., Horvath, V., Johansson, P. A., Pandiloski, N., et al. (2023). LINE-1 retrotransposons drive human neuronal transcriptome complexity and functional diversification. *Sci. Adv.* **9,** eadh9543.

Goodier, J. L. (2016). Restricting retrotransposons: a review. *Mob. DNA* **7**, 16.

Goodier, J. L., Cheung, L. E. and Kazazian, H. H. (2012). MOV10 RNA Helicase Is a Potent Inhibitor of Retrotransposition in Cells. *PLoS Genet.* **8**, e1002941.

Guler, G. D., Tindell, C. A., Pitti, R., Wilson, C., Nichols, K., KaiWai Cheung, T., Kim, H.-J., Wongchenko, M., Yan, Y., Haley, B., et al. (2017). Repression of Stress-Induced LINE-1 Expression Protects Cancer Cell Subpopulations from Lethal Drug Exposure. *Cancer Cell* **32**, 221-237.e13.

Hanashima, C., Li, S. C., Shen, L., Lai, E. and Fishell, G. (2004). Foxg1 suppresses early cortical cell fate. *Science* **303**, 56–59.

Development • Accepted manuscript

He, J., Fu, X., Zhang, M., He, F., Li, W., Abdul, M. M., Zhou, J., Sun, L., Chang, C., Li, Y., et al. (2019). Transposable elements are regulated by context-specific patterns of chromatin marks in mouse embryonic stem cells. *Nat. Commun.* **10**, 34.

He, J., Babarinde, I. A., Sun, L., Xu, S., Chen, R., Shi, J., Wei, Y., Li, Y., Ma, G., Zhuang, Q., et al. (2021). Identifying transposable element expression dynamics and heterogeneity during development at the single-cell level with a processing pipeline scTE. *Nat. Commun.* **12**, 1456.

Hébert, J. M. and McConnell, S. K. (2000). Targeting of cre to the Foxg1 (BF-1) locus mediates loxP recombination in the telencephalon and other developing head structures. *Dev. Biol.* **222**, 296–306.

Hou, P.-S., Miyoshi, G. and Hanashima, C. (2019). Sensory cortex wiring requires preselection of short- and long-range projection neurons through an Egr-Foxg1-COUP-TFI network. *Nat. Commun.* **10**, 3581.

Hutton, S. R. and Pevny, L. H. (2011). SOX2 expression levels distinguish between neural progenitor populations of the developing dorsal telencephalon. *Dev. Biol.* **352**, 40–47.

Ikeda, T., Abd El Galil, K. H., Tokunaga, K., Maeda, K., Sata, T., Sakaguchi, N., Heidmann, T. and Koito, A. (2011). Intrinsic restriction activity by apolipoprotein B mRNA editing enzyme APOBEC1 against the mobility of autonomous retrotransposons. *Nucleic Acids Res.* **39**, 5538–5554.

Jachowicz, J. W., Bing, X., Pontabry, J., Bošković, A., Rando, O. J. and Torres-Padilla, M.-E. (2017). LINE-1 activation after fertilization regulates global chromatin accessibility in the early mouse embryo. *Nat. Genet.* **49**, 1502–1510.

Kim, S., Günesdogan, U., Zylicz, J. J., Hackett, J. A., Cougot, D., Bao, S., Lee, C., Dietmann, S., Allen, G. E., Sengupta, R., et al. (2014). PRMT5 protects genomic integrity during global DNA demethylation in primordial germ cells and preimplantation embryos. *Mol. Cell* **56**, 564–579.

Development • Accepted manuscript

Kuwabara, T., Hsieh, J., Muotri, A., Yeo, G., Warashina, M., Lie, D. C., Moore, L., Nakashima, K., Asashima, M. and Gage, F. H. (2009). Wnt-mediated activation of NeuroD1 and retro-elements during adult neurogenesis. *Nat. Neurosci.* **12**, 1097–1105.

Li, X., Wang, W., Wang, J., Malovannaya, A., Xi, Y., Li, W., Guerra, R., Hawke, D. H., Qin, J. and Chen, J. (2015). Proteomic analyses reveal distinct chromatin-associated and soluble transcription factor complexes. *Mol. Syst. Biol.* **11**, 775.

Liu, E. Y., Russ, J., Cali, C. P., Phan, J. M., Amlie-Wolf, A. and Lee, E. B. (2019). Loss of Nuclear TDP-43 Is Associated with Decondensation of LINE Retrotransposons. *Cell Rep.* **27**, 1409-1421.e6.

Macfarlan, T. S., Gifford, W. D., Driscoll, S., Lettieri, K., Rowe, H. M., Bonanomi, D., Firth, A., Singer, O., Trono, D. and Pfaff, S. L. (2012). Embryonic stem cell potency fluctuates with endogenous retrovirus activity. *Nature* **487**, 57–63.

Mall, E. M., Herrmann, D. and Niemann, H. (2017). Murine pluripotent stem cells with a homozygous knockout of Foxg1 show reduced differentiation towards cortical progenitors in vitro. *Stem Cell Res.* **25**, 50–60.

Mangoni, D., Simi, A., Lau, P., Armaos, A., Ansaloni, F., Codino, A., Damiani, D., Floreani, L., Di Carlo, V., Vozzi, D., et al. (2023). LINE-1 regulates cortical development by acting as long non-coding RNAs. *Nat. Commun.* **14**, 4974.

Martynoga, B., Morrison, H., Price, D. J. and Mason, J. O. (2005). Foxg1 is required for specification of ventral telencephalon and region-specific regulation of dorsal telencephalic precursor proliferation and apoptosis. *Dev. Biol.* **283**, 113–127.

Mathelier, A., Fornes, O., Arenillas, D. J., Chen, C.-Y., Denay, G., Lee, J., Shi, W., Shyr, C., Tan, G., Worsley-Hunt, R., et al. (2016). JASPAR 2016: a major expansion and update of the open-access database of transcription factor binding profiles. *Nucleic Acids Res.* **44**, D110-115.

Development • Accepted manuscript

Menezes, J. R. and Luskin, M. B. (1994). Expression of neuron-specific tubulin defines a novel population in the proliferative layers of the developing telencephalon. *J. Neurosci. Off. J. Soc. Neurosci.* **14**, 5399–5416.

Mitter, D., Pringsheim, M., Kaulisch, M., Plümacher, K. S., Schröder, S., Warthemann, R., Abou Jamra, R., Baethmann, M., Bast, T., Büttel, H.-M., et al. (2018). FOXG1 syndrome: genotype–phenotype association in 83 patients with FOXG1 variants. *Genet. Med.* **20**, 98–108.

Miyoshi, G. and Fishell, G. (2012). Dynamic FoxG1 Expression Coordinates the Integration of Multipolar Pyramidal Neuron Precursors into the Cortical Plate. *Neuron* **74**, 1045–1058.

Miyoshi, G., Ueta, Y., Natsubori, A., Hiraga, K., Osaki, H., Yagasaki, Y., Kishi, Y., Yanagawa, Y., Fishell, G., Machold, R. P., et al. (2021). FoxG1 regulates the formation of cortical GABAergic circuit during an early postnatal critical period resulting in autism spectrum disorder-like phenotypes. *Nat. Commun.* **12**, 3773.

Muotri, A. R. and Gage, F. H. (2006). Generation of neuronal variability and complexity. *Nature* **441**, 1087–1093.

Muotri, A. R., Chu, V. T., Marchetto, M. C. N., Deng, W., Moran, J. V. and Gage, F. H. (2005). Somatic mosaicism in neuronal precursor cells mediated by L1 retrotransposition. *Nature* **435**, 903–910.

Muotri, A. R., Marchetto, M. C. N., Coufal, N. G., Oefner, R., Yeo, G., Nakashima, K. and Gage, F. H. (2010). L1 retrotransposition in neurons is modulated by MeCP2. *Nature* **468**, 443–446.

Muzio, L. and Mallamaci, A. (2005). Foxg1 confines Cajal-Retzius neuronogenesis and hippocampal morphogenesis to the dorsomedial pallium. *J. Neurosci. Off. J. Soc. Neurosci.* **25**, 4435–4441.

Development • Accepted manuscript

Nandi, S., Chandramohan, D., Fioriti, L., Melnick, A. M., Hébert, J. M., Mason, C. E., Rajasethupathy, P. and Kandel, E. R. (2016). Roles for small noncoding RNAs in silencing of retrotransposons in the mammalian brain. *Proc. Natl. Acad. Sci.* **113**, 12697–12702.

New drugs for HIV infection (1996). *Med. Lett. Drugs Ther.* **38**, 35–37.

Pancrazi, L., Di Benedetto, G., Colombaioni, L., Della Sala, G., Testa, G., Olimpico, F., Reyes, A., Zeviani, M., Pozzan, T. and Costa, M. (2015). Foxg1 localizes to mitochondria and coordinates cell differentiation and bioenergetics. *Proc. Natl. Acad. Sci. U. S. A.* **112**, 13910–13915.

Papandreou, A., Schneider, R. B., Augustine, E. F., Ng, J., Mankad, K., Meyer, E., McTague, A., Ngoh, A., Hemingway, C., Robinson, R., et al. (2016). Delineation of the movement disorders associated with *FOXG1* mutations: Table 1. *Neurology* **86**, 1794–1800.

Percharde, M., Lin, C.-J., Yin, Y., Guan, J., Peixoto, G. A., Bulut-Karslioglu, A., Biechele, S., Huang, B., Shen, X. and Ramalho-Santos, M. (2018). A LINE1-Nucleolin Partnership Regulates Early Development and ESC Identity. *Cell* **174**, 391-405.e19.

Pevny, L. H. and Lovell-Badge, R. (1997). Sox genes find their feet. *Curr. Opin. Genet. Dev.* **7**, 338–344.

Pinson, A. and Huttner, W. B. (2021). Neocortex expansion in development and evolution-from genes to progenitor cell biology. *Curr. Opin. Cell Biol.* **73**, 9–18.

Platt, R. J., Chen, S., Zhou, Y., Yim, M. J., Swiech, L., Kempton, H. R., Dahlman, J. E., Parnas, O., Eisenhaure, T. M., Jovanovic, M., et al. (2014). CRISPR-Cas9 Knockin Mice for Genome Editing and Cancer Modeling. *Cell* **159**, 440–455.

Protasova, M. S., Andreeva, T. V. and Rogaev, E. I. (2021). Factors Regulating the Activity of LINE1 Retrotransposons. *Genes* **12**, 1562.

Development • Accepted manuscript

Raciti, M., Granzotto, M., Duc, M. D., Fimiani, C., Cellot, G., Cherubini, E. and Mallamaci, A. (2013). Reprogramming fibroblasts to neural-precursor-like cells by structured overexpression of pallial patterning genes. *Mol. Cell. Neurosci.* **57**, 42–53.

Rangasamy, D. (2013). Distinctive patterns of epigenetic marks are associated with promoter regions of mouse LINE-1 and LTR retrotransposons. *Mob. DNA* **4**, 27.

Richardson, S. R., Morell, S. and Faulkner, G. J. (2014). L1 Retrotransposons and Somatic Mosaicism in the Brain. *Annu. Rev. Genet.* **48**, 1–27.

Rosser, J. M. and An, W. (2012). L1 expression and regulation in humans and rodents. *Front. Biosci. Elite Ed.* **4**, 2203–2225.

Sanchez-Luque, F. J., Kempen, M.-J. H. C., Gerdes, P., Vargas-Landin, D. B., Richardson, S. R., Troskie, R.-L., Jesuadian, J. S., Cheetham, S. W., Carreira, P. E., Salvador-Palomeque, C., et al. (2019). LINE-1 Evasion of Epigenetic Repression in Humans. *Mol. Cell* **75**, 590-604.e12.

Sastry, L., Johnson, T., Hobson, M. J., Smucker, B. and Cornetta, K. (2002). Titering lentiviral vectors: comparison of DNA, RNA and marker expression methods. *Gene Ther.* **9**, 1155–1162.

Seoane, J., Le, H.-V., Shen, L., Anderson, S. A. and Massagué, J. (2004). Integration of Smad and forkhead pathways in the control of neuroepithelial and glioblastoma cell proliferation. *Cell* **117**, 211–223.

SFARI db_FOXG1. https://gene.sfari.org/database/human-gene/Foxg1#variants-tab

Shen, L., Nam, H.-S., Song, P., Moore, H. and Anderson, S. A. (2006). FoxG1 haploinsufficiency results in impaired neurogenesis in the postnatal hippocampus and contextual memory deficits. *Hippocampus* **16**, 875–890.

Singer, T., McConnell, M. J., Marchetto, M. C. N., Coufal, N. G. and Gage, F. H. (2010). LINE-1 retrotransposons: mediators of somatic variation in neuronal genomes? *Trends Neurosci.* **33**, 345–354.

Development • Accepted manuscript

Sookdeo, A., Hepp, C. M., McClure, M. A. and Boissinot, S. (2013). Revisiting the evolution of mouse LINE-1 in the genomic era. *Mob. DNA* **4**, 3.

Spigoni, G., Gedressi, C. and Mallamaci, A. (2010). Regulation of Emx2 Expression by Antisense Transcripts in Murine Cortico-Cerebral Precursors. *PLoS ONE* **5**, e8658.

Storer, J., Hubley, R., Rosen, J., Wheeler, T. J. and Smit, A. F. (2021). The Dfam community resource of transposable element families, sequence models, and genome annotations. *Mob. DNA* **12**, 2.

Suarez, N. A., Macia, A. and Muotri, A. R. (2018). LINE-1 retrotransposons in healthy and diseased human brain: L1 Activity in the Human Brain. *Dev. Neurobiol.* **78**, 434–455.

Tang, S.-H. E., Silva, F. J., Tsark, W. M. K. and Mann, J. R. (2002). A cre/loxP-deleter transgenic line in mouse strain 129S1/SvImJ. *genesis* **32**, 199–202.

Tao, W. and Lai, E. (1992). Telencephalon-restricted expression of BF-1, a new member of the HNF-3/ fork head gene family, in the developing rat brain. *Neuron* **8**, 957–966.

Telley, L., Govindan, S., Prados, J., Stevant, I., Nef, S., Dermitzakis, E., Dayer, A. and Jabaudon, D. (2016). Sequential transcriptional waves direct the differentiation of newborn neurons in the mouse neocortex. *Science* **351**, 1443–1446.

Tigani, W., Rossi, M. P., Artimagnella, O., Santo, M., Rauti, R., Sorbo, T., Ulloa Severino, F. P., Provenzano, G., Allegra, M., Caleo, M., et al. (2020). Foxg1 Upregulation Enhances Neocortical Activity. *Cereb. Cortex N. Y. N 1991* **30**, 5147–5165.

Toma, K., Kumamoto, T. and Hanashima, C. (2014). The Timing of Upper-Layer Neurogenesis Is Conferred by Sequential Derepression and Negative Feedback from Deep-Layer Neurons. *J. Neurosci.* **34**, 13259–13276.

Upton, K. R., Gerhardt, D. J., Jesuadian, J. S., Richardson, S. R., Sánchez-Luque, F. J., Bodea, G. O., Ewing, A. D., Salvador-Palomeque, C., van der Knaap, M. S., Brennan, P. M., et al. (2015). Ubiquitous L1 Mosaicism in Hippocampal Neurons. *Cell* **161**, 228–239.

Development • Accepted manuscript

Vegas, N., Cavallin, M., Maillard, C., Boddaert, N., Toulouse, J., Schaefer, E., Lerman-Sagie, T., Lev, D., Magalie, B., Moutton, S., et al. (2018). Delineating *FOXG1* syndrome: From congenital microcephaly to hyperkinetic encephalopathy. *Neurol. Genet.* **4**, e281.

Weise, S. C., Arumugam, G., Villarreal, A., Videm, P., Heidrich, S., Nebel, N., Dumit, V. I., Sananbenesi, F., Reimann, V., Craske, M., et al. (2019). FOXG1 Regulates PRKAR2B Transcriptionally and Posttranscriptionally via miR200 in the Adult Hippocampus. *Mol. Neurobiol.* **56**, 5188–5201.

Yu, B., Liu, J., Su, M., Wang, C., Chen, H. and Zhao, C. (2019). Disruption of Foxg1 impairs neural plasticity leading to social and cognitive behavioral defects. *Mol. Brain* **12**, 63.

Zhou, L., Lim, Q.-E., Wan, G. and Too, H.-P. (2010). Normalization with genes encoding ribosomal proteins but not GAPDH provides an accurate quantification of gene expressions in neuronal differentiation of PC12 cells. *BMC Genomics* **11**, 75.

Zhu, W., Zhang, B., Li, M., Mo, F., Mi, T., Wu, Y., Teng, Z., Zhou, Q., Li, W. and Hu, B. (2019). Precisely controlling endogenous protein dosage in hPSCs and derivatives to model FOXG1 syndrome. *Nat. Commun.* **10**, 928.

Zhu, X., Zhou, B., Pattni, R., Gleason, K., Tan, C., Kalinowski, A., Sloan, S., Fiston-Lavier, A.-S., Mariani, J., Petrov, D., et al. (2021). Machine learning reveals bilateral distribution of somatic L1 insertions in human neurons and glia. *Nat. Neurosci.* **24**, 186–196.

Development • Accepted manuscript

Figures and Tables

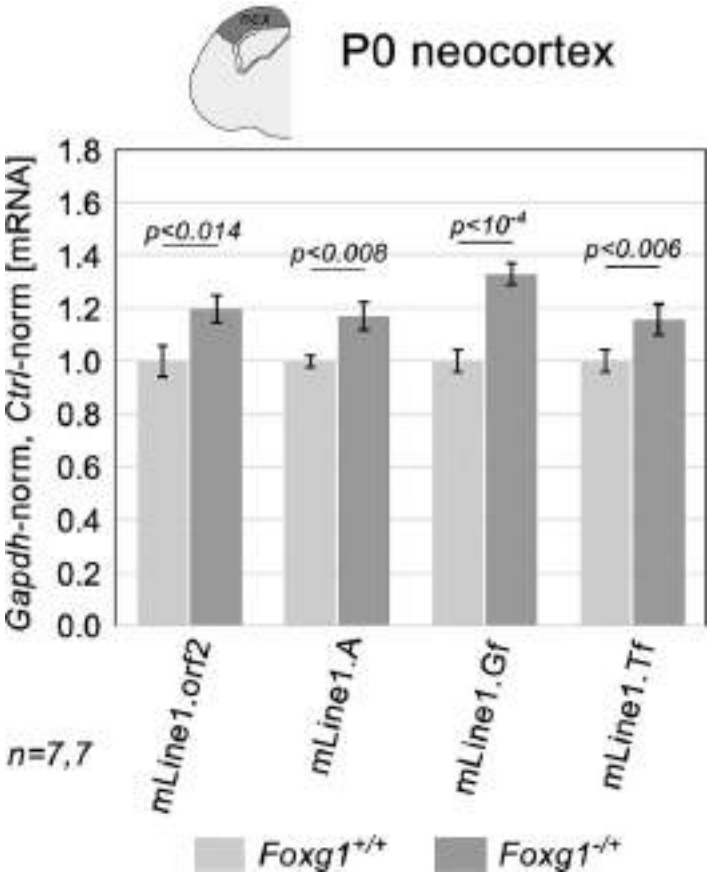

Fig. 1. L1 transcripts levels in neocortex of *Foxg1*$^{-/+}$ mouse neonates and controls. RT-PCR quantitation of pan-*L1* diagnostic amplicon "orf2", and family-specific amplicons, "A", "Gf" and "Tf". Data double normalized, against *Gapdh* and wild-type controls. Error-bars representing sem's. Statistical significance of results evaluated by t-test (one-tailed, unpaired). *n* is the number of biological replicates, i.e. neocortices taken from distinct pups.

Development • Accepted manuscript

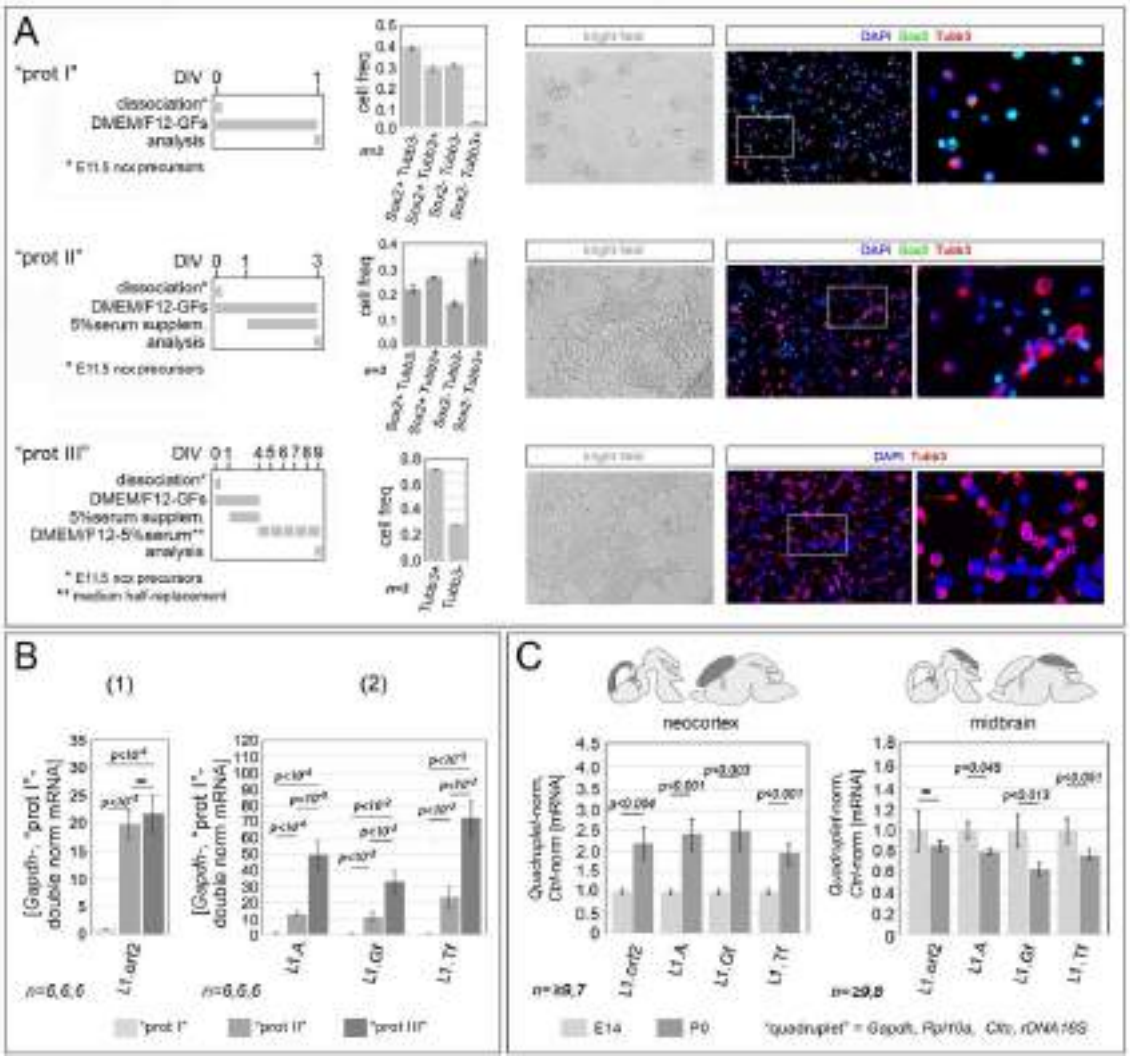

Fig. 2. In vitro modeling of *L1*-mRNA progression in murine developing neocortex. In (**A**), from left to right, shown are: [a] the three protocols (type I, II and III) employed to generate primary cultures, which model early, mid and late phases of neuronogenesis, respectively, and include neural cells terminally exposed to GFs, GFs and serum, and serum, respectively; [b] prevalences of distinctive cell types forming these cultures (type I cultures enriched in neural stem cells (NSCs, $Sox2^{+}Tubb3^{-}$) and neuronogenic progenitors (NPs, $Sox2^{-}Tubb3^{-}$), type II ones including comparable fractions of NSCs, NPs and neurons (Ns, $Tubb3^{+}$), and type III ones highly enriched in Ns); to note, here, low-Sox2-expressing cells (<2*background) were classified as $Sox2^{-}$, whereas all cells classified as $Sox2^{+}$ expressed such protein at much higher levels (>5*background); [c] examples of primary data; these include: bright field pictures of living cultures, taken just before their terminal analysis, and dark field images of aSox2/aTubb3 immunofluorescences, performed upon culture dissociation and fixation. In

Development • Accepted manuscript

(**B**) provided are RT-PCR quantitations of pan-*L1* diagnostic amplicon "orf2" (1), and family-specific amplicons, "A", "Gf" and "Tf" (2), in neural cultures set according to protocols I, II and III. Data double normalized, against *Gapdh* and "protocol I" values. In (**C**) shown are RT-PCR quantitations of the same diagnostic amplicons in neocortex and mesencephalic tectum at embryonic day 14.5 (E14.5) and birth (P0). Data double normalized against the geometric mean of *Gapdh*, *Rpl10a*, *Cltc* and *rDNA18S* ("quadruplet") and "E14.5" values. In (B,C) error-bars representing sem's. Statistical significance of results evaluated by t-test (one-tailed, unpaired). *n* is the number of biological replicates, i.e. independently cultured cell aliquots, originating from pooled, wild-type E11.5 neocortical primordia (B) or distinct embryos/pups (C).

Development • Accepted manuscript

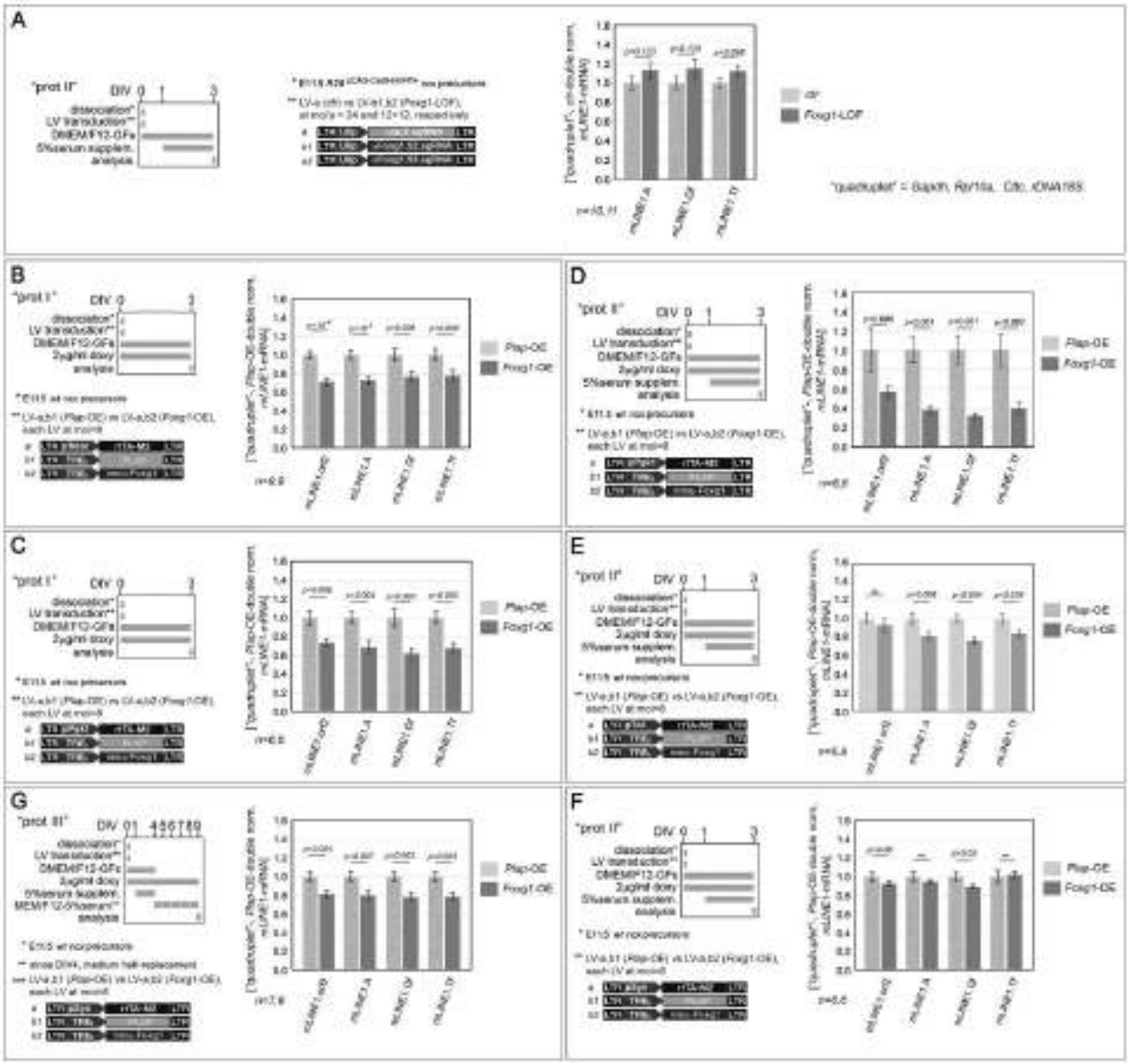

Fig. 3. Impact of *Foxg1* manipulation on *L1*-mRNA levels, in progressively more advanced neuronogenic pallial cultures. In (**A)** and (**B-G**), shown are outcomes of *Foxg1* downregulation (*Foxg1*-LOF) and overexpression (*Foxg1*-OE), respectively, in early- (B,C), mid- (A,D-F) and late- (G) neuronogenic cultures, set according to type I, II and III protocols, respectively. To left, protocols and lentiviral vectors employed. Transgenes driven by pNes, pTα1 and pSyn promoters, active in NSCs, NPs/Ns and Ns, respectively, and ubiquitously firing U6p and pPgk1 promoters. To right, results. RT-PCR quantitation of pan-*L1* diagnostic amplicon "orf2", and family-specific amplicons, "A", "Gf" and "Tf", in neural cultures set according to above-mentioned protocols. Data double normalized against gene quadruplet

Development • Accepted manuscript

(*Gapdh*, *Rpl10a*, *Cltc* and *rDNA 18S*) and control values. Error-bars representing sem's. Statistical significance of results evaluated by t-test (one-tailed, unpaired). *n* is the number of biological replicates, i.e. independently cultured and engineered cell aliquots, originating from pooled *R26*$^{pCAG\text{-}Cas9\text{-}EGFP/+}$ E11.5 neocortical primordia.

Development • Accepted manuscript

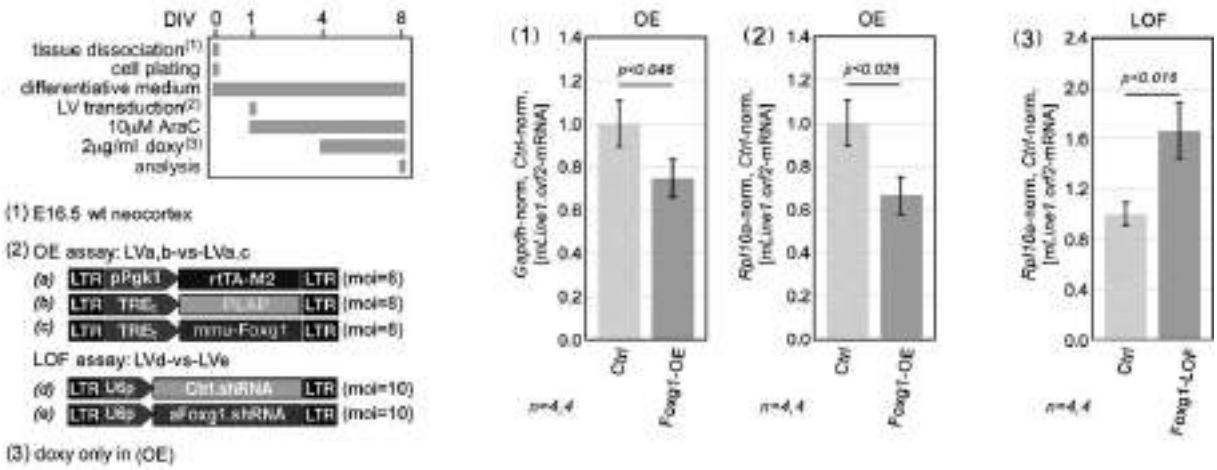

Fig. 4. Impact of constitutive *Foxg1* overexpression on *L1*-mRNA levels, in primary, neuron-enriched cultures. To left, protocols and lentiviral vectors employed, to right, results. Neuronal enrichment obtaind by early araC supplementation. Foxg1 constitutively overexpressed (OE) by a pPgk1-driven transgene, or down-regulated (LOF) by RNAi. *L1*-mRNA data double normalized against *Rpl10a* (or *Gapdh*) and control samples. Scalebars, sem's. Statistical evaluation of results by t-test (one-tail, unpaired). *n* = number of biological replicates, i.e. independently cultured and engineered cell aliquots originating from a common neural precursor pool.

Development • Accepted manuscript

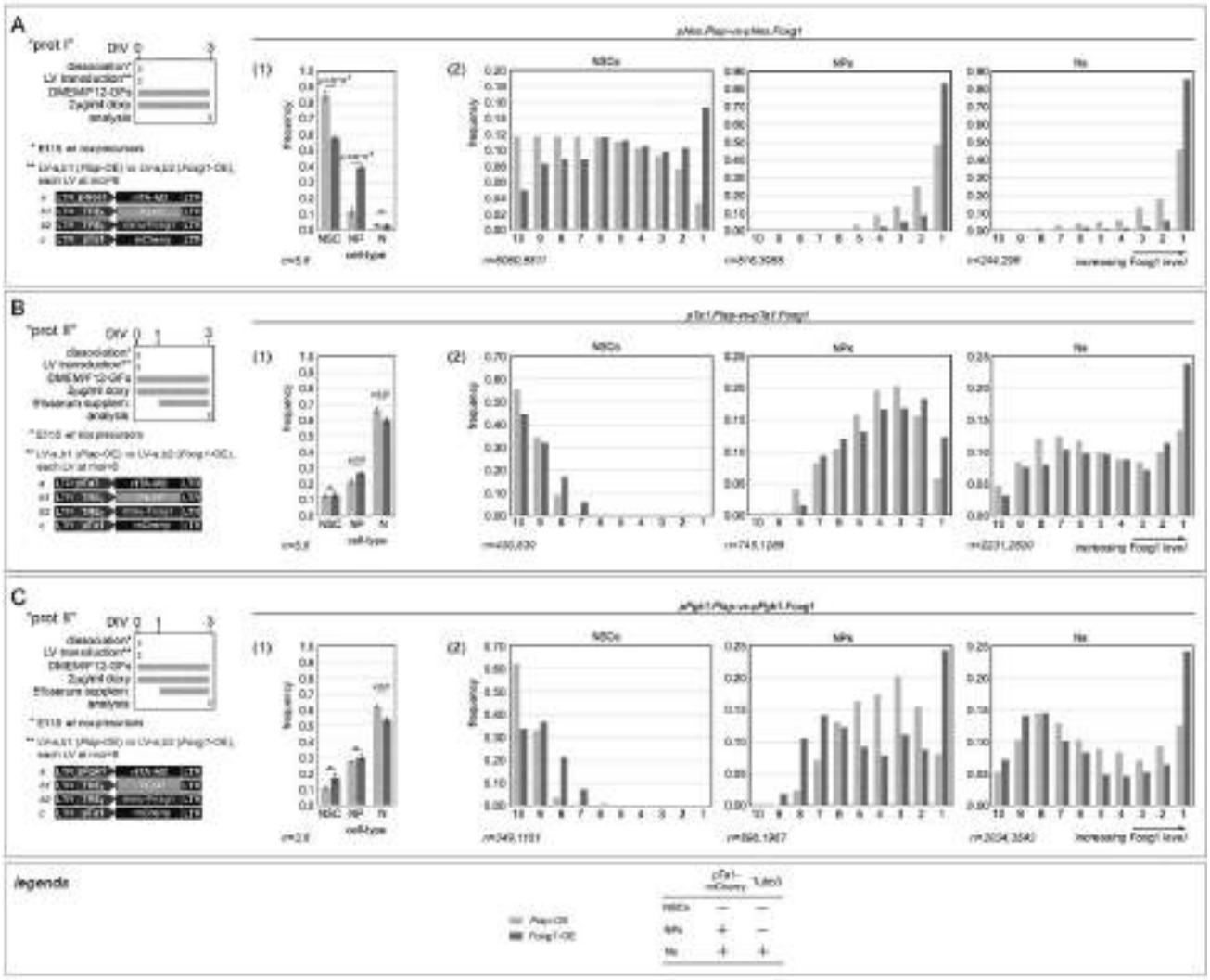

Fig. 5. Quantification of Foxg1 protein levels in distinctive neural precursor types, upon *Foxg1* over-expression driven by lentiviral vectors and cell-type specific promoters. Throughout the figure, to left, protocols and lentiviruses employed, to right, results. Assays run in early- (**A**), mid- (**B,C**) and late- (**D**) neuronogenic cultures, set according to type I, II and III protocols, respectively. Cultures over-expressing *Foxg1* or a control (*Plap*). Foxg1-encoding transgenes driven by pNes (A) and pTa1 (B) promoters, active in NSCs, and NPs/Ns, respectively, and ubiquitously firing pPgk1 promoter (C). NSCs, NPs and Ns recognized on the basis of their ^{pTa1}mCherry^{-}/Tubb3^{-}, ^{pTa1}mCherry^{+}/Tubb3^{-}, and ^{pTa1}mCherry$^{\pm}$/Tubb3^{+} profiles, respectively. Foxg1 cell content evaluated by quantitative immuno-fluorescence. In graphs (1), shown are prevalences of NSCs, NPs and Ns in neural cultures set according to the different protocols. Error-bars representing sem's. Statistical significance of results evaluated by t-test (one-tailed, unpaired). *n* is the number of biological replicates, i.e.

Development • Accepted manuscript

independently cultured and engineered cell aliquots, originating from pooled, *wild-type* E11.5 neocortical primordia. In graphs (2), shown are frequencies of NSCs, NPs and Ns falling within distinct Foxg1 expression deciles, i.e. normally equi-numerous bins characterized by decreasing (from 1 to 10) Foxg1 expression levels. n is the number of cells profiled, evenly pooled from the biological replicates referred to as for graph (1) series.

Development • Accepted manuscript

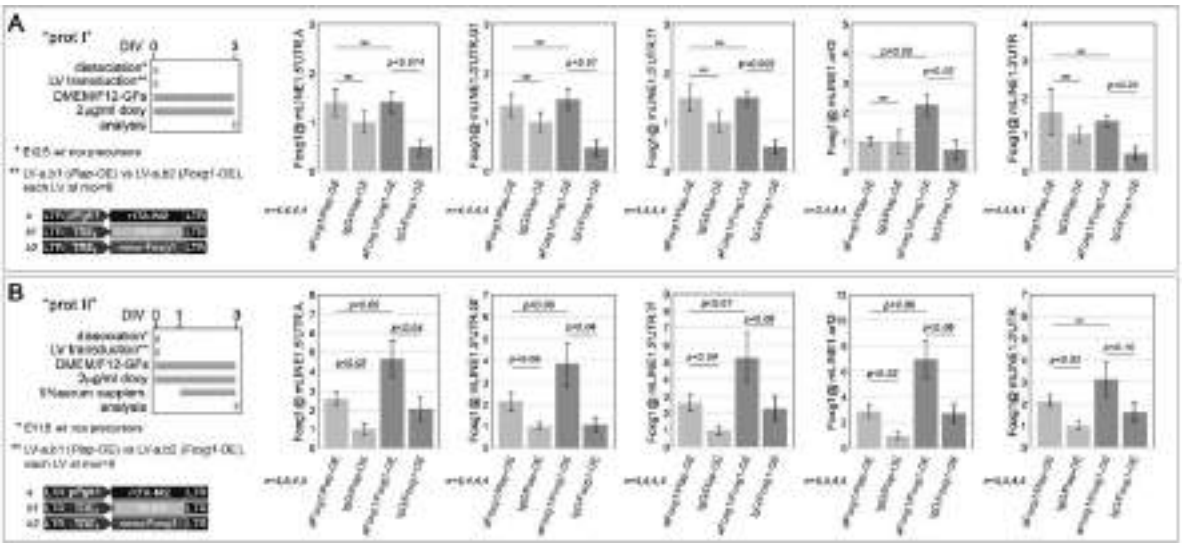

Fig. 6. Chromatin immunoprecipitation (ChIP) profiling of Foxg1 protein enrichment at L1 elements. To left, protocols and lentiviral vectors employed, to right, results. Analysis run in early- (**A**) and mid- (**B**) neuronogenic cultures, set according to type I and II protocols, respectively. Cultures constitutively overexpressing *Foxg1* (or a *Plap* control), driven by the pPgk1 promoter. Chromatin immunoprecipitation performed by anti-Foxg1 antibody and control IgG. PCR quantitation of pan-*L1* diagnostic amplicons "L1.orf2" and "L1.3'UTR", and family-specific "L1.5'UTR" amplicons, ".A", ".Gf" and ".Tf". Results normalized against input chromatin. Scalebars, sem's. Statistical evaluation of results by t-test (one-tail, unpaired). *n* = number of biological replicates, i.e. independently cultured and engineered cell aliquots originating from a common neural precursor pool.

Development • Accepted manuscript

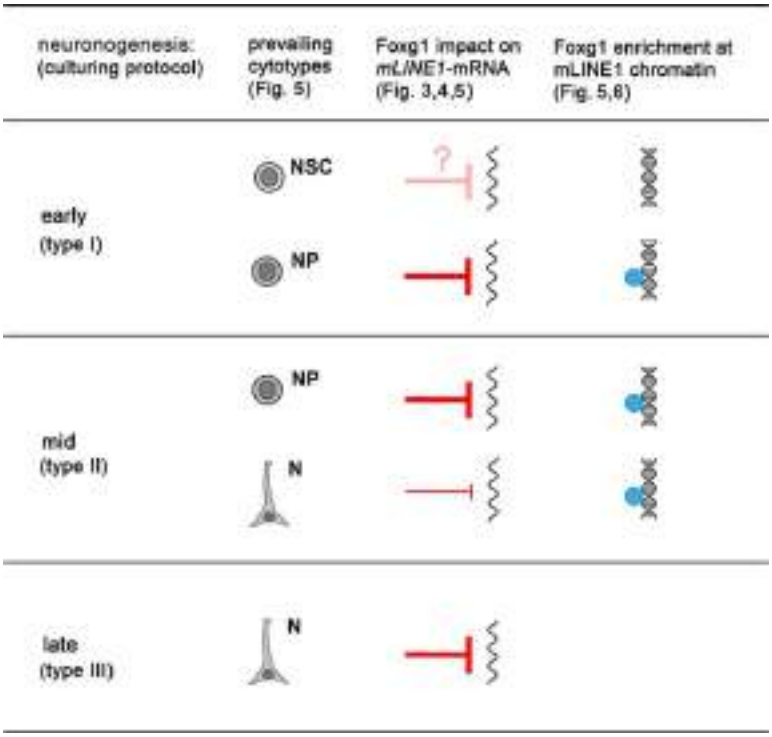

Fig. 7. Synopsis of Foxg1 inhibition of *L1* expression within the pallial neuronogenic lineage. Tentative, temporal progression of Foxg1 control of *L1* expression, based on integrated critical evaluation of L1-qRTPCR- (Fig. 3,4), Foxg1-qIF- (Fig. 5) and αFoxg1-ChIPqPCR- (Fig. 6) data.

Development • Accepted manuscript

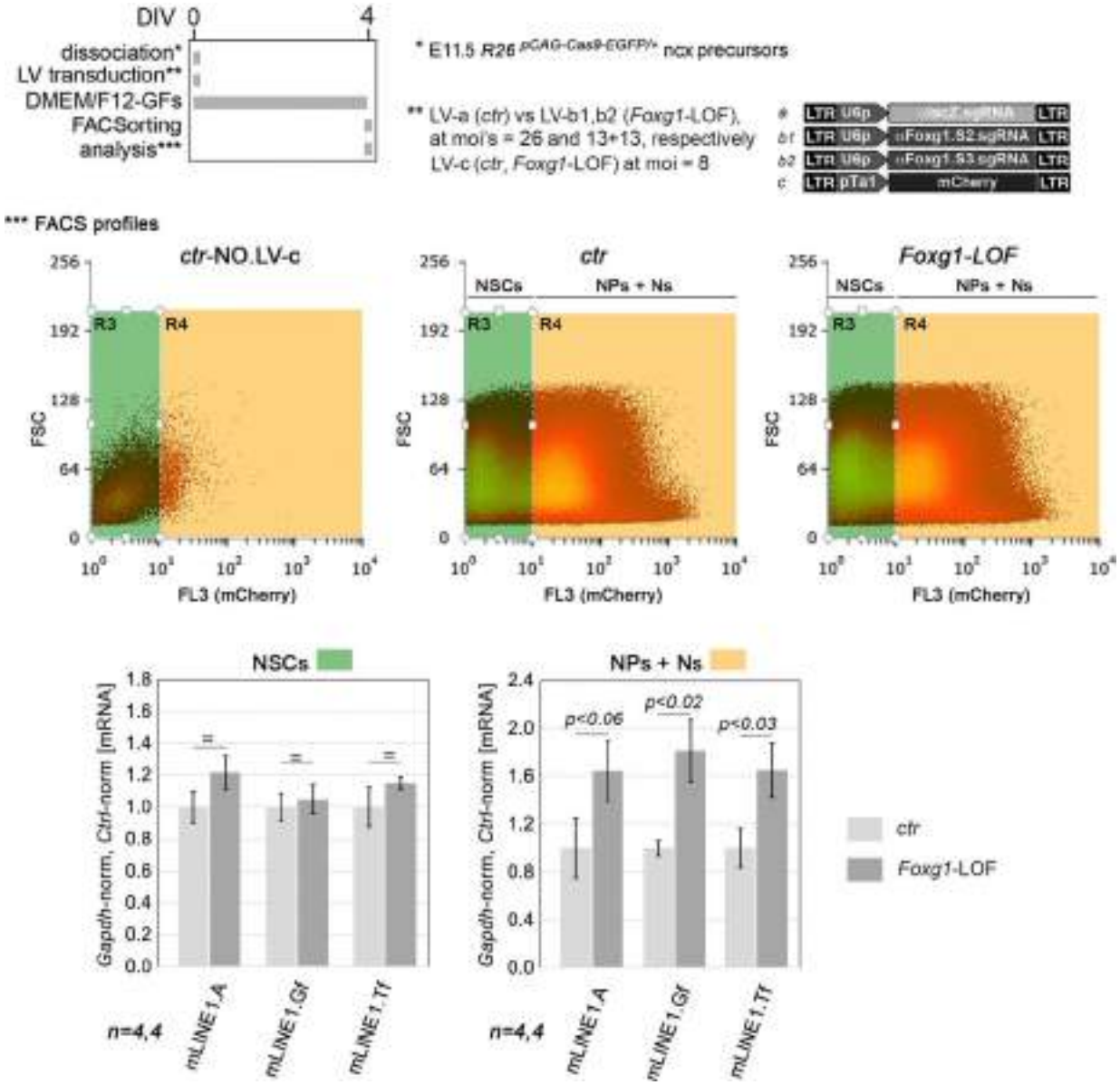

Fig. 8. Assessing *mL1*-mRNA dynamics in *Foxg1*-LOF vs control, NSC and neurono-genic (NP + N), sorted populations. To top, the experimental protocol, with details of neocortical (ncx) precursors and lentiviral vectors employed, as well as FSC/FL3 distributions of FACsorted cells. Of note, Foxg1 was constitutively knocked-down by a genetically encoded Cas9 nuclease programmed by two sgRNAs (aFoxg1.S2 and aFoxg1.S3). Non-NSC, neuronogenic committed cells, including NPs, neuronal progenitors, and Ns, postmitotic neurons, were labelled by a lentiviral mCherry transgene driven by the Tubulin-a1 promoter (pTa1). A stringent R3 gate, based on distribution of mCherry-untransduced cells, was applied for "clean" isolation of NSCs. To bottom, results of qRTPCR profiling of sorted cells, normalized

Development • Accepted manuscript

against *Gapdh* and further normalized against controls. Error-bars representing sem's. Statistical significance of results evaluated by t-test (one-tailed, unpaired). *n* is the number of biological replicates, i.e. independently cultured and engineered cell aliquots, originating from pooled *R26*$^{pCAG\text{-}Cas9\text{-}EGFP/+}$ E11.5 neocortical primordia.

Development • Accepted manuscript

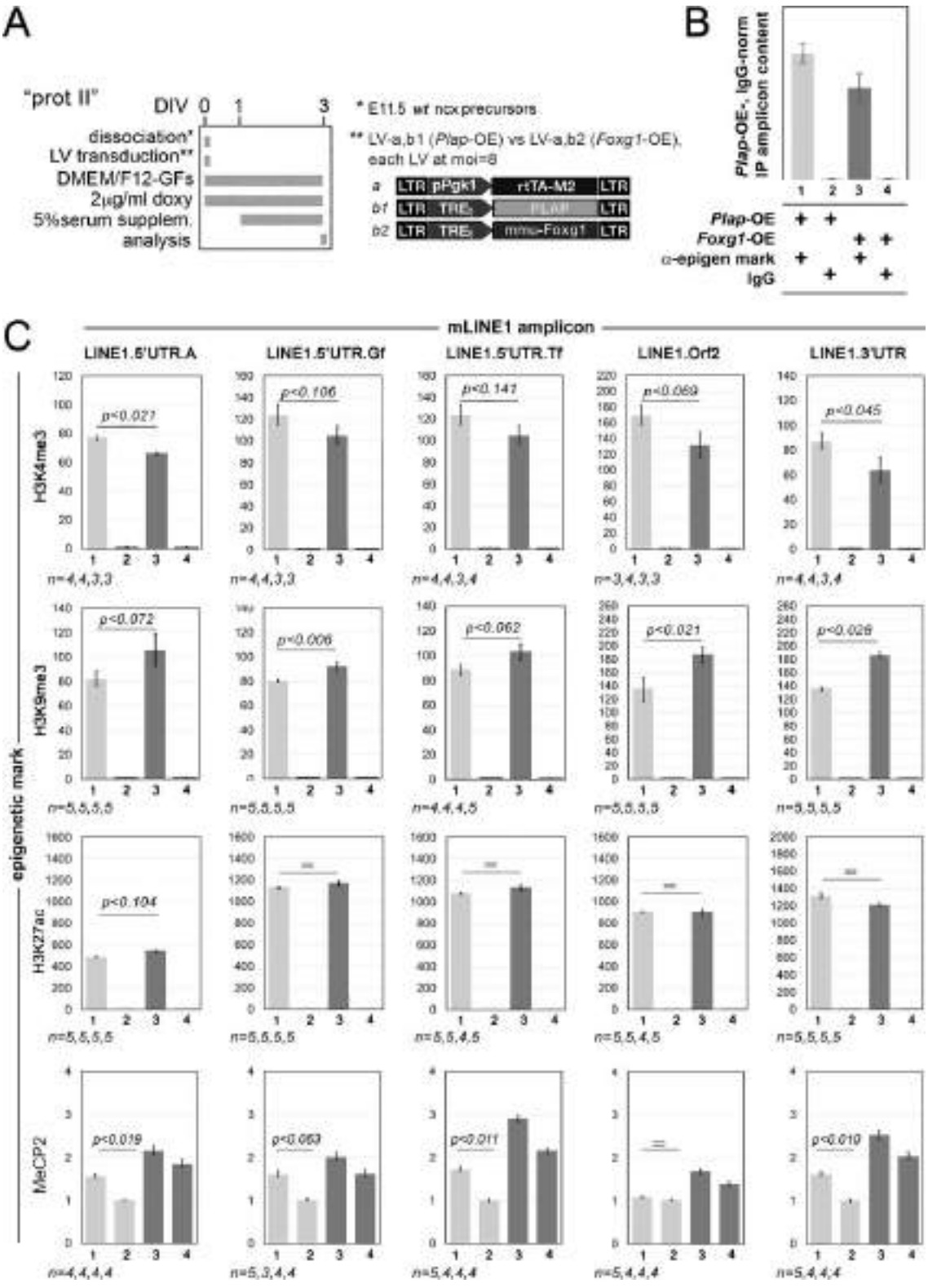

Fig. 9. Chromatin immunoprecipitation (ChIP) profiling of H3K4me3, H3K9me3, H3K27ac, and MeCP2 enrichment at *L1* elements. In (**A**), protocols and lentiviral vectors employed, in (**B**) an illustrative prototype of results presentation, in (**C**) results. Analyses run in mid-neuronogenic cultures, set according to a type II protocol. Cultures constitutively

Development • Accepted manuscript

overexpressing *Foxg1* (or a *Plap* control), driven by the pPgk1 promoter. Chromatin immunoprecipitation performed by αH3K4me3, αH3K9me3, αH3K27ac, and αMeCP2 antibodies and their isotypic IgG controls. PCR quantitation of pan-*L1* diagnostic amplicons "*L1*.orf2" and "*L1*.3'UTR", and family-specific "L1.5'UTR amplicons", ".A", ".Gf" and ".Tf". Results normalized against input chromatin. Scalebars, sem's. Statistical evaluation of results by t-test (one-tail, unpaired). *n* = number of biological replicates, i.e. independently cultured and engineered cell aliquots originating from a common neural precursor pool.

Development • Accepted manuscript

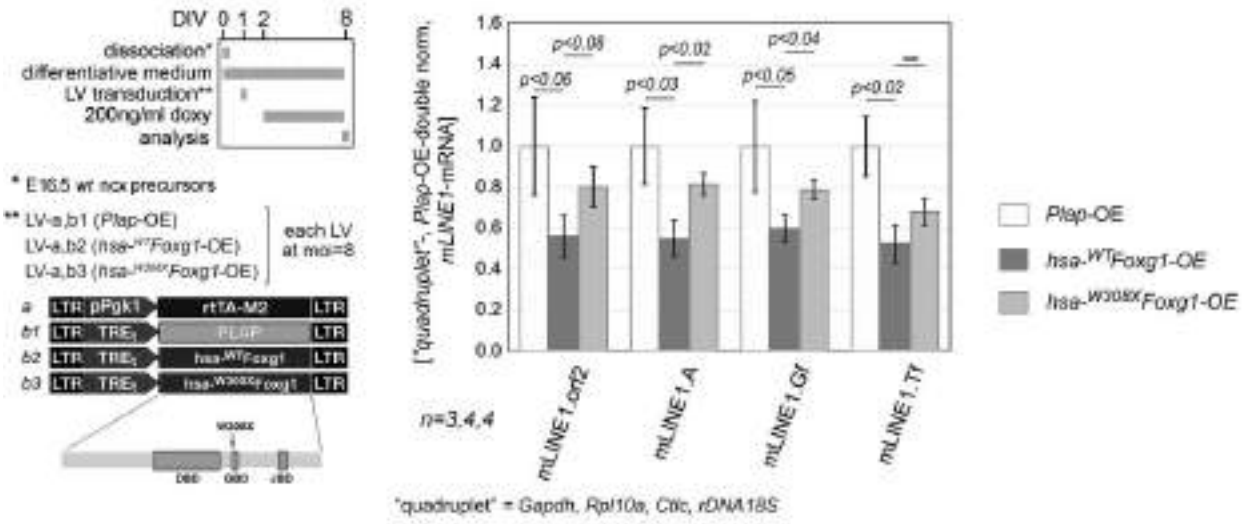

Fig. 10. Modulation of *L1*-mRNA levels in primary, neuron-enriched murine cultures overexpressing the human, wild-type and mutant, *hsa-*^{WT}*Foxg1* and *hsa-*^{W308X}*Foxg1* alleles. To left, protocol and lentiviral vectors employed. Transgenes driven by the constitutively firing pPgk1 promoter. The mutant allele in order encodes for a prematurely truncated protein, including the DNA-binding domain (DBD), but not the Groucho- and Jarid-binding domains (GBD and JBD, respectively). RT-PCR quantitation of pan-*L1* diagnostic amplicon "*L1*.orf2", and family-specific amplicons, "*L1*.A", "*L1*.Gf" and " *L1*.Tf", in neural cultures set according to a type II protocol. Data double normalized, against gene quadruplet (*Gapdh*, *Rpl10a*, *Cltc* and *rDNA 18S*) and control values. Error-bars representing sem's. Statistical significance of results evaluated by t-test (one-tailed, unpaired). *n* is the number of biological replicates, i.e. independently cultured and engineered cell aliquots, originating from pooled, *wild-type* E16.5 neocortical primordia.

Development • Accepted manuscript

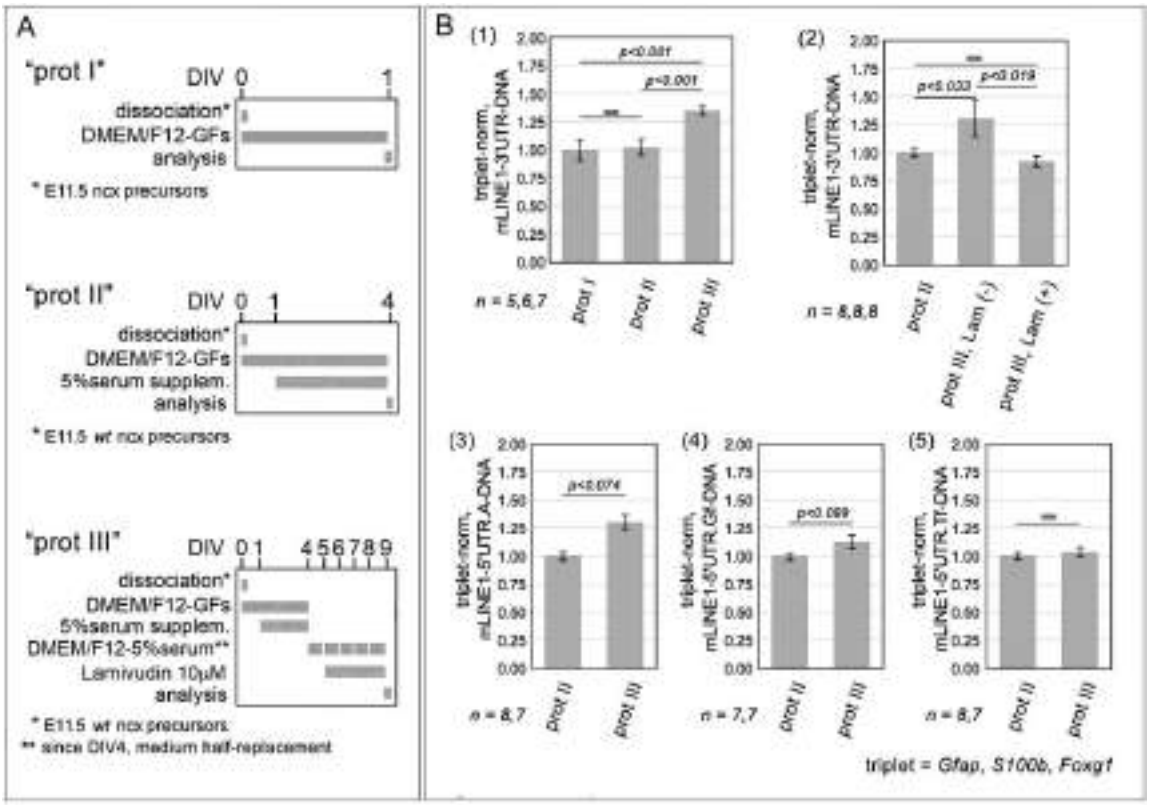

Fig. 11. *L1* DNA copy number variations (CNVs) in early- mid- and late-neuronogenic murine pallial cultures. (A) protocols, **(B)** results. Early- mid- and late-neuronogenic cultures set by means of type I, II and III protocols, respectively. DNA extraction performed by "high PK" (1) and "very high PK" procedure (2-4) (see Materials and Methods). DNA CNVs assessed by quantitative PCR, followed by normalization against endogenous *Gfap*, *S100b* and *Foxg1* (gene "triplet"). In graph (1), shown is the total *L1* copy number detectable in late- and mid- normalized against early-neuronogenic cultures. In graph (2), shown is the suppression of *L1* copy number variation which normally occurs between "mid-" and "late-neuronogenic" cultures, elicited by the pan-RT inhibitor lamivudine (aka 3T3). Finally, in graphs (3-5), as controls, shown are comparisons of family-specific, DNA copy numbers, as detected by "5'UTR.A", "5'UTR.Gf" and "5'UTR.Tf" diagnostic amplicons. Error-bars representing sem's. Statistical significance of results evaluated by t-test (one-tailed, unpaired). *n* is the number of biological replicates, i.e. independently cultured and engineered cell aliquots, originating from pooled, *wild-type* E11.5 neocortical primordia.

Development • Accepted manuscript

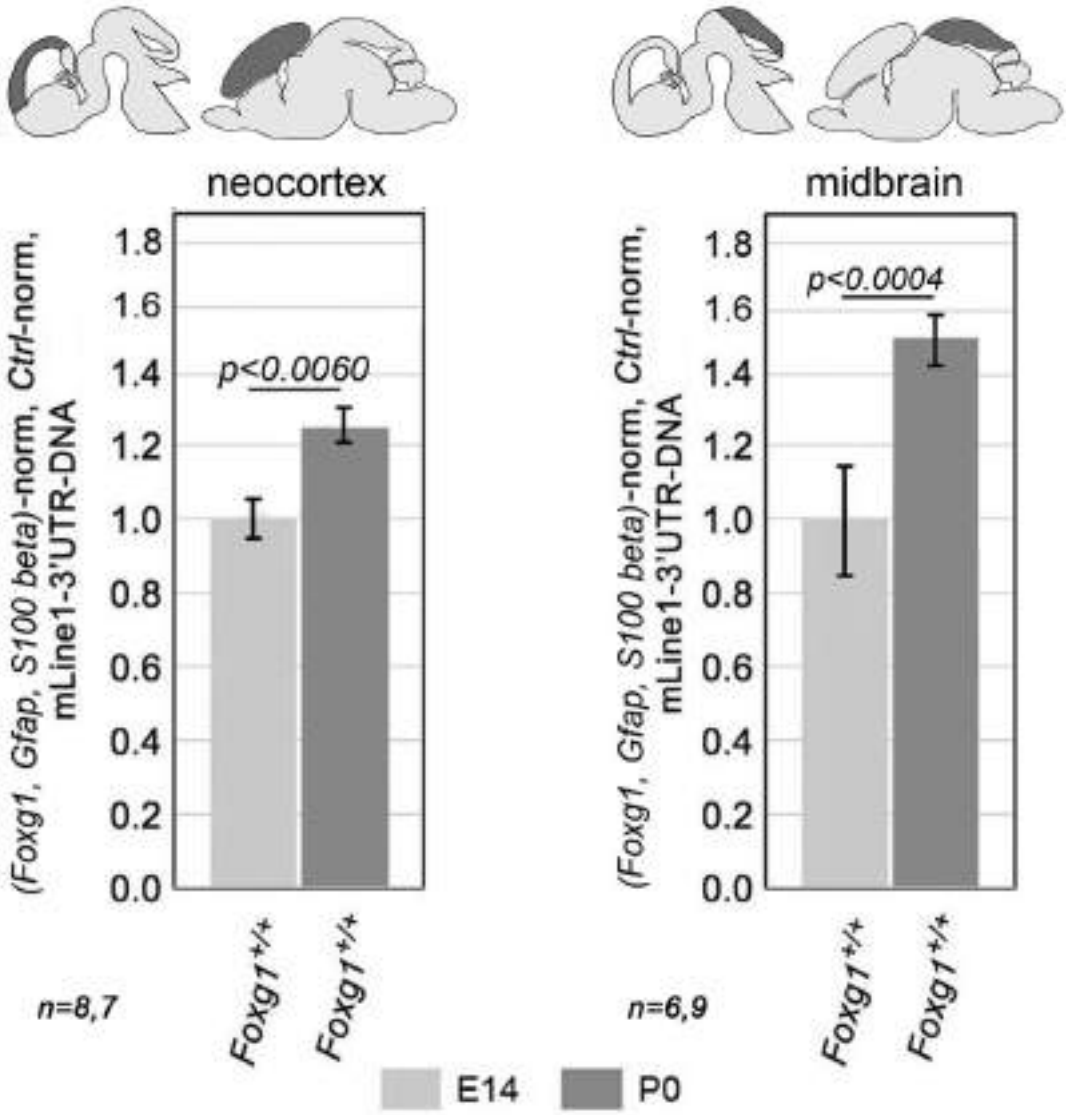

Fig. 12. *L1* DNA copy numbers in neocortex and tectum of wild type, mid-neuronogenic and perinatal mice. PCR quantitation of the pan-*L1* diagnostic amplicon "*L1*.3'UTR". Data normalized against the *Foxg1/Gfap/Nfia* gene triplet. Error-bars representing sem's. Statistical significance of results evaluated by t-test (one-tailed, unpaired). *n* is the number of biological replicates, i.e. neocortices taken from distinct pups.

Development • Accepted manuscript

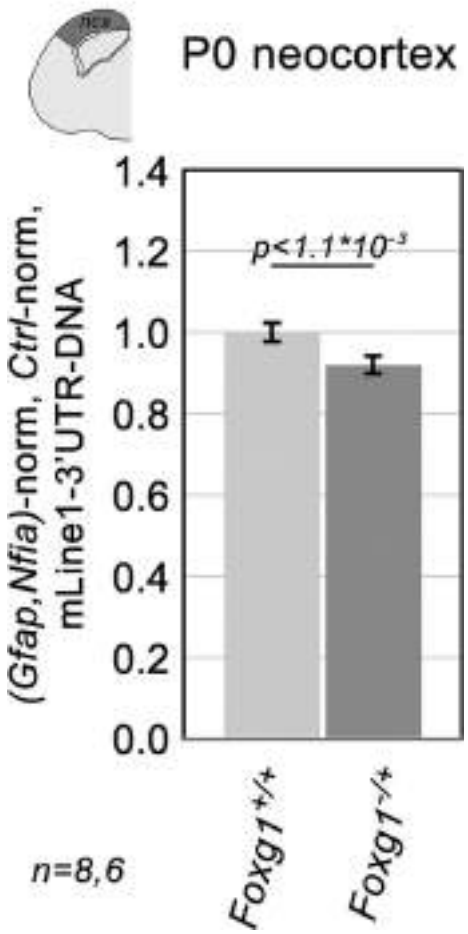

Fig. 13. *L1* DNA copy numbers in neocortex of *Foxg1*$^{-/+}$ mouse neonates and controls. PCR quantitation of the pan-*L1* diagnostic amplicon "*L1*.3'UTR". Data double normalized against the *Gfap/Nfia* gene doublet, and wild-type controls. Error-bars representing sem's. Statistical significance of results evaluated by t-test (two-tailed, unpaired). *n* is the number of biological replicates, i.e. neocortices taken from distinct pups.

Development • Accepted manuscript

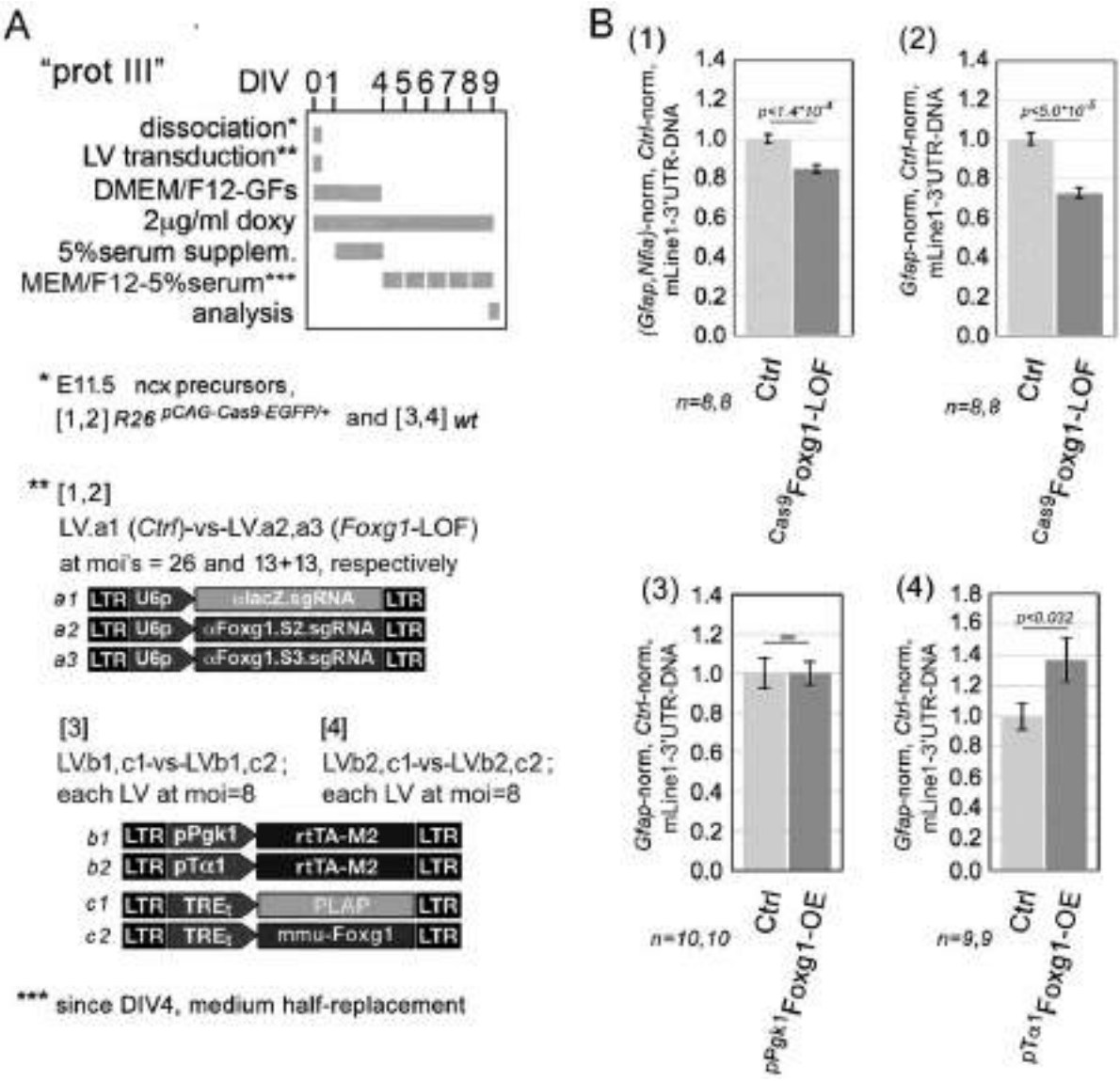

Fig. 14. Impact of *Foxg1*-knock-down (KD) and *Foxg1*-OE on *L1* DNA copy numbers in late-neuronogenic pallial cultures. In (**A**), protocols (with lentiviruses employed), in (**B**) results. CRISPR-Cas9 machinery driven by constitutively active U6p (sgRNAs) and R26/pCAG (Cas9) promoters, Foxg1 transgene led by constitutive Pgk1p and NP/N-restricted pTa1. Neural cultures set according to a "type III" protocol. Assesment of total L1 copies by quantitation of the "*L1*.3'UTR" amplicon. Data double-normalized, against *Gfap* (or the *Gfap/Nfia* gene doublet) and control values. Error-bars representing sem's. Statistical significance of results evaluated by t-test (one-tailed, unpaired). *n* is the number of biological replicates, i.e. independently cultured and engineered cell aliquots, originating from pooled, *R26*$^{pCAG\text{-}Cas9\text{-}EGFP/+}$ (1,2) and *wild-type* (3,4), E11.5 neocortical primordia.

Development • Accepted manuscript

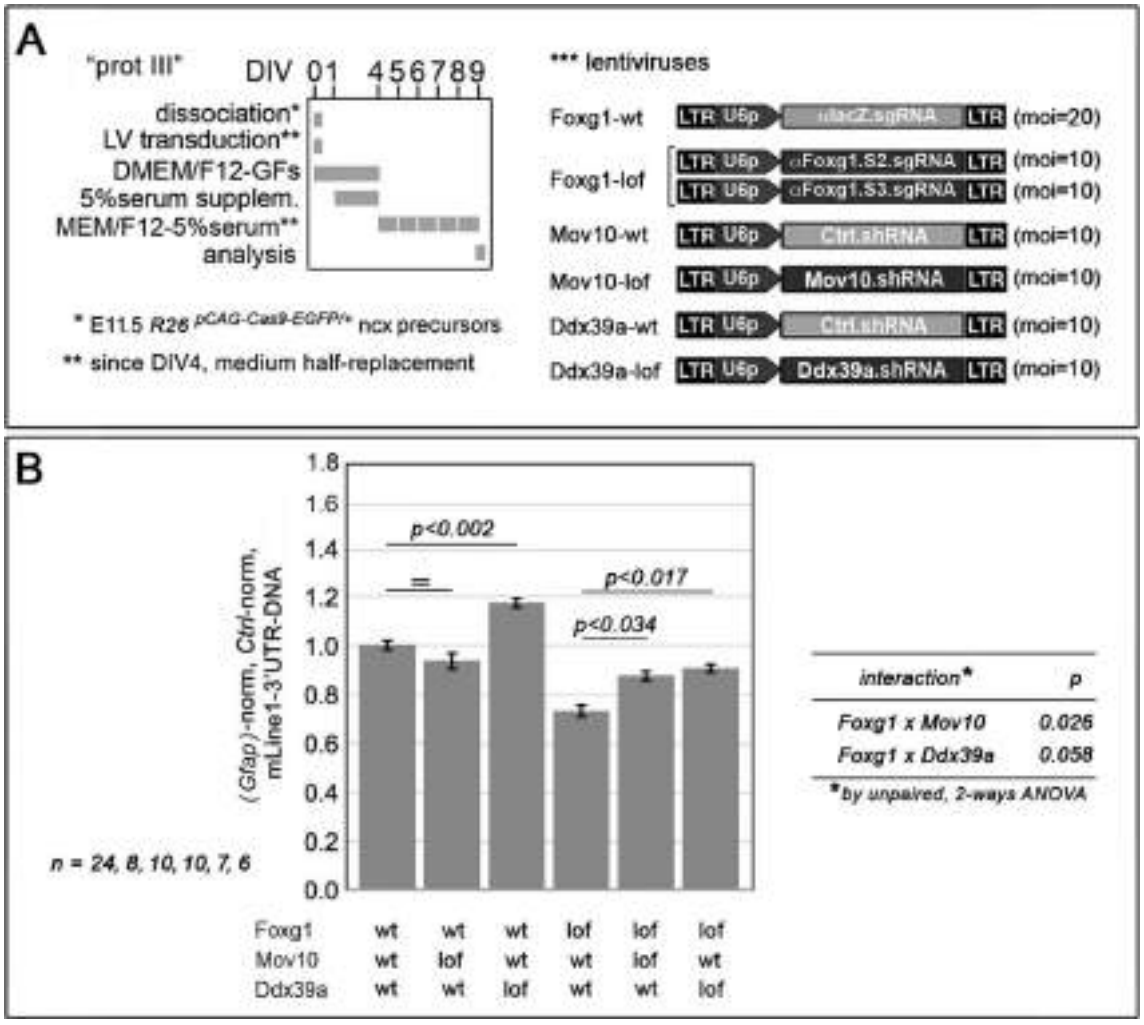

Fig. 15. Functional interaction among *Foxg1* and helicase genes *Mov10* and Ddx39a in modulation of L1 copy number. In (**A**), protocols (with lentiviruses employed). In (**B**) shown is the impact exerted by *Mov10* and *Ddx39a* downregulation, in *Foxg1*-wt and *Foxg1*-LOF environments, on L1 copy number, as evaluated in late-neuronogenic cultures by qPCR**.** Data double-normalized, against *Gfap* and control values. n is the number of biological replicates, i.e. independently cultured and engineered preparations, originating from a common neural cell pool. Statistical evaluation of results performed by t-test, one-tailed and unpaired, as well as by, unpaired, 2-ways ANOVA. Errors bars indicate s.e.m.

Development • Accepted manuscript

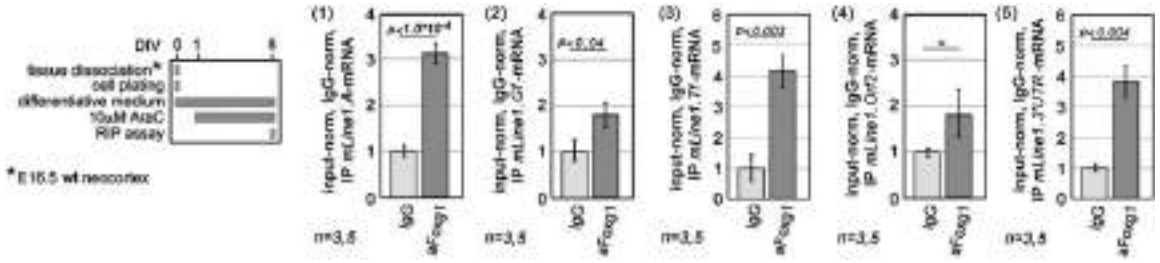

Fig. 16. Foxg1-protein/*L1*-mRNA interaction in neocortical neurons, as evaluated by RNA immunoprecipitation-quantitative PCR (qRIP-PCR) assay. To left, protocol, to right, results. Diagnostic amplicons, L1.5'UTR.A (1), L1.5'UTR.Gf (2), L1.5'UTR.Tf (3), L1.orf2 (4), and L1.3'UTR (5). Results double normalized, against input-RNA and IgG-IP samples. Througout figure, n is the number of biological replicates, i.e. independently cultured and engineered preparations, originating from a common neural cell pool. Statistical evaluation of results performed by t-test, one-tailed and unpaired. Errors bars indicate s.e.m.

Development • Accepted manuscript

Table 1. Primer sequences and mL1 thermal reaction profiles.

The following oligonucleotide pairs have been employed in this study:

Rpl10a/F,R

5’ CAG CAG CAC TGT GAT GAA GCC AAG G 3’

5’ GGG ATCT GCT TAA TCA GAG ACT CAG AGG 3’

mGapdh/F,R

5’ ATC TTC TTG TGC AGT GCC AGC CTC GTC 3’

5’ GAA CAT GTA GAC CAT GTA GTT GAG GTC AAT GAA GG 3’

mmuCltc/F,R

5' CTT GCT CAG CGT TTG GAA AAA CAC GAA CTC AT 3'

5' GCC AAT TCT GTG TCT TTA GAT TCA GAG GCA TAC 3'

mmuRn18s/F,R

5' AAT TGA CGG AAG GGC ACC ACC AGG AGT 3'

5' GCC ATG CAC CAC CAC CCA CGG AAT C 3'

Foxg1(cds)/F,R

5’ GAC AAG AAG AAC GGC AAG TAC GAG AAG C 3’

5’ GAA CTC ATA GAT GCC ATT GAG CGT CAG G 3’

Foxg1(Mid)/F,R

5’ GAC AAG AAG AAC GGC AAG TAC GAG AAG C 3’

5’ GAA CTC ATA GAT GCC ATT GAG CGT CAG G 3’

Couptf1_Foxg1-BS.a/F,R

5’ CCA TCT GAA TGC AAA ACG TAA GCA TG 3'

5’ ATG GAC CTC GCT CTA CTA ATT TGT TGG 3'

Gfap_Foxg1-BS.b/F,R

5’ GCA GGA ACT CCT GAG GCT GGC AGC ATT 3'

5 GTG TAA ACA AAA TTA CAG GAG CTT GTG TTG AAC TTG C 3'

Nfia_Foxg1-BS.h1/F,R

5’ CAG AAC TTG GTG GAT GGT GAG TTG GCA G 3'

Development • Accepted manuscript

5’ TGT GAG TTT GAT GAA TGT GAG GTC TGG GAC 3'

S100b_Foxg1-BS.x2/F,R

5’ TTG TGA GCC ACC CAA TGT GGT TCT GG 3'

5’ CCA CAA ATG TGT TGG AAA GAT ATA ACT CAA AG 3'

Sox9_Foxg1-BS.h1/F,R

5’ CCG TGA TTG GCC CGA GGT ATC TAA CGT G 3'

5’ AGT TGT CGC TCC CAC AGA AGT TTC CAG G 3'

A5utr.t3L(oM)/F,R

5' GAA TAC TCT GCC CAC TGA AAC TAA GGA GA 3'

5' GTT AAG AGC TTG TTC TTC AGG TGA CTC TGT 3'

Gf5utr.t3L(oM)/F,R

5' GGA GGT CCA AAC ACC AGA TAA CTG TAC ACC 3'

5' AGC AGG CGT GGG AGA CAA GCT CTC TT 3'

Tf5utr.t1L(M)/F,R

5' GAG AGT CTG TAC CAC CTG GGA ACT GC 3'

5' CCG AAG AAG AAG GCC CAA AAC AGG AC 3'

Orf2/F,R *

5' AGC TTT YAT YCC AGG GAT GCA GGG AT 3’

5' TGG GTG TTG GAT MTT GTC AAA TGC TT 3’

* Y = C or T; M = A or C

AM.mL1-pan3utr/F,R

5' GGT GGA ACA ACA TTA TGA ACT AAC CAG TAC C 3'

5' CCA ATG GGC CTC TCT TTC CAG TGA TG 3'

Cdkl5/F,R

5' GCA CTA CTT GAA AAT AAA GGA CGA AGG ATG GC 3’

5' CAG GCT GCG AGA TGA ACG TGA ATA TGA 3’

MeCP2/F,R

5' GTC CCC TGC CCA CAC TAA GTA TGA CAT 3’

5' GGG TCA CAT TGG GTA GCT GAA GGA GAT 3’

Development • Accepted manuscript

Uty/F,R

5' TGC TAT ACT GAT CTC ACA AGG AAC AAA GAG CA 3’

5' GGA GCA CCG ATT CTG GGA ACT TAA CAG 3’

NB. mL1 amplicons were quantified by PCR, run on a BioRad CFX96 thermocycler, according to the following thermal reaction profiles:

- *5'UTRs*

1x(98°C/4min); 40x(98°C/10sec, 68.4°C/15sec, 72°C/10sec, 74°C/3sec); 1x(72°C/10min)

- *orf2 & 3'UTR*

1x(98°C/4min); 40x(98°C/10sec, 68.4°C/15sec, 72°C/20sec, 74°C/3sec); 1x(72°C/10min)

Development • Accepted manuscript

Table 2. Lentiviruses list.

The lentiviruses (LVs) were used for this study were named according to the standard nomenclature: LV: pX-GOI, where pX is the promoter and GOI is the gene of interest. They were:

LV_pPgk1-rtTA2S-M2 (Spigoni et al., 2010)

LV_pNes-rtTA-M2, aka pNes/hsp68-rtTA2S-M2 (Brancaccio et al., 2010)

LV_pTα1-rtTA2S-M2 (Brancaccio et al., 2010)

LV_pSyn-rtTA2S-M2 (Tigani et al., 2020)

LV_TREt-PLAP (Falcone et al., 2019)

LV_TREt Foxg1 (Raciti et al., 2013)

LV_pU6 shFoxg1 (Sigma TRCN0000081746, in pLKO.1)

LV_pU6 shCtrl (Chiola et al., 2019)

LV_pTα1-mCherry (Brancaccio et al., 2010)

LV_pU6 shMov10 (Sigma TRCN0000097832, in pLKO.1)

LV_pU6 shDdx39a (Sigma TRCN0000071093, in pLKO.1)

LV_U6p-αLACZ.sgRNA [obtained by cloning the TGCGA ATACG CCCAC GCGAT guide (Platt et al., 2014) into BsmBI-cut, lentiCRISPR_v2ΔEB; lentiCRISPR_v2ΔEB was previously obtained starting from lentiCRISPR_v2 (Addgene #52961), deleting the EF1a-prom-Cas9 fragment by EcoRI/BamHI digestion, filling-in and religating]

LV_U6p-α Foxg1. S2.sgRNA sgRNA [obtained by cloning the GCCCG TCGGG CCGGA CGAGA guide (Mall et al., 2017) into BsmBI-cut, lentiCRISPR_v2ΔEB]

LV_U6p-αFoxg1. S3. sgRNA [obtained by cloning the CCCCG ACGCC TGGGT GATGC guide (Mall et al., 2017) into BsmBI-cut, lentiCRISPR_v2ΔEB]

LV_TREt-hsaFOXG1wt [built by transferring the AgeI-SalI fragment from pUC57 “hsaF1WT” (provided us on a commercial basis by Gene Universal) into the AgeI-SalI digested LV_TREt-IRES2- EGFP (Falcone et al., 2015)].

Development • Accepted manuscript

LV_TREt-hsaFoxg1(W308X) [built by transferring the AgeI-XhoI fragment from pUC57 “hsaF1-W308X” (provided us on a commercial basis by Gene Universal) into the AgeI-SalI digested LV_TREt-IRES2-EGFP (Falcone et al., 2015)].

NB. To build the last six LVs mentioned above, DNA manipulations (extraction, purification and ligation), bacterial cultures and transformations were performed according to standard methods. Restriction and modification enzymes were obtained from New England Biolabs and Promega; DNA fragments were purified from agarose gel by QIAquick Gel Extraction Kit (Qiagen); plasmid preparations were performed through DNA Plasmid Purification Kit (Qiagen). Plasmids were grown in E. Coli, Xl1-blue or ElectroMAX™ Stbl4™ Competent Cells (Invitrogen).

Development • Accepted manuscript

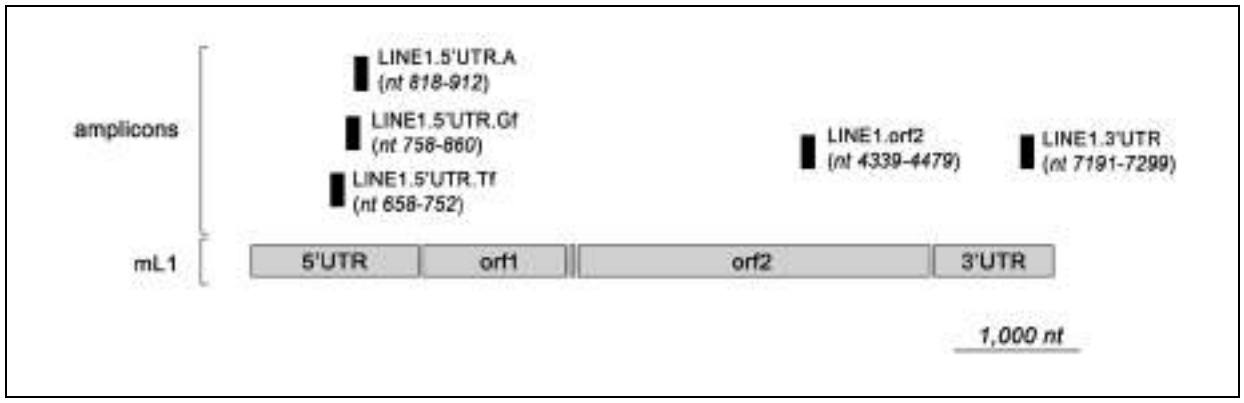

Fig. S1. Mapping diagnostic amplicons to mLINE1 elements. Shown are the five amplicons employed in this study and their locations. Coordinates refer to an idealized mLINE1 element obtained by juxtaposing: (a) Clustal Omega alignement of subfamily specific 5'UTRs (Dfam DF0001807, DF0001809, DF0001811, DF0001816, DF0001819, DF0001821, DF0001823, DF0001849, DF0001851, DF0001864, DF0001866 and DF0001868), (b) Clustal alignement of subfamily specific orf1 & orf2 elements reported in "Sookdeo et al (2013), doi: 10.1186/1759-8753-4-3, Additional File 1", and (c) Clustal Omega alignement of subfamily specific 3'UTRs (Dfam DF0001806, DF0001808, DF0001810, DF0001815, DF0001818, DF0001820, DF0001822, DF0001848, DF0001850, DF0001863, DF0001865, and DF0001867).

Development • Supplementary information

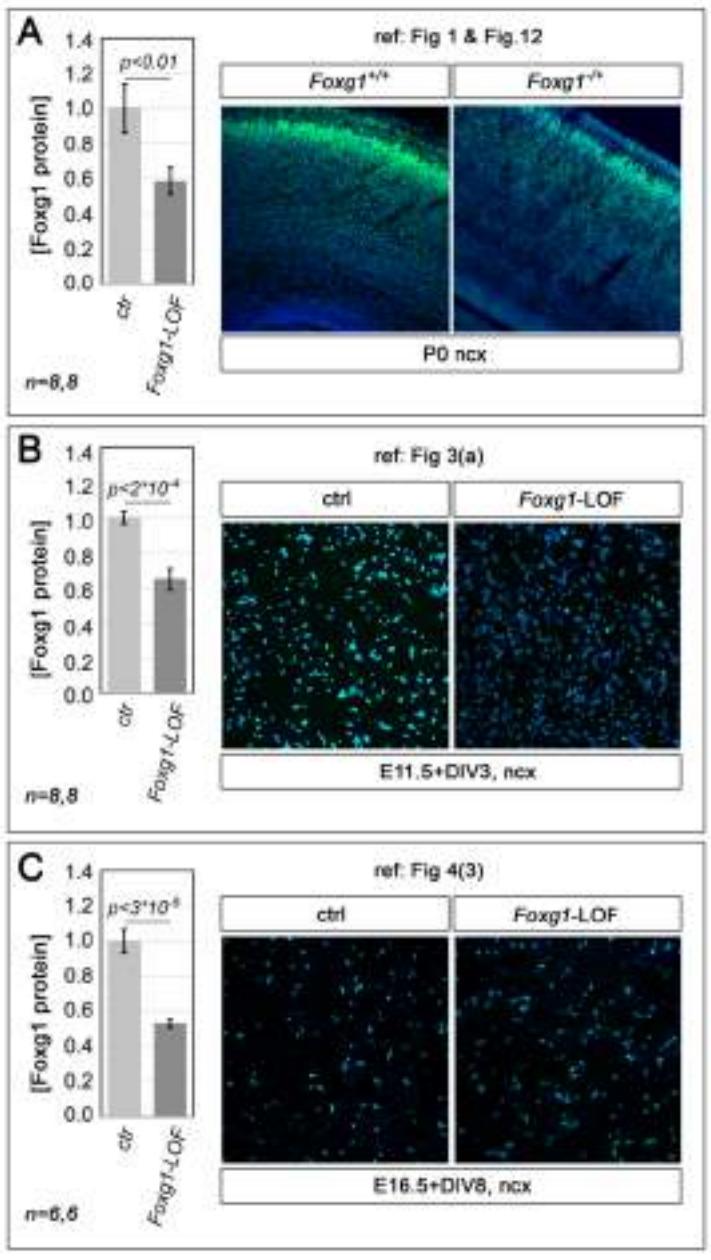

Development • Supplementary information

Figure S2

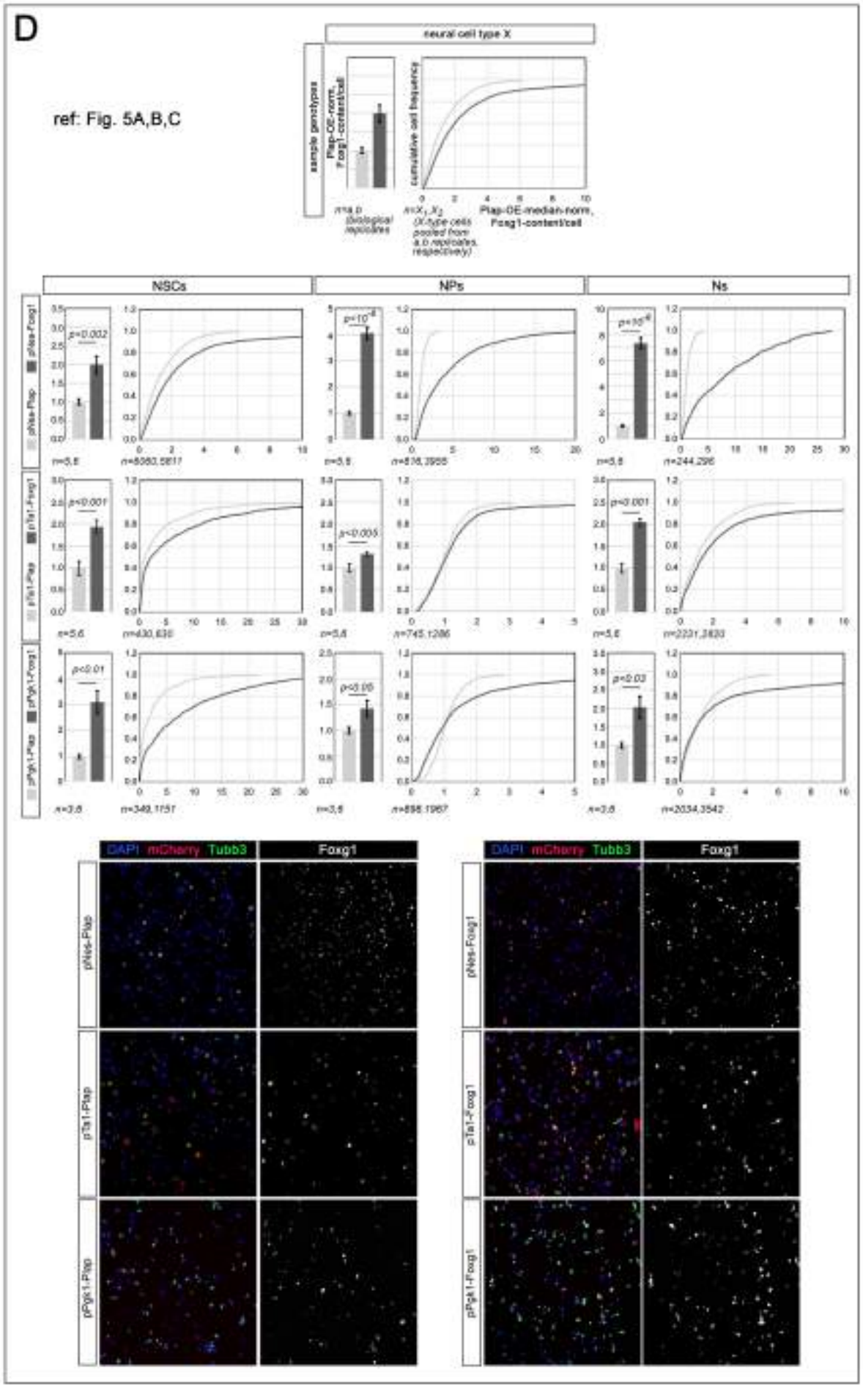
D
ref: Fig. 5A,B,C
neural cell type X
sample genotypes
Ptap-DE-norm, Foxg1-content/cell
cumulative cell frequency
n=4,5 (biological replicates)
n=X1,X2 (X-type cells pooled from 4,5 replicates, respectively)
Ptap-DE-median-norm, Foxg1-content/cell
NSCs
NPs
Ns
pNes-Ptap
pNes-Foxg1
pTa1-Ptap
pTa1-Foxg1
pPgk1-Ptap
pPgk1-Foxg1
p=0.002
p=10-6
p=0.001
p<0.005
p<0.01
p<0.05
p=0.03
n=5,6
n=5060,5811
n=576,3955
n=244,296
n=430,630
n=745,1286
n=2231,2820
n=3,6
n=349,1751
n=696,1967
n=2034,3542
DAPI mCherry Tubb3
Foxg1

Fig. S2. Foxg1 protein dynamics upon selected LOF- and GOF- manipulations. Here, reported are control-normalized Foxg1 protein levels in selected experiments of this study, each with reference Figures and panels, and indicative examples of the corresponding immunofluorescences. To note, Foxg1 protein downregulation was achieved by heterozygosity for a *Foxg1*-null allele (**A**), Cas9/sgRNA-driven knock-down (**B**) and shRNA-driven interference (**C**), Foxg1 protein upregulation by Tet^{ON}-controlled expression of a Foxg1-encoding transgene, driven by pNes, pTa1 and pPgk1 promoters (**D**). In case of overexpression assays, in addition to quantifications of average expression levels peculiar to distinctive neural cell types (NSCs, NPs, and Ns), shown also are cumulative distributions of protein levels displayed by single cells of different neural types. In such case, for the sake of clarity, a graph prototype with parameters represented in *x* and *y* is reported at the top of the panel. Error-bars representing sem's. Statistical significance of results evaluated by t-test (one-tailed, unpaired). *n* generally is the number of biological replicates, i.e. mouse individuals (A) and independently cultured and engineered cell aliquots, originating from pooled, *wild-type* E16.5 (B,C) or E11.5 (D) neocortical primordia. In the only case of graphs representing cumulative distributions (D), *n* is the number of cells pooled from distinctive biological replicates of each sample.

Development • Supplementary information

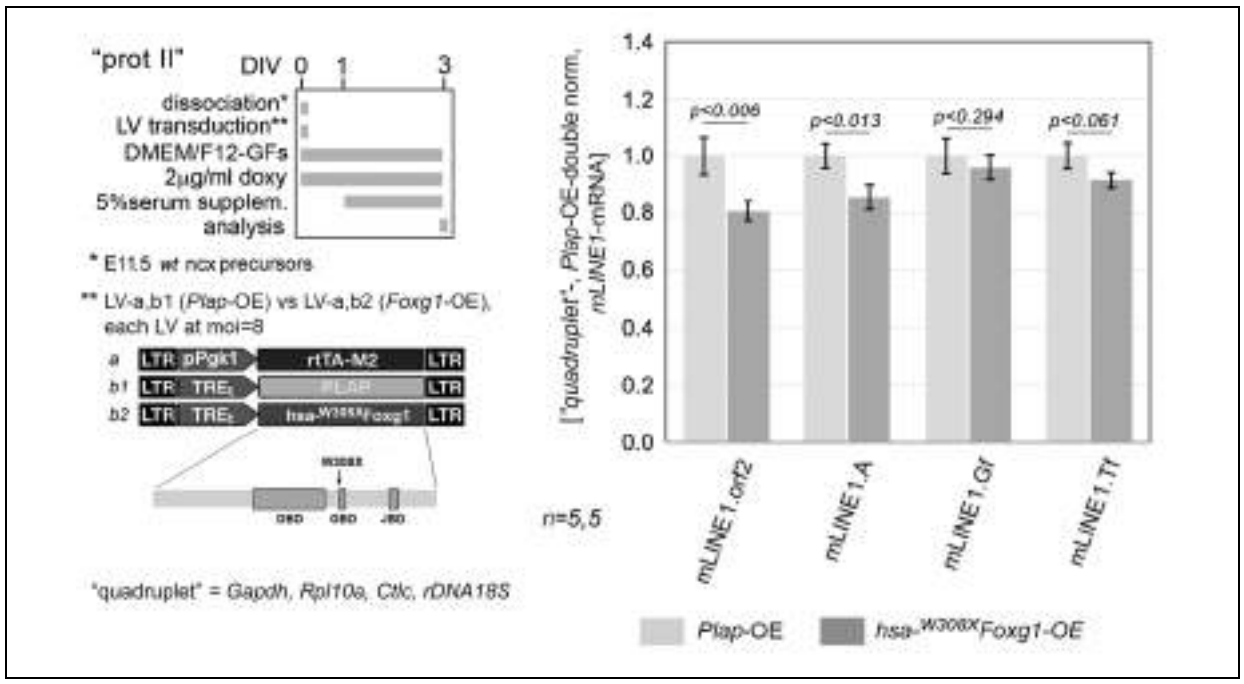

Fig. S3. Modulation of *L1*-mRNA levels in murine mid-neuronogenic pallial cultures overexpressing the *hsa-*^{W308X}*Foxg1* mutant allele. To left, protocol and lentiviral vectors employed. Transgenes driven by the constitutively firing pPgk1 promoter. The human (hsa) mutant allele in order encodes for a prematurely truncated protein, including the DNA-binding domain (DBD), but not the Groucho- and Jarid-binding domains (GBD and JBD, respectively). RT-PCR quantitation of pan-*L1* diagnostic amplicon "*L1*.orf2", and family-specific amplicons, "*L1*.A", "*L1*.Gf" and " *L1*.Tf", in neural cultures set according to a type II protocol. Data double normalized against gene quadruplet (*Gapdh*, *Rpl10a*, *Cltc* and *rDNA 18S*) and control values. Error-bars representing sem's. Statistical significance of results evaluated by t-test (one-tailed, unpaired). *n* is the number of biological replicates, i.e. independently cultured and engineered cell aliquots, originating from pooled, *wild-type* E11.5 neocortical primordia.

Development • Supplementary information

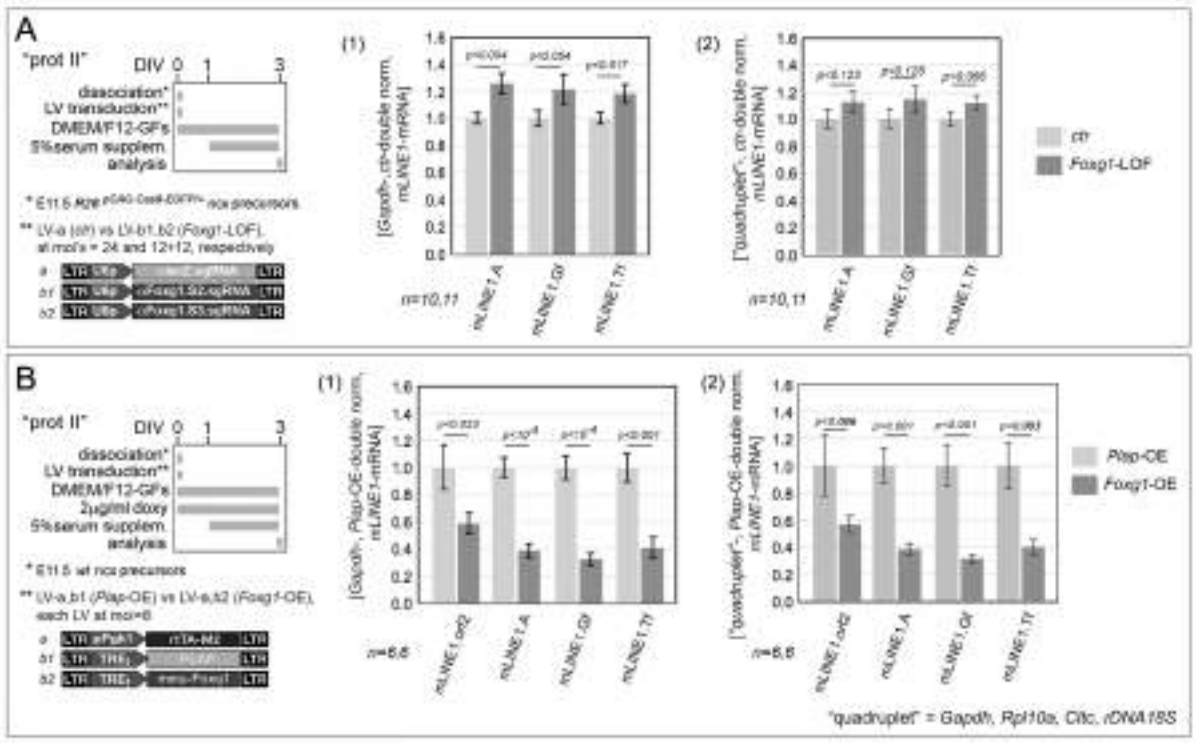

Fig. S4. Comparative evaluation of "quadruplet-" vs *Gapdh*-normalization of *L1*-mRNA expression levels. In (A) and (B) shown are data referred to in Fig. 3A and 3D, respectively, upon alternative normalization against *Gapdh* (1) and gene "quadruplet" (2).

Development • Supplementary information

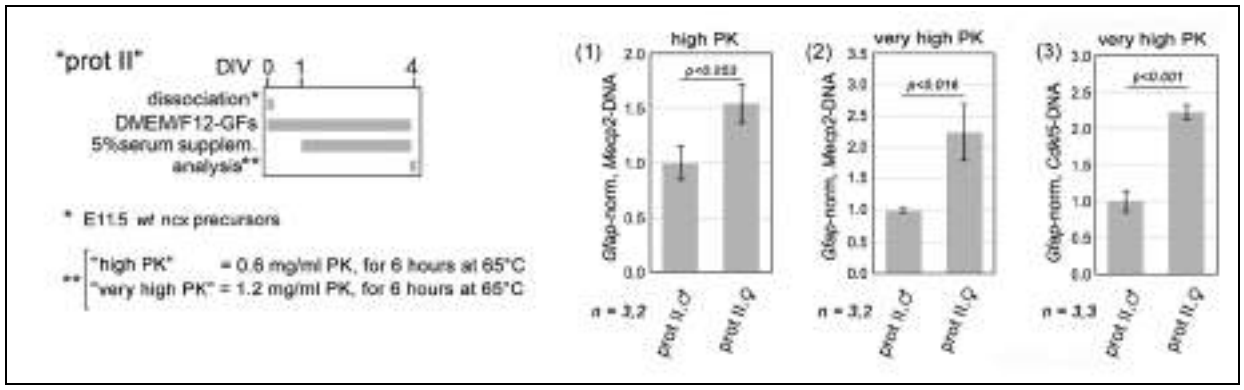

Fig. S5. Optimization of genomic DNA extraction. To left, protocol. Mid- neuronogenic cultures set by means of type II protocols. DNA extraction performed by a strong ("high PK", see Materials and Methods) or a very strong procedure ("very high PK", see Materials and Methods). To right, results. Graphs (1-3) providing a comparative assessment of "high PK" and "very high PK" procedures for their capability to extract with similar efficacy genomic DNA, regardless of chromatin accessibility. Such assesment was done by quantifying X-chromosomal *Mecp2* and *Cdkl5* sequences, amplified from female and male genomic DNA, and normalizing them against the euchromatic *Gfap* autosomal locus. Error-bars representing sem's. Statistical significance of results evaluated by t-test (one-tailed, unpaired). *n* is the number of biological replicates, i.e. independently cultured and engineered cell aliquots, originating from pooled, *wild-type* E11.5 neocortical primordia.

Development • Supplementary information

Table S1. Validating LINE1-diagnostic PCR primers. Sequences of DNA strings amplified by distinctive, family-specific (5'UTR) and shared (3'UTR), LINE1 primers were aligned by Clustal Omega and further processed to generate experimental, SEQ.A.x, SEQ.Gf.x, SEQ.Tf.x and SEQ.3'UTR.x consensuses. Similarly, subfamily specific LINE1 5'UTR and 3'UTR sequences harvested from Dfam database (listed in Legend to Fig. S1) were aligned by Clustal Omega and further processed to generate family-specific DFAM.A, DFAM.Gf and DFAM.Tf consensuses, as well as a shared DFAM.3'UTR consensus. Finally, each SEQ consensus was aligned against the corresponding DFAM consensus. Throughout the table, nucleotide numbers refer to the outputs of Clustal Omega alignments among Dfam consensus sequences.

```
[1] A family-specific primers: A5utr.t3L(oM)/F, A5utr.t3L(oM)/R
SEQ.A.x       GAATACTCTGCCCACTGAAACTAAGGA--GAGTGCTACCCT-CCAGRTCTGCTYATAGAGGCTAACAGAGTCACCKGAAGAACAAGCTCTTAAC
DFAM.A    818 GAATACTCTGCCCACTGAAACTAAGGA--GAGTGCTACCCT-CCAGGTCTGCTBATAGAGGCTAACAGAGTCACCTGAAGAACAAGCTCTTAAC 912
              ************************************************************************************************

DFAM.Gf   818 GACTGCTCTGACCACTGAAACTCAGAGAAGAGAGCTTGTCTCCCACGCCTGCTGATAGAGGGTAACAAAATCAACAGAGGAACAATCTCTTAAC 912
              ** * ***** *********** **    *** ***   ** *** * ******************* * *** * ** ****** ********

DFAM.Tf   818 GAGTGCTCTGAGCACTGAAACTCAGAGGAGAGAATCTGTCTCCCAGGTCTGCTGATAGACGGTAACAGAATCACCAGAAGAACAATCTCTAAAC 912
              ** * *****  ********** **    *** *     ** ***************** ********* ***** ********* ********

NB. "-" replaced by "C" in LINE1.A.III-VII


[2] Gf family-specific primers: Gf5utr.t3L(oM)/F, Gf5utr.t3L(oM)/R
SEQ.Gf.x      GGAGGTCCAAACACCAGATAACTGTACACCTTCCCTGAGAGAGGAGAGCTTGCCTACAGAGACTGCTCTGACCACTGAAACTCAGAGAAGAGAGCTTGTCTCCCACGCCTGCT
DFAM.A    758 KCTGGTTCGAACACCAGATATCTGGGTACCTGCCTTGCAAGAAGAGAGCTTGCCTGCAGAGARTACTCTGCCCACTGAAACTMAGGAKAGTGCTASYCTC--CCAGGTCTGCT  870
              *  *** * *********** ***   **** ***** **** ******************* * ***** **************   ** *    * **  *** * *****

DFAM.Gf   758 GGAGGTCCAAACACCAGATAACTGTRCACCTTCCCTGARAGAGGAGAGCTTGCCTACAGAGACTGCTCTGACCACTGAAACTCAGAGAAGAGAGCTNGTCTCCCACGCCTGCT  870
              ************************************************************************************************************

DFAM.Tf   758 GGAGGTCCAAAWACAAGATATCTGCGCACCTTC---CCTGTAAGAGAGCTTGCCAGCAGAGAGTGCTCTGAGCACTGAAACTCAGAGGAGAGAATCTGTCTCCCAGGTCTGCT  870
              *********** ** ***** *** * **** *        * ***********  ****** ******** *************** *****   ********* * *****

NB. "T" replaced by "-" in LINE1.Gf.II


[3] Tf family-specific primers: Tf5utr.t1L(M)/F, Tf5utr.t1L(M)/R
SEQ.Tf.x.     GAGAGTCTGTAC------------------CACCTGGGAACTGCCAAAGCAACACAGTGTCTGAGAAAGGTCCTGTTTTGGGCCTTCTTCTTCGG
DFAM.A    658 GAGYKKSSSVGSKGAGTCKCCBGACACCCNCAAGGDNCCWCACRGGAYYCYNCACGNGATCCTAAGACCYYYDGTGAGTGGAWCACAACTTCTGC 752
              *** *** *  *                  **   **  **     *  * **** *  **  *  *   **      ***  *      *  *
DFAM.Gf   658 CCA-MYWKMTTCKRSKMCWGMS---MASYNGSCMSCYTNCNGGCCAAAGCAACACAGCTTCTGGGAAAGATCCTGTTTTGGGCCTTCACCTTCRG 752
                    * * *                    **    * * ********************** ***** ****************  ******
DFAM.Tf   658 GAGAGKSTGTAC------------------CWYCTGGGAACTGCCAAAGCAACACAGYKTCTGAGARAGGYCCTGTTTTGGGCCTTCTTCTTCGR 752
              ************                   ************************************************************

NB. "------------------" replaced by "ACAGAAGCT---GACAGC" in DFAM.Tf.III


[4] 3'UTR primers: AM.mL1-pan3utr/F, AM.mL1-pan3utr/R
SEQ.3'UTR.x       GGTGGAACAACATTATGAACTAACCAGTACCCCDGAGBTCKTGWCTCTWGCTGCATRTGYATCARAAGATGRMCTARTHGGYCATCACTGGAAAGAGAGGCCCATTGG
DFAM.3'UTR        GGYGSAWCAACATTATGARCTAACCAGTACCCCKGAGCTCTTGACTCTAGCTGCATATRYATCAAAAGATGGCCTAGTCGGCCATCACTGGAAAGAGAGGCCCATTGG   108
                  ************************************************************************************************************
```

Table S2. Foxg1-mRNA dynamics upon OE- and LOF-manipulations of this study. Here, reported are control-normalized *Foxg1*-mRNA levels in selected experiments of this study, each with reference Figures and panels, and normalizer gene(s) employed for their evaluation.

ref		*Foxg1-mRNA manipulation*	
Fig. #	*panel, graph*	*ctr-norm Foxg1-mRNA levels*	*normalizer(s)*
1	---	0.64	*Gapdh*
3	A	0.64	*gene quadruplet**
	B	2.74	*gene quadruplet**
	C	3.63	*gene quadruplet**
	D	2.84	*gene quadruplet**
	E	4.02	*gene quadruplet**
4	graph (1)	4.84	*Gapdh*
	graph (2)	4.27	*Rpl10a*
	graph (3)	0.28	*Rpl10a*
8	NSCs	0.59	*Gapdh*
	NPs + Ns	0.40	
13	---	0.64	*Gapdh*
14	B, graph (1)	0.35	*Gapdh*
	B, graph (3)	3.05	*Gapdh*
S3	---	14.08	*"quadruplet"*

**(Gapdh; Rpl10a; Cltc and rDNA 18S)*

Development • Supplementary information

Table S3. "Quadruplet", RNA-pol II-transcribed normalizers: fluctuations of their mRNA levels throughout normal neuronogenesis as well as upon *Foxg1* manipulation in differentiating neurons. (A) Violin plots representing single cell mRNA levels, in pallial apical precursors (AP), basal precursors (BP), early neurons (EN) and late neurons (LN). Downloaded from http://genebrowser.unige.ch/science 2016 (Telley et al., 2016). **(B)** Modulation of average mRNA levels in differentiating neuronal cultures overexpressing *Foxg1* (Artimagnella and Mallamaci, 2020 i.e doi:10.5281/zenodo.3739467).

A

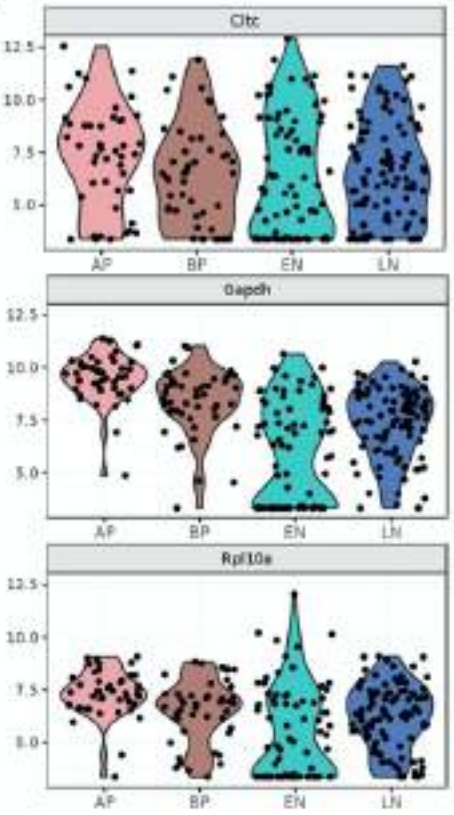

B

Locus	log2FC	logCPM	P-value	FDR	Gene Name
ENSMUSG00000047126	0,01	9,73	0,94	0,96	Cltc

Locus	log2FC	logCPM	P-value	FDR	Gene Name
ENSMUSG00000057666	-0,16	9,44	0,15	0,24	Gapdh

Locus	log2FC	logCPM	P-value	FDR	Gene Name
ENSMUSG00000037805	0,07	6,50	0,68	0,77	Rpl10a

Development • Supplementary information

Table S4. Putative mediators of Foxg1 impact on L1 retro-transcription. Shown are selected genes impacting on L1 retro-transcription/transposition rates, (A) whose mRNA levels are sensitive to Foxg1 overexpression, or (B) whose protein products physically interact with Foxg1 protein.

Foxg1-responsive gene (ref 1)	*impact on retro-transcription/transposition*	*mRNA dynamics upon Foxg1 overexpression in ncx neurons*				
		Locus	*log2FC*	*logCPM*	*P-value*	*FDR*
Apobec1	limits Line1 retrotransposition (ref 2)	ENSMUSG00000040613	-1.01	2.02	0.00	0.00

Foxg1 interactor (ref 3)	*impact on retro-transcription/transposition*	*Foxg1-protein interaction details (Biogrid #)*
MOV10	limits Line1 retrotransposition (ref 4)	1507467
DDX39A	limits Line1 retrotransposition (ref 4)	1507432

REFERENCES

1 doi: 10.5281/zenodo.2849656.
2 doi: 10.1093/nar/gkr124
3 https://thebiogrid.org/
4 doi: 10.1371/journal.pgen.1002941

Table S5. Full primary data
(referring to: Figures 1,2,3,4,5,6,8,9,10,11,12,13,14,15,16,S2,S3,S4,S5)

Figure 1

P0 neocortex

Gadph-norm, Ctr-norm [mRNA]								
	1.00							
	0.87	1.27		1.28	1.17	1.45	1.07	1.44
	0.81	1.05	0.99	0.94	0.97	1.13	0.98	1.03
	1.10	0.97	0.94	1.03	0.87	1.29	0.83	1.05
	0.82	1.24	0.97	1.17	1.07	1.32	1.07	1.26
	0.95	1.21	1.01	1.22	0.85	1.35	0.88	1.10
	1.27	1.36	0.98	1.25	0.99	1.34	1.05	1.24
	1.17	1.28	1.11	1.31	1.07	1.43	1.13	1.34
	Foxg1 (+/+)	Foxg1 (+/-)	Foxg1 (+/+)	Foxg1 (+/-)	Foxg1 (+/+)	Foxg1 (+/-)	Foxg1 (+/+)	Foxg1 (+/-)
	mLine1.orf2		mLine1.A		mLine1.Gf		mLine1.Tf	

Figure 2

A

"prot I"

cell freq				
	0.41	0.28	0.02	0.29
	0.38	0.31	0.02	0.29
	0.39	0.27	0.02	0.32
	Sox2+ Tubb3-	Sox2+ Tubb3+	Sox2- Tubb3+	Sox2- Tubb3-

"prot II"

cell freq				
	0.23	0.26	0.14	0.39
	0.24	0.27	0.15	0.33
	0.19	0.27	0.16	0.41
	Sox2+ Tubb3-	Sox2+ Tubb3+	Sox2- Tubb3+	Sox2- Tubb3-

"prot III"

cell freq		
	0.72	0.28
	0.72	0.28
	0.72	0.28
	Tubb3+	Tubb3-

B

(1)

Gapdh-, "prot I"-double-norm mRNA			
	0.95	20.59	18.91
	0.83	24.61	26.32
	1.07	18.40	30.29
	0.67	25.92	27.82
	1.48	8.18	17.66
	1.00	21.40	8.92
	E12	E14	E20
	orf2		

(2)

Gapdh-, "prot I"-double-norm mRNA									
	0.54	10.40	36.28		7.51	23.39		15.66	
	2.95	10.18	44.18	1.11	6.91	28.72	1.02	13.70	52.68
	0.63	9.36	32.65	0.96	7.23	16.95	1.04	14.26	78.68
	0.57	13.33	41.51	1.05	9.79	23.11	1.04	19.29	56.39
	0.81	17.40	89.81	1.25	26.47	63.74	1.11	59.45	59.86
	0.50	17.39	54.80	0.64	9.03	43.93	0.79	18.11	114.81
	E12	E14	E20	E12	E14	E20	E12	E14	E20
	mLine1.A-5'UTR			mLine1.Gf-5'UTR			mLine1.Tf-5'UTR		

C

neocortex

quadruplet-norm, ctrl-norm [mRNA]								
	1.16		1.01				1.18	
	1.05		0.95		1.24		1.11	
	0.98		0.95		0.81		0.93	
	1.10	3.03	1.13	3.16	0.97	3.14	1.05	2.53
	0.77	1.48	0.78	1.86	1.19	1.89	0.85	1.53
	0.91	1.44	0.92	1.92	0.77	1.43	0.92	1.43
	1.17	1.77	1.30	2.34	0.86	2.19	1.05	1.77
	0.88	4.78	1.06	4.68	1.09	5.29	0.98	3.32
	0.84	1.65	0.84	1.32	0.90	2.09	1.02	1.47
	1.13	1.41	1.06	1.57	1.17	1.44	0.93	1.32
	E14	P0	E14	P0	E14	P0	E14	P0
	mLine1.orf2		mLine1.A		mLine1.Gf		mLine1.Tf	

mesencephalon

quadruplet-norm, ctrl-norm [mRNA]								
	0.63		0.77		0.89		0.95	
	0.76	0.64	0.81	0.82	0.81		0.81	
	1.64	0.67	1.34	0.72	1.33	0.75	1.24	0.81
	0.84	1.20	0.84	0.98	0.95	0.56	1.52	0.66
	0.29	0.71	1.44	0.71	0.38	0.76	0.37	0.86
	1.74	0.95	1.19	0.78	1.82	0.54	1.46	0.67
	1.40	0.73	1.14	0.58	1.28	0.58	1.10	0.95
	0.96	1.19	0.92	1.02	1.00	0.45	1.08	0.52
	0.73	0.71	0.55	0.73	0.96	0.83	0.95	0.92
	E14	P0	E14	P0	E14	P0	E14	P0
	mLine1.orf2		mLine1.A		mLine1.Gf		mLine1.Tf	

Figure 3

A

["quadruplet"-, ctrl-double-norm *mLINE1*-mRNA]						
	1.18		1.22		1.11	
0.77	1.35	1.11	1.41	0.89	1.37	
0.89	1.43	0.84	1.00	0.99	1.05	
0.97	1.58	1.07	1.37	1.03	1.38	
0.83	0.86	0.73	1.79	0.93	1.34	
1.31	0.77	1.12	0.60	1.01	0.81	
0.83	1.09	0.80	1.17	0.90	1.12	
0.82	0.82	0.76	0.80	0.80	0.88	
1.02	1.31	0.97	1.31	0.93	1.11	
1.32	1.09	1.27	1.11	1.26	1.20	
1.23	0.93	1.34	0.84	1.26	0.96	
ctr	Foxg1-LOF	ctr	Foxg1-LOF	ctr	Foxg1-LOF	
mLine1.A		mLine1.Gf		mLine1.Tf		

B

["quadruplet"-, *Plap*-OE-double norm mLINE1-mRNA]								
1.05	0.89	1.00	0.95	0.97	1.04	0.98	1.08	
0.92	0.75	1.00	0.68	0.99	0.75	0.96	0.69	
0.94	0.75	0.81	0.69	0.83	0.70	0.73	0.72	
0.89	0.64	0.97	0.69	0.97	0.74	0.98	0.77	
1.08	0.87	1.32	0.87	1.47	0.98	1.37	1.00	
1.18	0.71	1.03	0.72	0.96	0.70	1.08	0.74	
0.93	0.59	0.93	0.62	1.00	0.55	0.96	0.65	
1.08	0.66	1.08	0.74	1.00	0.76	1.11	0.78	
0.93	0.52	0.86	0.59	0.81	0.69	0.83	0.55	
ctr	Foxg1-OE	ctr	Foxg1-OE	ctr	Foxg1-OE	ctr	Foxg1-OE	
mLine1.orf2		mLine1.A		mLine1.Gf		mLine1.Tf		

D

["quadruplet"-, *Plap*-OE-double norm mLINE1-mRNA]								
0.95	0.74	0.87	0.31	0.99	0.28	0.89	0.38	
0.48	0.72	0.67	0.35	0.65	0.30	0.78	0.41	
1.96	0.35	1.60	0.26	1.67	0.24	1.75	0.26	
1.04	0.57	0.98	0.48	1.08	0.44	1.14	0.65	
1.09	0.46	1.03	0.54	0.85	0.29	0.83	0.34	
0.48	0.58	0.85	0.37	0.76	0.36	0.62	0.35	
ctr	Foxg1-OE	ctr	Foxg1-OE	ctr	Foxg1-OE	ctr	Foxg1-OE	
mLine1.orf2		mLine1.A		mLine1.Gf		mLine1.Tf		

C

["quadruplet"-, *Plap*-OE-double norm mLINE1-mRNA]								
0.90	0.75	1.01	0.65	0.88	0.68	1.05	0.74	
1.10	0.92	1.09	0.73	1.10	0.74	1.03	0.67	
1.15	0.59	1.06	0.54	1.02	0.47	0.98	0.55	
0.97	0.77	0.89	0.99	0.87	0.81	0.97	0.85	
0.70	0.70	0.76	0.67	0.75	0.58	0.73	0.73	
1.19	0.67	1.19	0.55	1.38	0.42	1.24	0.53	
ctr	Foxg1-OE	ctr	Foxg1-OE	ctr	Foxg1-OE	ctr	Foxg1-OE	
mLine1.orf2		mLine1.A		mLine1.Gf		mLine1.Tf		

E

["quadruplet"-, *Plap*-OE-double norm mLINE1-mRNA]								
0.98		1.01		0.97		0.99		
1.05		1.15		1.11		1.03		
1.21	0.85	1.15	0.76	1.09	0.74	1.15	0.80	
0.79	1.05	0.85	0.86	0.92	0.75	0.87	0.86	
1.14	1.16	1.13	0.98	1.19	0.90	1.22	1.00	
0.83	0.79	0.74	0.72	0.78	0.69	0.76	0.75	
1.01	0.79	0.97	0.77	0.94	0.76	0.99	0.79	
ctr	Foxg1-OE	ctr	Foxg1-OE	ctr	Foxg1-OE	ctr	Foxg1-OE	
mLine1.orf2		mLine1.A		mLine1.Gf		mLine1.Tf		

G

["quadruplet"-, *Plap*-OE-double norm mLINE1-mRNA]								
0.77		0.87		0.86				
0.86	0.73	0.82	0.71	0.80	0.69	0.84	0.88	
0.95	0.65	1.06	0.67	1.06	0.60	1.02	0.69	
0.88	0.71	0.86	0.69	0.87	0.72	0.86	0.63	
1.10	0.87	1.04	0.82	1.07	0.85	1.06	0.70	
0.95	0.92	0.98	0.97	0.99	0.91	1.00	0.83	
1.02	0.88	0.97	0.88	1.00	0.84	0.96	0.89	
1.24	0.93	1.27	1.25	1.20	1.28	1.25	0.87	
ctr	Foxg1-OE	ctr	Foxg1-OE	ctr	Foxg1-OE	ctr	Foxg1-OE	
mLine1.orf2		mLine1.A		mLine1.Gf		mLine1.Tf		

F

["quadruplet"-, *Plap*-OE-double norm mLINE1-mRNA]								
0.84		0.87		0.89	0.87	0.83		
1.05	0.86	1.10	0.89	1.07	0.89	1.05	0.91	
0.95	0.93	1.03	0.93	1.10	0.92	1.09	1.01	
0.93	0.91	0.90	0.97	0.93	0.89	0.84	1.02	
1.02	0.90	0.94	0.97	0.89	0.82	0.93	1.05	
1.21	0.92	1.15	0.89	1.11	0.97	1.25	0.98	
ctr	Foxg1-OE	ctr	Foxg1-OE	ctr	Foxg1-OE	ctr	Foxg1-OE	
mLine1.orf2		mLine1.A		mLine1.Gf		mLine1.Tf		

Figure 4

(1)

[*Gapdh*-, ctrl-double-norm *mLINE1.orf2*-mRNA]	
1.03	0.65
0.74	0.80
1.05	0.97
1.18	0.57
ctr	*Foxg1*-OE

(2)

[*Rpl10a*-, ctrl-double-norm *mLINE1.orf2*-mRNA]	
0.97	0.54
0.71	0.82
1.16	0.81
1.16	0.49
ctr	*Foxg1*-OE

(3)

[*Rpl10a*-, ctrl-double-norm *mLINE1.orf2*-mRNA]	
0.72	1.42
1.10	1.47
1.12	2.32
1.06	1.45
ctr	*Foxg1*-LOF

Development • Supplementary information

Figure 5

A

(1)

frequency						
	0.84	0.52	0.12	0.43	0.04	0.06
	0.83	0.56	0.13	0.41	0.04	0.02
	0.75	0.63	0.21	0.35	0.04	0.02
	0.92	0.59	0.06	0.37	0.02	0.04
	0.88	0.57	0.08	0.40	0.03	0.02
	Plap-OE	*Foxg1*-OE	*Plap*-OE	*Foxg1*-OE	*Plap*-OE	*Foxg1*-OE
	NSC		NP		N	

(2)

NSC	^{pNes}Plap-OE cell n = 6060		^{pNes}Foxg1-OE cell n = 5811							
cell fraction	^{pNes}Plap-OE	0.12	0.12	0.12	0.12	0.12	0.11	0.10	0.09	0.08	0.03
	^{pNes}Foxg1-OE	0.05	0.08	0.09	0.09	0.12	0.11	0.10	0.10	0.10	0.15
	expr decile	10	9	8	7	6	5	4	3	2	1

NP	^{pNes}Plap-OE cell n = 816		^{pNes}Foxg1-OE cell n = 3955							
cell fraction	^{pNes}Plap-OE	0.00	0.00	0.00	0.00	0.00	0.03	0.09	0.14	0.25	0.49
	^{pNes}Foxg1-OE	0.00	0.00	0.00	0.00	0.00	0.01	0.02	0.05	0.09	0.83
	expr decile	10	9	8	7	6	5	4	3	2	1

N	^{pNes}Plap-OE cell n = 244		^{pNes}Foxg1-OE cell n = 296							
cell fraction	^{pNes}Plap-OE	0.01	0.01	0.02	0.03	0.04	0.05	0.07	0.14	0.18	0.46
	^{pNes}Foxg1-OE	0.00	0.00	0.00	0.01	0.02	0.01	0.02	0.02	0.06	0.85
	expr decile	10	9	8	7	6	5	4	3	2	1

B

(1)

frequency						
	0.12	0.12	0.15	0.26	0.73	0.62
	0.13	0.17	0.20	0.25	0.67	0.59
	0.14	0.08	0.23	0.24	0.62	0.68
	0.12	0.16	0.25	0.26	0.63	0.58
	0.11	0.14	0.23	0.29	0.65	0.57
	Plap-OE	*Foxg1*-OE	*Plap*-OE	*Foxg1*-OE	*Plap*-OE	*Foxg1*-OE
	NSC		NP		N	

(2)

NSC	^{pTa1}Plap-OE cell n = 430		^{pTa1}Foxg1-OE cell n = 630							
cell fraction	^{pTa1}Plap-OE	0.55	0.34	0.09	0.01	0.00	0.00	0.00	0.00	0.00	0.00
	^{pTa1}Foxg1-OE	0.44	0.32	0.17	0.06	0.00	0.00	0.00	0.00	0.00	0.00
	expr decile	10	9	8	7	6	5	4	3	2	1

NP	^{pTa1}Plap-OE cell n = 745		^{pTa1}Foxg1-OE cell n = 1286							
cell fraction	^{pTa1}Plap-OE	0.00	0.00	0.04	0.08	0.10	0.16	0.19	0.20	0.16	0.06
	^{pTa1}Foxg1-OE	0.00	0.00	0.02	0.09	0.12	0.13	0.17	0.17	0.18	0.12
	expr decile	10	9	8	7	6	5	4	3	2	1

N	^{pTa1}Plap-OE cell n = 2231		^{pTa1}Foxg1-OE cell n = 2820							
cell fraction	^{pTa1}Plap-OE	0.05	0.08	0.12	0.12	0.12	0.10	0.09	0.08	0.10	0.13
	^{pTa1}Foxg1-OE	0.03	0.08	0.08	0.10	0.10	0.10	0.09	0.07	0.11	0.24
	expr decile	10	9	8	7	6	5	4	3	2	1

C

(1)

frequency						
		0.28		0.20		0.52
		0.21		0.27		0.52
		0.11		0.37		0.52
	0.10	0.09	0.27	0.29	0.62	0.61
	0.10	0.14	0.27	0.31	0.63	0.54
	0.12	0.17	0.28	0.32	0.60	0.51
	Plap-OE	*Foxg1*-OE	*Plap*-OE	*Foxg1*-OE	*Plap*-OE	*Foxg1*-OE
	NSC		NP		N	

(2)

NSC	^{pPgk1}Plap-OE cell n = 349		^{pPgk1}Foxg1-OE cell n = 1151							
cell fraction	^{pPgk1}Plap-OE	0.62	0.33	0.04	0.01	0.00	0.00	0.00	0.00	0.00	0.00
	^{pPgk1}Foxg1-OE	0.34	0.37	0.21	0.07	0.01	0.00	0.00	0.00	0.00	0.00
	expr decile	10	9	8	7	6	5	4	3	2	1

NP	^{pPgk1}Plap-OE cell n = 898		^{pPgk1}Foxg1-OE cell n = 1967							
cell fraction	^{pPgk1}Plap-OE	0.00	0.00	0.02	0.07	0.13	0.16	0.17	0.20	0.15	0.08
	^{pPgk1}Foxg1-OE	0.00	0.02	0.11	0.14	0.12	0.09	0.08	0.11	0.09	0.24
	expr decile	10	9	8	7	6	5	4	3	2	1

N	^{pPgk1}Plap-OE cell n = 2034		^{pPgk1}Foxg1-OE cell n = 3542							
cell fraction	^{pPgk1}Plap-OE	0.05	0.10	0.14	0.13	0.10	0.09	0.08	0.07	0.09	0.13
	^{pPgk1}Foxg1-OE	0.07	0.14	0.14	0.10	0.08	0.05	0.05	0.05	0.06	0.24
	expr decile	10	9	8	7	6	5	4	3	2	1

Figure 6

A

Foxg1@mLINE1.5'UTR.A, IgG/Plap-OE-norm enrichment				
	1.60	1.34	1.71	0.64
	1.08	1.39	0.90	0.26
	0.90	0.48	1.85	0.60
	2.03	0.78	1.21	1.05
	aFoxg1 / Plap-OE	IgG / Plap-OE	aFoxg1 / Foxg1-OE	IgG / Foxg1-OE
IgG/Plap-OE, abs enrichment	0.0023			

Foxg1@mLINE1.5'UTR.Gf, IgG/Plap-OE-norm enrichment				
	1.43	1.33	1.41	0.60
	0.93	1.33	1.11	0.24
	1.02	0.53	2.04	0.61
	1.99	0.81	1.29	1.05
	aFoxg1 / Plap-OE	IgG / Plap-OE	aFoxg1 / Foxg1-OE	IgG / Foxg1-OE
IgG/Plap-OE, abs enrichment	0.0024			

Foxg1@mLINE1.5'UTR.Tf, IgG/Plap-OE-norm enrichment				
	1.78	1.35	1.74	0.61
	1.12	1.36	1.26	0.28
	0.96	0.56	1.77	0.61
	2.09	0.73	1.24	0.97
	aFoxg1 / Plap-OE	IgG / Plap-OE	aFoxg1 / Foxg1-OE	IgG / Foxg1-OE
IgG/Plap-OE, abs enrichment	0.0020			

Foxg1@mLINE1.orf2, IgG/Plap-OE-norm enrichment				
	0.81	2.12	1.36	0.50
	1.25	0.34	2.70	1.02
	1.04	0.49	2.97	2.07
	aFoxg1 / Plap-OE	IgG / Plap-OE	aFoxg1 / Foxg1-OE	IgG / Foxg1-OE
IgG/Plap-OE, abs enrichment	0.0012			

Foxg1@mLINE1.3'UTR, IgG/Plap-OE-norm enrichment				
	1.16	0.98	1.43	0.65
	0.76	1.61	1.15	0.18
	0.97	0.66	1.75	0.66
	3.46	0.74	1.15	1.03
	aFoxg1 / Plap-OE	IgG / Plap-OE	aFoxg1 / Foxg1-OE	IgG / Foxg1-OE
IgG/Plap-OE, abs enrichment	0.0032			

B

Foxg1@mLINE1.5'UTR.A, IgG/Plap-OE-norm enrichment				
	3.49	1.81		1.13
	1.62	0.34	3.74	1.62
	1.97	0.45	7.47	4.03
	2.72	1.41	3.54	0.60
	3.05	0.99	3.88	2.83
	aFoxg1 / Plap-OE	IgG / Plap-OE	aFoxg1 / Foxg1-OE	IgG / Foxg1-OE
IgG/Plap-OE, abs enrichment	0.0044			

Foxg1@mLINE1.5'UTR.Gf, IgG/Plap-OE-norm enrichment				
	2.63			
	1.01	1.24	2.45	0.82
	1.41	0.63	6.76	0.86
	3.27	1.27	3.02	0.64
	2.49	0.86	3.13	2.03
	aFoxg1 / Plap-OE	IgG / Plap-OE	aFoxg1 / Foxg1-OE	IgG / Foxg1-OE
IgG/Plap-OE, abs enrichment	0.0130			

Foxg1@mLINE1.5'UTR.Tf, IgG/Plap-OE-norm enrichment				
	3.34	1.60		1.33
	1.44	0.39	4.44	1.58
	1.57	0.45	9.54	4.82
	3.84	1.64	3.21	0.62
	2.98	0.92	3.82	3.02
	aFoxg1 / Plap-OE	IgG / Plap-OE	aFoxg1 / Foxg1-OE	IgG / Foxg1-OE
IgG/Plap-OE, abs enrichment	0.0040			

Foxg1@mLINE1.orf2, IgG/Plap-OE-norm enrichment				
	4.45	1.82		1.38
	0.95	0.19	3.68	1.50
	1.59	0.47	13.86	6.57
	4.07	1.57	5.20	0.62
	3.48	0.95	5.02	3.61
	aFoxg1 / Plap-OE	IgG / Plap-OE	aFoxg1 / Foxg1-OE	IgG / Foxg1-OE
IgG/Plap-OE, abs enrichment	0.0011			

Foxg1@mLINE1.3'UTR, IgG/Plap-OE-norm enrichment				
	2.54	1.48		0.92
	1.37	0.48	1.41	0.98
	1.68	0.67	5.25	3.27
	2.48	1.35	3.12	0.80
	2.56	1.02	2.76	2.22
	aFoxg1 / Plap-OE	IgG / Plap-OE	aFoxg1 / Foxg1-OE	IgG / Foxg1-OE
IgG/Plap-OE, abs enrichment	0.0060			

Development • Supplementary information

Figure 8

NSCs

		Gapdh-norm, *Ctrl*-norm *mLINE1 [*mRNA]					
mLine1.A	ctr	0.82	0.83	1.25	0.73	1.05	2.11
		1.17	1.12	0.88	0.86	1.23	1.19
		1.16	1.18	1.16	1.18	1.15	1.95
	Foxg1-LOF	0.85	0.88	0.91	1.23	1.18	1.35
		1.26	1.30	1.16	1.18	1.15	1.95
		1.40	1.18	1.16	1.18	1.15	1.95
mLine1.Gf	ctr	0.91	0.83	1.25	0.73	1.05	2.11
		1.26	1.12	0.88	0.86	1.23	1.19
		1.30	1.18	1.16	1.18	1.15	1.95
	Foxg1-LOF	1.40	0.88	0.91	1.23	1.18	1.35
		1.30	1.18	1.16	1.18	1.15	1.95
		1.30	1.18	1.16	1.18	1.15	1.95
mLine1.Tf	ctr	0.82	0.83	1.25	0.73	1.05	2.11
		1.17	1.12	0.88	0.86	1.23	1.19
		1.16	1.18	1.16	1.18	1.15	1.95
	Foxg1-LOF	1.40	0.88	0.91	1.23	1.18	1.35
		1.26	1.30	1.16	1.18	1.15	1.95
		1.30	1.18	1.16	1.18	1.15	1.95

NPs + Ns

		Gapdh-norm, *Ctrl*-norm *mLINE1 [*mRNA]					
mLine1.A	ctr	0.69	0.74	2.20	0.93	1.84	0.76	2.11
		0.74	1.15	0.96	2.54	0.87	1.19
		0.83	1.91	0.92	1.50	0.89	1.95
	Foxg1-LOF	1.74	1.31	1.20	1.37	1.48	1.35
		1.15	1.91	0.92	1.50	0.89	1.95
		1.15	1.91	0.92	1.50	0.89	1.95
mLine1.Gf	ctr	0.73	0.86	1.18	1.18	1.05	2.11
		0.86	0.88	1.18	1.18	1.05	2.11
		1.23	1.18	1.18	1.18	1.05	2.11
	Foxg1-LOF	1.18	1.18	1.18	1.18	1.05	2.11
		1.18	1.18	1.18	1.18	1.05	2.11
		1.18	1.18	1.18	1.18	1.05	2.11
mLine1.Tf	ctr	0.69	0.74	2.20	0.93	1.84	0.76	2.11
		0.74	1.15	0.96	2.54	0.87	1.19
		0.83	1.91	0.92	1.50	0.89	1.95
	Foxg1-LOF	1.74	1.31	1.20	1.37	1.48	1.35
		1.15	1.91	0.92	1.50	0.89	1.95
		1.15	1.91	0.92	1.50	0.89	1.95

Figure 9

c

mLINE1.5'UTR.A

H3K4me3

H3K4me3@mLINE1.5'UTR.A, IgG/Plap-OE-norm enrichment

aH3K4me3 / Plap-OE	76.3	76.6	82.6	71.5
IgG / Plap-OE	0.8	1.2	0.5	1.5
aH3K4me3 / Foxg1-OE	71.7	59.7	66.6	
IgG / Foxg1-OE	0.9	0.9	1.1	

IgG/Plap-OE, abs enrichment: 0.001149219

H3K9me3

H3K9me3@mLINE1.5'UTR.A, IgG/Plap-OE-norm enrichment

aH3K9me3 / Plap-OE	73.7	65.3	82.0	91.6	99.9
IgG / Plap-OE	1.0	1.0	0.7	1.3	
aH3K9me3 / Foxg1-OE	155.1	85.2	86.3	91.1	112.6
IgG / Foxg1-OE	1.6	1.1	0.5	0.6	0.7

IgG/Plap-OE, abs enrichment: 0.002083091

H3K27aac

H3K27ac@mLINE1.5'UTR.A, IgG/Plap-OE-norm enrichment

aH3K27ac / Plap-OE	524.5	484.4	458.0	489.0	530.7
IgG / Plap-OE	1.3	0.7	1.2	0.9	
aH3K27ac / Foxg1-OE	605.2	455.2	607.0	554.3	491.3
IgG / Foxg1-OE	2.7	3.3	2.2	0.0	1.8

IgG/Plap-OE, abs enrichment: 0.001826347

MeCP2

MeCP2@mLINE1.5'UTR.A, IgG/Plap-OE-norm enrichment

aMeCP2 / Plap-OE	1.6	1.1	1.5	2.1
IgG / Plap-OE	1.0	1.0	0.9	1.1
aMeCP2 / Foxg1-OE	3.5	2.0	1.6	1.6
IgG / Foxg1-OE	2.9	1.4	1.8	1.3

IgG/Plap-OE, abs enrichment: 0.000934096

mLINE1.5'UTR.Gf

H3K4me3

H3K4me3@mLINE1.5'UTR.Gf, IgG/Plap-OE-norm enrichment

aH3K4me3 / Plap-OE	119.5	125.4	148.3	103.0
IgG / Plap-OE	0.7	1.3	0.5	1.6
aH3K4me3 / Foxg1-OE	106.6	89.4	119.5	
IgG / Foxg1-OE	1.0	1.1	1.0	

IgG/Plap-OE, abs enrichment: 0.000689949

H3K9me3

H3K9me3@mLINE1.5'UTR.Gf, IgG/Plap-OE-norm enrichment

aH3K9me3 / Plap-OE	78.6	83.6	79.5	81.0	79.4
IgG / Plap-OE	1.0	1.0	0.8	1.2	
aH3K9me3 / Foxg1-OE	88.6	104.0	88.7	83.6	94.0
IgG / Foxg1-OE	1.6	1.2	0.7	0.7	0.7

IgG/Plap-OE, abs enrichment: 0.002339303

H3K27aac

H3K27ac@mLINE1.5'UTR.Gf, IgG/Plap-OE-norm enrichment

aH3K27ac / Plap-OE	969.9	1142.8	1272.5	1092.1	1159.5
IgG / Plap-OE	1.5	0.6	1.1	0.7	
aH3K27ac / Foxg1-OE	1500.0	785.1	1261.2	1110.7	1187.2
IgG / Foxg1-OE	2.0	3.4	2.9	0.0	2.3

IgG/Plap-OE, abs enrichment: 0.001087686

MeCP2

MeCP2@mLINE1.5'UTR.Gf, IgG/Plap-OE-norm enrichment

aMeCP2 / Plap-OE	1.7	1.2	1.0	1.7	2.5
IgG / Plap-OE	1.1	0.8	1.1		
aMeCP2 / Foxg1-OE	3.0	1.6	2.1	1.4	
IgG / Foxg1-OE	2.4	1.3	1.6	1.3	

IgG/Plap-OE, abs enrichment: 0.000777261

mLINE1.5'UTR.Tf

H3K4me3

H3K4me3@mLINE1.5'UTR.Tf, IgG/Plap-OE-norm enrichment

aH3K4me3 / Plap-OE	103.3	118.8	146.4	116.1	1.6
IgG / Plap-OE	0.7	1.2	0.5	1.6	
aH3K4me3 / Foxg1-OE	133.1	81.2	117.4		
IgG / Foxg1-OE	1.0	0.7	1.2	1.1	

IgG/Plap-OE, abs enrichment: 0.000750664

H3K9me3

H3K9me3@mLINE1.5'UTR.Tf, IgG/Plap-OE-norm enrichment

aH3K9me3 / Plap-OE	82.6	81.6	89.8	100.1		
IgG / Plap-OE	1.0	0.9	1.1			
aH3K9me3 / Foxg1-OE	110.7	91.4	91.4	118.0	0.6	
IgG / Foxg1-OE	1.3	1.0	0.6	0.6	0.6	

IgG/Plap-OE, abs enrichment: 0.002191176

H3K27aac

H3K27ac@mLINE1.5'UTR.Tf, IgG/Plap-OE-norm enrichment

aH3K27ac / Plap-OE	962.4	1074.1	1219.0	1025.9	1104.1
IgG / Plap-OE	1.3	0.7	1.1	0.9	
aH3K27ac / Foxg1-OE	799.9	1355.9	1131.1	1221.4	
IgG / Foxg1-OE	2.1	3.3	3.1	0.0	2.0

IgG/Plap-OE, abs enrichment: 0.000980244

MeCP2

MeCP2@mLINE1.5'UTR.Tf, IgG/Plap-OE-norm enrichment

aMeCP2 / Plap-OE	2.1	1.5	1.1	1.7	2.4
IgG / Plap-OE	0.9	1.0	1.0	1.0	
aMeCP2 / Foxg1-OE	5.0	3.1	1.6	1.9	
IgG / Foxg1-OE	3.3	1.8	2.2	1.3	

IgG/Plap-OE, abs enrichment: 0.001044369

mLINE1.orf2

H3K4me3

H3K4me3@mLINE1.orf2, IgG/Plap-OE-norm enrichment

aH3K4me3 / Plap-OE	152.2	193.4	163.2	1.4
IgG / Plap-OE	0.8	1.3	0.5	
aH3K4me3 / Foxg1-OE	163.1	108.8	124.5	
IgG / Foxg1-OE	0.9	1.0	0.8	

IgG/Plap-OE, abs enrichment: 0.000466815

H3K9me3

H3K9me3@mLINE1.orf2, IgG/Plap-OE-norm enrichment

aH3K9me3 / Plap-OE	71.6	119.5	165.6	150.6	167.7
IgG / Plap-OE	0.9	0.9	0.6	1.5	
aH3K9me3 / Foxg1-OE	180.7	156.2	168.3	216.4	210.7
IgG / Foxg1-OE	1.7	1.2	0.5	0.6	0.6

IgG/Plap-OE, abs enrichment: 0.000911135

H3K27aac

H3K27ac@mLINE1.orf2, IgG/Plap-OE-norm enrichment

aH3K27ac / Plap-OE	814.7	893.7	933.1	848.1	1028.8
IgG / Plap-OE	1.5	0.7	0.9	0.9	
aH3K27ac / Foxg1-OE	1121.4	608.1	922.0	955.9	
IgG / Foxg1-OE	2.0	2.6	3.9	0.0	3.1

IgG/Plap-OE, abs enrichment: 0.001110746

MeCP2

MeCP2@mLINE1.orf2, IgG/Plap-OE-norm enrichment

aMeCP2 / Plap-OE	1.3	1.0	0.8	1.0	1.4
IgG / Plap-OE	0.9	1.1	1.1	0.9	
aMeCP2 / Foxg1-OE	2.3	1.8	1.3	1.3	
IgG / Foxg1-OE	1.7	1.8	1.2	0.9	

IgG/Plap-OE, abs enrichment: 0.001918216

mLINE1.3'UTR

H3K4me3

H3K4me3@mLINE1.3'UTR, IgG/Plap-OE-norm enrichment

aH3K4me3 / Plap-OE	83.4	85.2	105.9	75.8	1.6
IgG / Plap-OE	0.7	1.2	0.4		
aH3K4me3 / Foxg1-OE	47.8	61.3	82.5		
IgG / Foxg1-OE	0.5	0.6	1.0	1.0	

IgG/Plap-OE, abs enrichment: 0.000820073

H3K9me3

H3K9me3@mLINE1.3'UTR, IgG/Plap-OE-norm enrichment

aH3K9me3 / Plap-OE	54.1	45.1	58.8	61.4	63.2
IgG / Plap-OE	1.0	1.0	0.7	1.3	
aH3K9me3 / Foxg1-OE	78.2	69.2	59.9	58.6	70.6
IgG / Foxg1-OE	1.7	1.2	0.7	0.6	0.7

IgG/Plap-OE, abs enrichment: 0.002530524

H3K27aac

H3K27ac@mLINE1.3'UTR, IgG/Plap-OE-norm enrichment

aH3K27ac / Plap-OE	1107.3	1530.8	1190.2	1059.0	1690.3
IgG / Plap-OE	1.6	0.6	1.1	0.8	0.0
aH3K27ac / Foxg1-OE	1131.6	926.3	1442.5	1162.5	1402.9
IgG / Foxg1-OE	1.4	3.4	3.5	0.0	2.2

IgG/Plap-OE, abs enrichment: 0.001167836

MeCP2

MeCP2@mLINE1.3'UTR, IgG/Plap-OE-norm enrichment

aMeCP2 / Plap-OE	1.9	1.4	1.1	1.6	2.1
IgG / Plap-OE	0.9	1.3	1.0	0.8	
aMeCP2 / Foxg1-OE	3.2	3.3	1.7	1.8	
IgG / Foxg1-OE	2.8	1.9	2.1	1.4	

IgG/Plap-OE, abs enrichment: 0.000483773

Figure 10

"quadruplet", Plap-OE double-normalized *mLINE1-*												
	0.90	0.37 0.57	0.60 0.86	0.87	0.35 0.52	0.70 0.85	0.90	0.45 0.56	0.77	0.93	0.33 0.46	0.54 0.70
	0.64	0.46	0.70	0.76	0.56	0.77	0.68	0.63	0.88	0.79	0.54	0.64
	1.45	0.85	1.05	1.36	0.77	0.94	1.43	0.76	0.72	1.28	0.77	0.84
	PLAP	Foxg1 (WT)	Foxg1 (W308X)	PLAP	Foxg1 (WT)	Foxg1 (W308X)	PLAP	Foxg1 (WT)	Foxg1 (W308X)	PLAP	Foxg1 (WT)	Foxg1 (W308X)
	mLINE1 Orf2			*mLINE1-5'UTR.A*			*mLINE1-5'UTR.Gf*			*mLINE1-5'UTR.Tf*		

Figure 11

B1

[Gfap-S100β, Foxg1] ctrl-double-norm *mLINE1-3'UTR DNA*			
			1.31
		1.12	1.36
	0.89	1.13	1.24
	1.11	1.05	1.44
	1.19	1.24	1.25
	1.12	0.82	1.51
	0.69	0.79	1.35
	Prot I	Prot II	Prot III
	mLine1.3'UTR		

B2

[Gfap-S100β, Foxg1] ctrl-double-norm *mLINE1-3'UTR DNA*			
	0.99	1.00	1.00
	1.15	1.02	0.88
	0.85	1.66	0.90
	1.05	1.11	1.15
	1.00	1.14	0.91
	1.03	1.26	1.00
	0.97	1.05	0.85
	0.97	2.25	0.93
	E15.5	E20.5 Lam-	E20.5 Lam+
	mLine1.3'UTR		

B3

[Gfap-S100β, Foxg1] ctrl-double-norm *mLINE1-3'UTR DNA*		
	1.09	
	1.10	1.06
	0.82	1.31
	0.94	0.73
	1.02	0.96
	1.07	1.25
	1.08	1.27
	0.89	1.39
	E15.5	E20.5
	mLine1.3'UTR	

B4

[Gfap-S100β, Foxg1] ctrl-double-norm *mLINE1-3'UTR DNA*		
	0.93	0.97
	0.92	1.09
	0.96	0.81
	1.00	1.27
	0.99	1.48
	1.14	1.15
	1.05	1.06
	E15.5	E20.5
	mLine1.3'UTR	

B5

[Gfap-S100β, Foxg1] ctrl-double-norm *mLINE1-3'UTR DNA*		
	0.97	
	0.97	0.99
	0.83	1.27
	1.04	0.73
	1.06	1.04
	1.00	1.18
	0.95	1.11
	1.17	1.12
	E15.5	E20.5
	mLine1.3'UTR	

Figure 12

Neocortex

[Gfap-S100β, Foxg1] ctrl-double-norm *mLINE1-3'UTR DNA*		
	0.72	
	1.04	1.30
	0.79	1.01
	0.88	1.24
	1.11	1.26
	1.13	1.41
	1.11	1.17
	1.22	1.27
	Foxg1 $^{+/+}$ E14	*Foxg1* $^{+/+}$ P0
	mLine1.3'UTR	

Mesencephalon

[Gfap-S100β, Foxg1] ctrl-double-norm *mLINE1-3'UTR DNA*		
		1.25
		1.45
	0.60	1.25
	1.09	1.50
	1.21	1.91
	0.88	1.86
	1.08	1.72
	1.14	1.56
	Foxg1 $^{+/+}$ E14	*Foxg1* $^{+/+}$ P0
	mLine1.3'UTR	

Figure 13

[Gfap-Nfia] ctrl-double-norm *mLINE1-3'UTR DNA*		
	0.96	
	0.96	
	0.99	0.92
	0.98	0.91
	1.05	0.93
	1.06	0.94
	0.98	0.89
	1.03	0.96
	Foxg1 $^{+/+}$ P0	*Foxg1* $^{+/-}$ P0
	mLine1.3'UTR	

Figure 14

B1

Gfap- ctrl-double-norm *mLINE1-3'UTR DNA*	
0.97	0.80
0.91	0.92
1.00	0.92
0.93	0.82
1.08	0.92
0.99	0.83
1.07	0.76
1.05	0.82
Ctrl	*Foxg1* - LOF
mLINE1 .3'UTR	

B2

Gfap- ctrl-double-norm *mLINE1-3'UTR DNA*	
0.96	0.71
0.83	0.85
0.93	0.79
0.87	0.63
1.12	0.81
1.11	0.72
1.09	0.62
1.09	0.69
Ctrl	*Foxg1* - LOF
mLINE1 .3'UTR	

B3

Gfap- ctrl-double-norm *mLINE1-3'UTR DNA*	
1.00	0.95
1.22	0.83
1.04	1.08
1.10	1.04
1.22	0.66
0.95	0.96
0.44	1.05
1.04	0.96
0.81	1.06
1.20	1.39
Ctrl	*Foxg1* - OE
mLINE1 .3'UTR	

B4

Gfap- ctrl-double-norm *mLINE1-3'UTR DNA*	
0.89	2.43
1.17	1.44
1.26	1.44
0.64	0.89
0.82	1.40
1.18	1.33
1.15	1.24
0.62	1.52
1.29	0.65
Ctrl	*Foxg1* - OE
mLINE1 .3'UTR	

Figure 15

Gfap -, "prot III"-double-norm DNA						
1.20						
1.07						
0.97						
1.02						
0.95						
0.88						
0.91						
0.97						
0.97						
0.97						
1.16						
1.15						
1.30						
0.66						
0.82			1.05	0.65		
1.06			1.27	0.70		
0.83	0.64		1.06	0.88		
1.12	0.74		1.02	0.98	0.83	
1.16	1.15		1.20	0.85	0.94	0.89
0.94	0.90		1.27	0.78	0.87	0.88
0.95	1.03		1.20	0.74	0.99	0.89
1.00	0.96		1.13	0.67	0.83	0.94
0.93	0.98		1.18	0.53	0.92	0.97
1.01	0.97		1.31	0.58	0.73	0.81
Foxg1	wt	wt	wt	lof	lof	lof
Mov10	wt	lof	wt	wt	lof	wt
Ddx39a	wt	wt	lof	wt	wt	lof
	mLine1. 3'UTR					

Figure 16

(1)

Foxg1@mLINE1.5'UTR.A, IgG/Plap-OE-norm enrichment	
2.68	
2.73	
3.54	0.98
2.95	0.82
3.63	1.20
aFoxg1 / Plap-OE	IgG / Plap-OE

(2)

Foxg1@mLINE1.5'UTR.Gf, IgG/Plap-OE-norm enrichment	
1.49	
1.17	
2.26	0.55
1.61	1.05
2.73	1.40
aFoxg1 / Plap-OE	IgG / Plap-OE

(3)

Foxg1@mLINE1.5'UTR.Tf, IgG/Plap-OE-norm enrichment	
5.34	
2.80	
3.50	0.57
3.69	0.56
5.32	1.87
aFoxg1 / Plap-OE	IgG / Plap-OE

(4)

Foxg1@mLINE1.Orf2, IgG/Plap-OE-norm enrichment	
2.23	
0.74	
1.06	0.93
1.95	1.13
3.34	0.95
aFoxg1 / Plap-OE	IgG / Plap-OE

(5)

Foxg1@mLINE1.3'UTR., IgG/Plap-OE-norm enrichment	
3.81	
2.35	
3.58	0.84
3.91	1.24
5.78	0.92
aFoxg1 / Plap-OE	IgG / Plap-OE

Fig. S1. Sanger sequences of amplicons employed to generate experimental, SEQ.A.x, SEQ.Gf.x, SEQ.Tf.x and SEQ.3'UTR.x consensuses

```
>SEQ.A.1
GAATACTCTGCCCACTGAAACTAAGGAGAGTGCTACCCTCCAGGTCTGCTCATAGAGGCTAACAGAGTCACCGGAAGAACAAGCTCTTAAC
>SEQ.A.2
GAATACTCTGCCCACTGAAACTAAGGAGAGTGCTACCCTCCAGATCTGCTTATAGAGGCTAACAGAGTCACCTGAAGAACAAGCTCTTAACT
>SEQ.A.3
GAATACTCTGCCCACTGAAACTAAGGAGAGTGCTACCCTCCAGGTCTGCTCATAGAGGCTAACAGAGTCACCTGAAGAACAAGCTCTTAAC
>SEQ.A.4
GAATACTCTGCCCACTGAAACTAAGGAGAGTGCTACCCTCCAGGTCTGCTCATAGAGGCTAACAGAGTCACCTGAAGAACAAGCTCTTAAC
>SEQ.A.5
GAATACTCTGCCCACTGAAACTAAGGAGAGTGCTACCCTCCAGGTCTGCTCATAGAGGCTAACAGAGTCACCTGAAGAACAAGCTCTTAAC
>SEQ.A.6
GAATACTCTGCCCACTGAAACTAAGGAGAATGCTACCCTCCAGGTCTGCTCATAGAGGCTAACAGAGTCACCTGAAGAACAAGCTCTTAAC
>SEQ.A.7
GAATACTCTGCCCACTGAAACTAAGGAGAGTGCTACCCTCCAGGTCTGCTTATAGAGGCTAACAGAGTCACCTGAAGAACAAGCTCTTAAC
>SEQ.A.8
GAATACTCTGCCCACTGAAACTAAGGAGAGTGCTACCCTCCAGGTCTGCTTATAGAGGCTAACAGAGTCACCTGAAGAACAAGCTCTTAAC
```

```
>SEQ.Gf.1
GGAGGTCCAAACACCAGATAACTGTACACCTTCCCTGAGAGAGGAGAGCTTGCCTACAGAGACTGCTCTGACCACTGAAACTCAGAGAAGAGAGCTTGTCT
CCCACGCCTGCT
>SEQ.Gf.2
GGAGGTCCAAACACCAGATAACTGTACACCTTCCCTGAGAGAGGAGAGCTTGCCTACAGAGACTGCTCTGACCACTGAAACTCAGAGAAGAGAGCTTGTCT
CCCACGCCTGCT
>SEQ.Gf.3
GGAGGTCCAAACACCAGATAACTGTACACCTTCCCTGAGAGAGGAGAGCTTGCCTACAGAGACTGCTCTGACCACTGAAACTCAGAGAAGAGAGCTTGTCT
CCCACGCCTGCT
>SEQ.Gf.4
GGAGGTCCAAACACCAGATAACTGTACACCTTCCCTGAGAGAGGAGAGCTTGCCTACAGAGACTGCTCTGACCACTGAAACTCAGAGAAGAGAGCTTGTCT
CCCACGCCTGCT
>SEQ.Gf.5
GGAGGTCCAAACACCAGATAACTGTACACCTTCCCTGAGAGAGGAGAGCTTGCCTACAGAGACTGCTCTGACCACTGAAACTCAGAGAAGAGAGCTTGTCT
CCCACGCCTGCT
>SEQ.Gf.6
GGAGGTCCAAACACCAGATAACTGTACACCTTCCCTGAGAGAGGAGAGCTTGCCTACAGAGACTGCTCTGACCACTGAAACTCAGAGAAGAGAGCTTGTCT
CCCACGCCTGCT
```

```
>SEQ.Tf.1
GAGAGTCTGTACCACCTGGGAACTGCCAAAGCAACACAGTGTCTGAGAAAGGTCCTGTTTTGGGCCTTCTTCTTCGG
>SEQ.Tf.2
GAGAGTCTGTACCACCTGGGAACTGCCAAAGCAACACAGTGTCTGAGAAAGGTCCTGTTTTGGGCCTTCTTCTTCGG
>SEQ.Tf.3
GAGAGTCTGTACCACCTGGGAACTGCCAAAGCAACACAGTGTCTGAGAAAGGTCCTGTTTTGGGCCTTCTTCTTCGG
>SEQ.Tf.4
GAGAGTCTGTACCACCTGGGAACTGCCAAAGCAACACAGTGTCTGAGAAAGGTCCTGTTTTGGGCCTTCTTCTTCGG
>SEQ.Tf.5
GAGAGTCTGTACCACCTGGGAACTGCCAAAGCAACACAGTGTCTGAGAAAGGTCCTGTTTTGGGCCTTCTTCTTCGG
>SEQ.Tf.6
GAGAGTCTGTACCACCTGGGAACTGCCAAAGCAACACAGTGTCTGAGAAAGGTCCTGTTTTGGGCCTTCTTCTTCGG
>SEQ.Tf.7
GAGAGTCTGTACCACCTGGGAACTGCCAAAGCAACACAGTGTCTGAGAAAGGTCCTGTTTTGGGCCTTCTTCTTCGG
>SEQ.Tf.8
GAGAGTCTGTACCACCTGGGAACTGCCAAAGCAACACAGTGTCTGAGAAAGGTCCTGTTTTGGGCCTTCTTCTTCGG
```

```
>SEQ.3'UTR.1
GGTGGAACAACATTATGAACTAACCAGTACCCAGGAGGTCTTGACTCTAGCTGCATATGTATCAAAAGATGGCCTAATCGGCCATCACTGGAAAGAGAGGC
CCATTGG
>SEQ.3'UTR.2
GGTGGAACAACATTATGAACTAACCAGTACCCCGGAGCTCTTGACTCTAGCTGCATATGTATCAAAAGATGGCCTAGTCGGCCATCACTGGAAAGAGAGGC
CCATTGG
>SEQ.3'UTR.3
GGTGGAACAACATTATGAACTAACCAGTACCCCTGAGCTCTTGACTCTAGCTGCATATGTATCAAAAGATGGCCTAGTCGGCCATCACTGGAAAGAGAGGC
CCATTGG
>SEQ.3'UTR.4
GGTGGAACAACATTATGAACTAACCAGTACCCCAGAGCTCTTGACTCTAGCTGCATATGTATCAAAAGATGACCTAGTCGGCCATCACTGGAAAGAGAGGC
CCATTGG
>SEQ.3'UTR.5
GGTGGAACAACATTATGAACTAACCAGTACCCCTGAGCTCTTGACTCTAGCTGCATATGTATCAAAAGATGGCCTAGTCGGCCATCACTGGAAAGAGAGGC
CCATTGG
>SEQ.3'UTR.6
GGTGGAACAACATTATGAACTAACCAGTACCCCGGAGCTCTTGACTCTAGCTGCATATGTATCAAAAGATGGCCTAGTCGGCCATCACTGGAAAGAGAGGC
CCATTGG
>SEQ.3'UTR.7
GGTGGAACAACATTATGAACTAACCAGTACCCCCCAGAGTTCGTGTCTCTAGCTGCATATGCATCAGAAGATGAACTAGTAGGTCATCACTGGAAAGAGAG
GCCCATTGG
>SEQ.3'UTR.8
GGTGGAACAACATTATGAACTAACCAGTACCCCGGAGCTCTTGACTCTTGCTGCATGTGTATCAAAAGATGGCCTAGTTGGCCATCACTGGAAAGAGAGGC
CCATTGG
```

Development • Supplementary information

Figure S2

A

Ctrl-norm [Foxg1 protein]	ctr	Foxg1-LOF
	1.30	0.50
	1.49	0.31
	1.36	0.41
	1.26	0.81
	0.68	0.83
	0.78	0.56
	0.68	0.39
	0.45	0.86

B

Ctrl-norm [Foxg1 protein]	ctr	Foxg1-LOF
		0.94
	1.14	0.50
	0.94	0.83
	1.01	0.87
	1.02	0.53
	0.92	0.59
	1.03	0.64
	1.10	0.54
	0.85	0.42

C

Ctrl-norm [Foxg1 protein]	ctr	Foxg1-LOF
	0.89	0.47
	0.93	0.48
	1.23	0.50
	1.08	0.61
	0.79	0.59
	1.08	0.51

D

promoter = pNes

Plap-OE-norm Foxg1 content/cell	NSCs Plap-OE	NSCs Foxg1-OE	NPs Plap-OE	NPs Foxg1-OE	Ns Plap-OE	Ns Foxg1-OE
		1.83		3.82		6.83
	1.17	2.80	1.16	4.71	1.21	6.47
	1.16	2.12	0.95	4.35	1.16	7.63
	0.87	1.69	0.89	3.89	0.97	7.93
	0.79	2.33	0.91	4.33	0.83	8.89
	1.00	1.20	1.09	3.13	0.83	6.30

promoter = pTa1

Plap-OE-norm Foxg1 content/cell	NSCs Plap-OE	NSCs Foxg1-OE	NPs Plap-OE	NPs Foxg1-OE	Ns Plap-OE	Ns Foxg1-OE
		2.10		1.13		1.88
	1.30	2.41	1.20	1.27	1.37	2.01
	0.82	1.33	0.89	1.39	0.79	2.24
	0.98	1.89	1.12	1.31	1.00	2.33
	1.46	1.80	1.11	1.41	0.96	1.79
	0.45	2.07	0.67	1.39	0.88	2.04

promoter = pPgk1

Plap-OE-norm Foxg1 content/cell	NSCs Plap-OE	NSCs Foxg1-OE	NPs Plap-OE	NPs Foxg1-OE	Ns Plap-OE	Ns Foxg1-OE
		1.58		0.72		0.79
		3.68		1.33		1.65
		4.02		1.60		2.38
	1.08	2.83	0.89	1.79	1.14	2.91
	1.07	2.14	1.10	1.55	0.96	2.28
	0.85	4.36	1.01	1.55	0.90	2.17

Figure S3

"quadruplet", Plap-OE double-normalized *mLINE1-mRNA*	Foxg1 (W308X)	PLAP	Foxg1 (W308X)	PLAP	Foxg1 (W308X)	PLAP	Foxg1 (W308X)	PLAP
	mLINE1-5'UTR.A		*mLINE1-5'UTR.Gf*		*mLINE1-5'UTR.Tf*		*mLINE1 Orf2*	
	0.77	0.99	1.00	1.04	0.81	1.03	0.75	1.08
	0.91	1.09	1.01	1.13	1.05	1.06	0.78	1.00
	0.82	1.06	0.87	0.93	0.85	1.02	0.69	0.91
	0.80	0.99	0.79	0.99	0.91	0.96	0.81	1.00
	0.97	0.88	1.14	0.91	0.97	0.93	1.01	1.01

Figure S4

A

Gapdh-, ctrl-double-norm *mLINE1*-mRNA						
	1.09		1.14		1.03	
0.76	1.23	1.11	1.30	0.89	1.26	
0.92	1.32	0.88	0.94	1.04	0.98	
0.78	1.28	0.87	1.12	0.83	1.12	
0.86	0.66	0.76	1.39	0.97	1.04	
1.55	1.18	1.33	0.93	1.20	1.25	
0.98	1.48	0.94	1.59	1.06	1.52	
0.82	0.87	0.76	0.85	0.80	0.93	
1.15	2.09	1.10	2.11	1.05	1.77	
1.11	1.13	1.07	1.16	1.07	1.26	
1.07	0.99	1.17	0.89	1.10	1.03	
ctr	Foxg1-LOF	ctr	Foxg1-LOF	ctr	Foxg1-LOF	
mLine1.A		mLine1.Gf		mLine1.Tf		

["quadruplet"-, ctrl-double-norm *mLINE1*- mRNA]						
	1.18		1.22		1.11	
0.77	1.35	1.11	1.41	0.89	1.37	
0.89	1.43	0.84	1.00	0.99	1.05	
0.97	1.58	1.07	1.37	1.03	1.38	
0.83	0.86	0.73	1.79	0.93	1.34	
1.31	0.77	1.12	0.60	1.01	0.81	
0.83	1.09	0.80	1.17	0.90	1.12	
0.82	0.82	0.76	0.80	0.80	0.88	
1.02	1.31	0.97	1.31	0.93	1.11	
1.32	1.09	1.27	1.11	1.26	1.20	
1.23	0.93	1.34	0.84	1.26	0.96	
ctr	Foxg1-LOF	ctr	Foxg1-LOF	ctr	Foxg1-LOF	
mLine1.A		mLine1.Gf		mLine1.Tf		

B

Gapdh-, ctrl-double-norm *mLINE1*-mRNA								
0.94	0.85	0.84	0.35	0.96	0.31	0.86	0.43	
0.58	0.60	0.80	0.28	0.77	0.25	0.93	0.34	
1.64	0.33	1.30	0.23	1.37	0.22	1.43	0.24	
1.12	0.68	1.03	0.56	1.14	0.51	1.21	0.76	
1.15	0.41	1.06	0.47	0.88	0.26	0.86	0.30	
0.57	0.66	0.98	0.41	0.88	0.40	0.72	0.39	
ctr	Foxg1-OE	ctr	Foxg1-OE	ctr	Foxg1-OE	ctr	Foxg1-OE	
mLine1.orf2		mLine1.A		mLine1.Gf		mLine1.Tf		

["quadruplet"-, *Plap* -OE-double norm mLINE1- mRNA]								
0.95	0.74	0.87	0.31	0.99	0.28	0.89	0.38	
0.48	0.72	0.67	0.35	0.65	0.30	0.78	0.41	
1.96	0.35	1.60	0.26	1.67	0.24	1.75	0.26	
1.04	0.57	0.98	0.48	1.08	0.44	1.14	0.65	
1.09	0.46	1.03	0.54	0.85	0.29	0.83	0.34	
0.48	0.58	0.85	0.37	0.76	0.36	0.62	0.35	
ctr	Foxg1-OE	ctr	Foxg1-OE	ctr	Foxg1-OE	ctr	Foxg1-OE	
mLine1.orf2		mLine1.A		mLine1.Gf		mLine1.Tf		

Figure S5

(1) *high Pk*

Gfap -,ctrl-double-norm *Mecp2 DNA*		
0.97		
1.28	1.72	
0.75	1.36	
E15.5 males	E15,5 females	

(2) *very high Pk*

Gfap, - ctrl-double-norm *Mecp2 DNA*		
1.02		
1.04	1.80	
0.94	2.69	
E15.5 males	E15,5 females	

(3) *very high Pk*

Gfap, - ctrl-double-norm *Cdkl5 DNA*		
0.73	2.04	
1.23	2.26	
1.04	2.37	
E15.5 males	E15,5 females	

Development • Supplementary information